Estimating particle size of hydrocyclone underflow discharge using image analysis

by

Foibe Dimbulukwa Lawanifwa Uahengo

Thesis presented in partial fulfilment
of the requirements for the Degree

of

MASTER OF SCIENCE IN ENGINEERING
(EXTRACTIVE METALLURGICAL ENGINEERING)

in the Faculty of Engineering
at Stellenbosch University

Supervisor
Prof. C. Aldrich

April 2014

Declaration

By submitting this thesis electronically, I declare that the entirety of the work contained therein is my own, original work, that I am the sole author thereof (save to the extent explicitly otherwise stated), that reproduction and publication thereof by Stellenbosch University will not infringe any third party rights and that I have not previously in its entirety or in part submitted it for obtaining any qualification.

Foibe Dimbulukwa Lawanifwa Uahengo 22 April 2014

…… …….

Signature Date

Abstract

Hydrocyclones are stationary separating machines that separate materials based on centrifugal separation and are widely used in chemical engineering and mineral processing industries. Their design and operation, compact structure, low running costs and versatility all contribute to their applications in liquid clarification, slurry thickening, solid washing and classification. With any of these operations, the overall profitability of the process relies on the effective control of the process equipment. However, in practice, hydrocyclones are difficult to monitor and control, owing to the complexity and difficulty in measuring internal flows in the equipment.

Several studies have indicated that hydrocyclone underflow images can be used to monitor process conditions. The research described in this thesis considers the use of image analysis to monitor particle size and solids concentration in the underflow discharge of a hydrocyclone.

The experimental work consisted of laboratory and industrial-based case studies. The laboratory cyclone used was a 76 mm general laboratory cyclone. A Canon EOS 400D digital camera was used for the underflow imaging. Image features such as pixel intensity values, underflow discharge width and grey level co-occurrence matrix (GLCM) were extracted from the images using MATLAB Toolbox software.

Linear discriminant analysis (LDA) and neural network (NN) classification models were used to discriminate between different PGM ore types based on features extracted from the underflow of the hydrocyclone. Likewise, multiple linear regression and neural network models were used to estimate the underflow solids content and mean particle size in the hydrocyclone underflow.

The LDA model could predict the PGM ore types with 61% reliability, while the NN model could do so with a statistically similar 62% reliability. The multiple linear regression models could explain 56% and 40% of variance in the mean particle size and solids content respectively. In contrast, the neural network model could explain 67% and 45% of the variance of the mean particle size and solids content respectively. For the industrial system, a

100% correct classification was achieved with all methods. However, these results are regarded as unreliable, owing to the insufficient data used in the models.

Keywords: Hydrocyclone, image features, classification, co-occurrence matrix, image analysis

Opsomming

Hidrosiklone is stasionêre skeidingsmasjiene wat materiale skei op grond van sentrifugale skeiding en word algemeen gebruik in die chemiese ingenieurswese en mineraalprosessering industrieë. Hul ontwerp en werking, kompakte struktuur, lae bedryfskoste en veelsydigheid dra by tot hul gebruik vir toepassings in vloeistofsuiwering, slykverdikking, vastestof wassing en klassifikasie. In enige van hierdie prosesse hang die oorhoofse winsgewendheid van die proses af van die effektiewe beheer van die prosestoerusting. In die praktyk is hidrosiklone egter moeilik om te monitor en beheer weens die kompleksiteit en moeilikheidsgraad daarvan om die interne vloei in die apparaat te meet.

Verskeie studies het aangedui dat hidrosikloon ondervloeibeelde gebruik kan word om die proseskondisies te monitor. Die navorsing beskryf in hierdie tesis maak gebruik van beeldanalise moniteringstegnieke om die ertstipes en grootte- verspreidingsgebiede/ klasse van die ondervloei afvoerpartikels te bepaal. Sodoende word ‘n grondslag gelê vir verbeterde sikloon monitering en beheer.

Die eksperimentele werk het bestaan uit beide laboratorium en industrieel-gebaseerde studies. Die laboratorium sikloon wat gebruik is, was ‘n 76 mm algemene laboratorium sikloon. ‘n Canon EOS 400D digitale kamera is gebruik om die hidrosikloon ondervloei beelde vas te vang. Beeldeienskappe soos beeldelement intensiteitswaardes, ondervloei afvoerwydte en grysvlak mede-voorkoms matriks is onttrek uit die beelde deur gebruik te maak van MATLAB Toolbox sagteware.

Lineêre diskriminantanalise (LDA) en neural netwerk (NN) klassifikasiemodelle is gebou om te onderskei tussen die verskillende PGM ertse en gebaseer op veranderlikes wat afgelei is uit beelde van die ondervloei van die sikloon. Net so is daar ook gebruik gemaak van lineêre regressie- en neural netwerkmodelle om die vasestofkonsentrasie en gemiddelde partikelgrootte in die ondervloei van die sikloon te beraam.

Die LDA model kon die PGM ertstipes met 61% betroubaarheid voorspel, terwyl die neural netwerkmodel dit kon doen met statisties dieselfde betroubaarheid van 62%. Die lineêre

regressiemodelle kon onderskeidelik 56% en 40% van die variansie in die gemiddelde partikelgrootte en vastestofkonsentrasie verduidelik. In teenstelling iermee, kon die neurale netwerkmodel 67% en 45% van die variansie in die gemiddelde partikelgrootte en vastestofkonsentrasie verduidelik. In die nywerheidstelsel kon beide tipe modelle perfekte onderskeid tref tussen die partikelgroottes wat gemeet is op opeenvolgende dae van die bedryf van die siklone. Hierdie resultate is egter nie betroubaar nie, a.g.v. die beperkte hoeveelheid data wat beskikbaar was vir modellering.

Trefwoorde: Hidrosikloon, beeldeienskappe, klassifikasie, grysvlak mede-voorkomsmatriks, beeldanalise.

Table of Contents

Nomenclature

a) Symbols

C_x = Corrected efficiency for a particle of size class x

E_T = Total efficiency in the hydrocyclone

F = Hydrocyclone feed stream mass flow rate

f = Known function of the covariate vector

f_x = Fraction of the feed stream particles in size class x

G_x = Grade efficiency for a particle of size class x

i,j = Co-occurring pair in GLCM

M = Total mass flow rate

M_f = Mass flow rate for the feed

M_o = Mass flow rate for the overflow products

M_u = Mass flow rate for the underflow products

N = Number of grey levels in the image

o_x = Fraction of the overflow stream particles in size class x

P_{ij} = Co-occurring probability of elements i,j in GLCM

u_x = Fraction of the underflow stream particles in size class x

U = Hydrocyclone underflow mass flow rate

x = Particles' size class

y_1, y_2 = Hydrocyclone flow ratio

β = vector parameter in a linear regression method formula

ϵ = Parameter vector of disturbance terms in a non-linear regression formula

σ^2 = Variance

μ = Mean of grey level co-occurrence matrices

μ = Vector of disturbance term in a non-linear formula

ϖ = random error in non-linear formula

Y_i = Non-linear model responses

Y^* = vector of observations of dependent variable

γ = Grand mean of the dependent variable

b) Acronyms

AES = Acoustic Emission Sensor

BFGS = Broyden-Fletcher-Goldfarb-Shanno, a neural network training algorithm

CCD = Charge-Coupled Device (CCD Camera)

CCD = Counter Current Decantation (CCD circuit in mineral processing industry)

CFD = Computer Fluid Dynamic

ECT = Electrical Capacitance Tomography

EIT = Electrical Impedance Tomography

EOS = Electro-Optical System

ERT = Electrical Resistance Tomography

ISO = International Standard Organization

JPEG = Joint Photographic Experts Group

LDA = Linear Discriminant Analysis

MCA = Multiple Classification Analysis

MER = Merensky ore

MLP = Multilayer Perception

MLR = Multiple Linear Regression

MPS = Mean Particle Size

O/F = Overflow

PC = Personal Computer

PGM = Platinum-Group Metals

PLAT = Plat Reef ore

PPE = Personal Protective Equipment

PSD = Particle Size Distribution

RF = Random Forest

RUL = Rössing Uranium Ltd

R/S = Rotoscoop

UG2 = Upper Ground Reef 2 (ore)

U/F = Underflow

VHSC = Video Home System Camcoder

List of Figures

List of Tables

Acknowledgements

It is by God's grace that I have come to the completion of this research project. He has given me the wisdom, knowledge, skills and strength I needed to do my work. I praise Him for the wonders of His work.

I would like to give my sincere appreciation to my sponsor, Rio Tinto Rössing Uranium Ltd (RUL) and its caring personnel for making it possible for me to do my research and encouragement during hard times. I further extend my gratitude to my supervisors, Prof. Chris Aldrich, Jeanette Janse van Vuuren and Prof. Andre Burger for their proficient supervision. Thank you. I have learned a lot from you. It was a great pleasure working with the laboratory team, both maintenance and technical teams. I couldn't have enjoyed my practical work if it was not for the undivided attention you have given me despite your tight schedules. Special thanks to Mr. Vincent and Lukas for helping me with the hard physical work and to Phillip John and Manda Rossouw for editing my work.

I further extent my gratitude to Corné Yzelle, Lidia Auret, Edson Charikinya and Mohsen Karimi for constant assistance especially with my experimental work and data analysis; plus Tyrone Kotze, Andrew Luke, Nicole Jansen van Rensburg and the Processing Improvement Team at Rössing. Thank you to Bernard Sililo and Tinashe Tendayi for sharing the hard long hours of putting this thesis together with me. I wouldn't have made it this smoothly if it was not for you. I also would like to extend my thanksgiving to all the Stellenbosch University Process Department personnel for assuring a smooth research for me and all my colleagues and friends who stood by me throughout my study time.

Finally, I would also like to thank my mother, Naemi Uahengo and family for their unceasing prayers and encouragement. On this note, I express my gratitude to Mrs. Bresler for believing in me, Sara Mwoonde, Rachel Shanyanana, Frondina Mweudina, Mr. and Mrs. Goosens, and Mamorabeli Kobo. Thank you for your emotional and spiritual support plus Saimi Uukule for body feeding.

It was a long and bumpy road but you all have been my support. May the Lord God Almighty bless you all!

Conference Presentation

A presentation titled: Inference of underflow cut sizes in hydrocyclones by use of multivariate image analysis. This paper was presented at the annual conference of the Southern African Institute of Mining and Metallurgy (SAIMM) on Mineral Processing, held on the 4th - 5th of August 2011 at Vineyard Conference Centre, Cape Town, South Africa.

Chapter 1: Introduction

This chapter introduces the hydrocyclone as well as its use and significance in the mineral processing industries. It outlines the importance of the monitoring and proper control of this device and evaluates monitoring techniques. From this evaluation, the potential of the use of image analysis methods for the online monitoring of the hydrocyclone is illustrated. Furthermore, the project objectives, scope and thesis layout are also outlined.

1.1 The hydrocyclone in mineral processing industries

The ore processed in mineral processing and chemical industries consist of valuable minerals and gangue which need to be separated, both chemically and physically, in order to extract the minerals of interest. Hydrocyclones are primarily used for particle size separation as well as the solid/liquid separation of minerals, rendering them vital to these processes (Wills, 2006). They are ubiquitous in mineral processing industries, replacing large mechanical spiral and rake classifiers. The wide use of cyclones by industry is due to their simplicity, versatility, low maintenance cost and small size as opposed to other equipment (Bergstrom & Vomhoff, 2007; Napier-Munn *et al*., 1996).

Furthermore, hydrocyclones[1] are commonly used in closed-circuit grinding operations (Napier-Munn *et al*., 1996) but are also used in de-sliming, de-gritting and thickening (Wills, 2006). Apart from chemical engineering and mineral processing, hydrocyclone applications have been extended to several industries such as oil refineries, petrochemical and textile industries, and many others (Janse van Vuuren, 2011; Svarovsky, 1984).

Hydrocyclones are operated either as a single unit, in series, or in parallel depending on the specific application in the process. They are used to improve overall recoveries in clarification, to simultaneously produce thicker underflows and clearer overflows, to sharpen the classification/sorting and for washing solids (Svarovsky *et al*., 2001b). The performance of a single unit can be improved by multiple cyclones.

[1] The words, hydrocyclone and cyclone are interchangeably used in this thesis.

1.1.1 Hydrocyclone monitoring and control in grinding circuits

This section illustrates the significance of hydrocyclone monitoring and control in grinding circuits. This project focused on the application of the hydrocyclone in the context of grinding and washing circuits.

A hydrocyclone requires proper monitoring of its operation for it to deliver the desired products. Therefore, it is critical in grinding circuits to maintain optimum cyclone operations, as the overall grinding efficiency depends on the hydrocyclone performance. Satisfactory hydrocyclone performance can be achieved by having the appropriate control measures in place (Daniel, 2011). This in turn aids the determination of the circuit performance, and consequently the overall process product. Janse van Vuuren (2011) emphasised the importance of controlling the hydrocyclone operations in order to reduce the energy consumption caused by poor cyclone performance. In addition, hydrocyclone performance optimisation is the best and easiest way of improving grinding and mill throughput (Kawatra *et al.*, 2002; Napier-Munn *et al*., 1996).

The classification hydrocyclone is used to select material to pass to the next phase of the process which could be the next size reduction, or a beneficiation stage e.g. floatation, leaching or gravity concentration (Napier-Munn *et al*., 1996). As such, efficient cyclone operation is crucial in maintaining downstream product efficiencies.

1.1.2 Hydrocyclone monitoring and control in washing circuits

Another application of the hydrocyclone is in washing circuits where the dissolved minerals of interest are washed off the barren solids material. The hydrocyclone overflow is transported downstream for further processing. Figure 1-1 shows a diagram of the washing circuit studied.

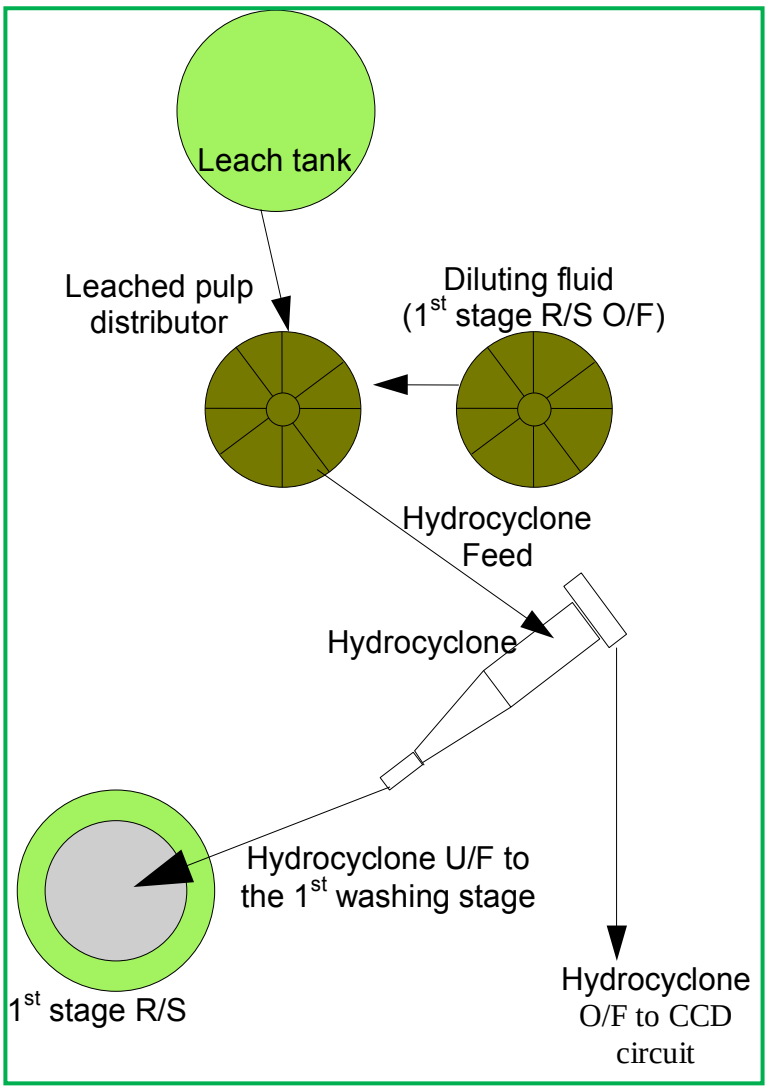

Figure 1-1: The washing circuit diagram (redrawn from Rössing, 1995)

The correct hydrocyclone operation states are essential for the required product efficiency of a specific process. Different mineral processes may require varying hydrocyclone operating parameters like: separation size, wash flow rate, inlet pressure, etc. Maintaining these parameters would thus produce high cyclone product efficiencies. This calls for proper monitoring of the operation states that eventually leads to adequate control of the hydrocyclone performance.

1.2 Overview of hydrocyclone monitoring and control

The hydrocyclone has a critical influence on mineral processing operations. Despite this, it is often neglected in industry. Due to its versatility, robustness and simple nature to operate,

people may tend to neglect the unit's required overall maintenance and the necessity for its optimum operating conditions. In addition, hydrocyclone modelling is difficult due to the complexity of its flow (Napier-Munn *et al.*, 1996). As a result, the modelling is often not performed.

Although the hydrocyclone operation advantages far outweigh its disadvantages, the complexity of its inner flow makes it difficult to control. Therefore, more research work is continuously being conducted to fully understand this flow and the hydrocyclone operational variables in terms of fluctuating hydrocyclone feed conditions (Machado, 1992).

Multiple investigations have been carried out which attempt to put hydrocyclone control measures in place. However, due to a poor understanding of fluid dynamics, hydrocyclone performance management greatly depends on theoretical and empirical modelling methods (Dyakowski & Williams, 1993; Gutiérrez *et al.*, 2000; Hararah *et al.*, 2010; Janse van Vuuren, 2011). Limitations to these modelling methods demonstrate the requirement for hydrocyclone operational monitoring as an alternative measure of hydrocyclone control.

1.2.1 Empirical and theoretical modelling

Modelling of hydrocyclone performance is hindered by its complex fluid mechanism and this is due, in part, to multiple phases (liquid, air and solid particles) as well as the turbulent flow inside the hydrocyclone (Hsieh & Rajamani, 1991). This complexity makes it difficult for one model code to be applied directly without modifications. Therefore theoretical and empirical models are at times combined to attain the desired results (Kraipech *et al.*, 2006).

Of the two models, empirical models are commonly applied to the hydrocyclone, with Lynch and Rao (1975) models being the first commonly used, and Plitt (1976) and Nageswararao (1995) the most recently applied. These empirical models work well only over a range of hydrocyclone conditions and they use material specific constants (Janse van Vuuren, 2011; Wills, 2006).

Theoretical models are highly dependent on either hydrocyclone operating conditions, designs or sizes. For each particular model, a specific hydrocyclone geometry or operating condition is required. These models cover a wider range of operation in comparison to the empirical ones, and hence are more useful tools. Furthermore, Computational Fluid Dynamic (CFD) hydrocyclone modelling found a wide application in the field and it is used to provide

solutions for the theoretical models (Wills, 2006). However, the CFD consumes high computer power and much time. Therefore the use of empirical models are preferred or the combination of both models (Nageswararao *et al.*, 2004).

1.2.2 Process conditions monitoring techniques

Changes in hydrocyclone operating conditions alter its performance (Bradley, 1965; Sripriya *et al.*, 2007). The ability to control hydrocyclone operation could address this issue, ensuring smooth running and improved performance of the device. Since this is not presently attainable, online monitoring is used to oversee changes in cyclone operating conditions. Studies done using online monitoring approaches (Galvin & Smitham, 1994; Gutiérrez *et al.*, 2000; Hou *et al.*, 1998; Williams *et al.*, 1999) yielded some recommendations as to alternative methods of monitoring hydrocyclone operating conditions. Although many techniques were proposed, sensing techniques proved to be the most practical as they provide real-time process information.

Hydrocyclone operating states give information concerning the cyclone's performance and are used to identify faulty conditions in the hydrocyclone. These operating states could be improved for control scheme developments. Three hydrocyclone operating states can be inspected. These are: normal state, spray-shaped state and roping shape, with the roping shape indicating the separation inefficiencies.

The methods used for the process state monitoring mainly focused on the study of the air core shape and this used electrical impedance tomography, electrical resistance tomography, ultrasound tomography and data acquisition card as sensor techniques (Gutiérrez *et al.*, 2000; Hararah *et al.*, 2010; Krishna *et al.*, 2010; Neesse and Dueck, 2007a; Williams *et al.*, 1999). Other methods were used to study the operating states on internal solids concentration (Dyakowski & Williams, 1996; Galvin & Smitham, 1994; Gutiérrez *et al.*, 2000; Hou *et al.*, 2002; Neesse *et al.*, 2004b). Furthermore, sensor techniques and mechanical detection methods were used to determine operating states from underflow discharge shapes (Dyakowski & Williams, 1996; Galvin & Smitham, 1994; Gutiérrez *et al.*, 2000; Hou *et al.*, 2002; Neesse *et al.*, 2004b).

Hydrocyclone underflow monitoring was also studied using image analysis (Petersen *et al.* (1996); Janse van Vuuren, 2011), and a laser-optical measuring device as used by Neese *et al.*

(2004b). These methods proved to be more viable and robust as well as less invasive and of lower equipment cost in comparison to the techniques mentioned in the previous paragraph. Furthermore, they revealed a correlation between the underflow discharge shapes and the hydrocyclone operating conditions. Images of the hydrocyclone underflow were studied to investigate the hydrocyclone underflow discharge particles in order to form a basis of improved monitoring and control of a hydrocyclone.

1.3 Project objectives

The main aim of this research project was to determine whether image analysis can be used to estimate particle sizes and solids loadings in hydrocyclone underflows. This was done in order to form a basis for improved monitoring and control of the hydrocyclone and in so doing to reaffirm the viability of image analysis as an online monitoring technique.

1.4 Project scope

In order to achieve the objectives of this research project, a thorough review was completed of past and present studies of online monitoring and control of hydrocyclones. This review was done in parallel to experimental work that aimed to collect photographic images and the associated particle size measurements for a laboratory hydrocyclone. An industrial-based cyclone system was also studied in the same way. Ultimately, an image processing methodology was developed by the use of MATLAB software that aimed at image feature extraction and the additional use of STATISTICA Software, to assess the relationship between the underflow image features and particle sizes.

1.5 Thesis layout

This thesis is comprised of seven chapters which are laid out as follows: The first chapter introduces the use and importance of the hydrocyclone in mineral processing industries. It outlines the importance of its monitoring and control. Furthermore, the monitoring techniques used to study the hydrocyclone operating states are discussed. Moreover, the objectives and scope of the project are presented.

The second and third chapters give a review of the hydrocyclone and its monitoring. Chapter two provides some background information on the hydrocyclone, briefly discussing its theory and the factors affecting its performance efficiency. Chapter three concentrates on online monitoring techniques, whereby an overview is provided of the past and present work that employed online monitoring.

The fourth chapter presents the methodology used in this research project. The experimental procedures performed and their layouts are described here. Furthermore, the underflow images and manual sample analysis are defined in chapter five, whereas the results are presented and discussed in the sixth chapter. The concluding chapter summarises the findings of this research followed by the reference and appendices sections.

Chapter Summary

The hydrocyclone is ubiquitous and important in mineral processing industries and its control is therefore essential. Though the hydrocyclone is versatile and simple to operate, the complexity in its flow behaviors makes it difficult to control and model. Due to this, hydrocyclone monitoring techniques are alternatively used to determine the cyclone operating states. Many techniques studied are expensive, fragile, time consuming and invasive sensing methods.

However, an alternative sensing technique was identified that proved to be robust and viable for use in the processes. It used image analysis to monitor the operating states of the cyclone. The objective of this study was formulated with this approach in mind where image analysis was used to relate hydrocyclone underflow particle sizes to corresponding underflow image features.

Chapter 2: Hydrocyclone Theory and Literature Review

This chapter presents the theoretical knowledge concerning the hydrocyclone, giving a brief description of hydrocyclone types, basic cyclone design, mode of operation and flow structure. It further describes the factors affecting the hydrocyclone performance efficiency as well as the influence of operating variables on the hydrocyclone operation conditions.

2.1 Hydrocyclone definition

Hydrocyclones are stationary and continuously operating, classifying equipment that separate materials using centrifugal forces to hasten the settling rate of particles (Wills, 2006). They are designed for separation of particles in liquids. These devices are small in size, simple in structure; there is nothing adjustable inside the cyclones. Furthermore, they are cost effective and have low residence time (Svarovsky, 1984). Due to less mechanical maintenance required, hydrocyclones are manageable devices in industry.

Although there are advantages to using hydrocyclones, there are also some disadvantages as stipulated by Svarovsky (1984). These include:

- Inflexibility –they are not adjustable according to flow fluctuations.
- Limitations to their separation performance in terms of sharpness of cut-range, of operating cut size and clarification power.
- They require routine spigot maintenance.
- They have optimal operation at low viscosity.

However, some of the shortcomings can be circumvented by hydrocyclone adjustments and improvements of operation conditions, though this normally comes at an additional cost.

2.2 Types of and basic design structure of a hydrocyclone

There are several types of hydrocyclones with different design structures to fit their specific applications and operations. For example, the water injected hydrocyclone, the air-sparged hydrocyclone with a solid core and a thick-wall vortex finder and the conventional hydrocyclone (Chu & Luo, 1994; Maurice *et al.*, 2003). The hydrocyclone used in this study

is the conventional one. Moreover, hydrocyclone application is determined by its design and operation because there are particular requirements and targets for every application (Svarovsky, 1984).

A typical hydrocyclone consists of a cylindrical section with a tangential feed inlet and an overflow pipe connected to the plate covering the top of the cylindrical part. To this section a conically shaped section with an opening at its apex[2] is joined to it (Wills, 1997). Figure 2-1 illustrates this description and it shows the basic features of a conventional hydrocyclone as used for the experimental work of this research project.

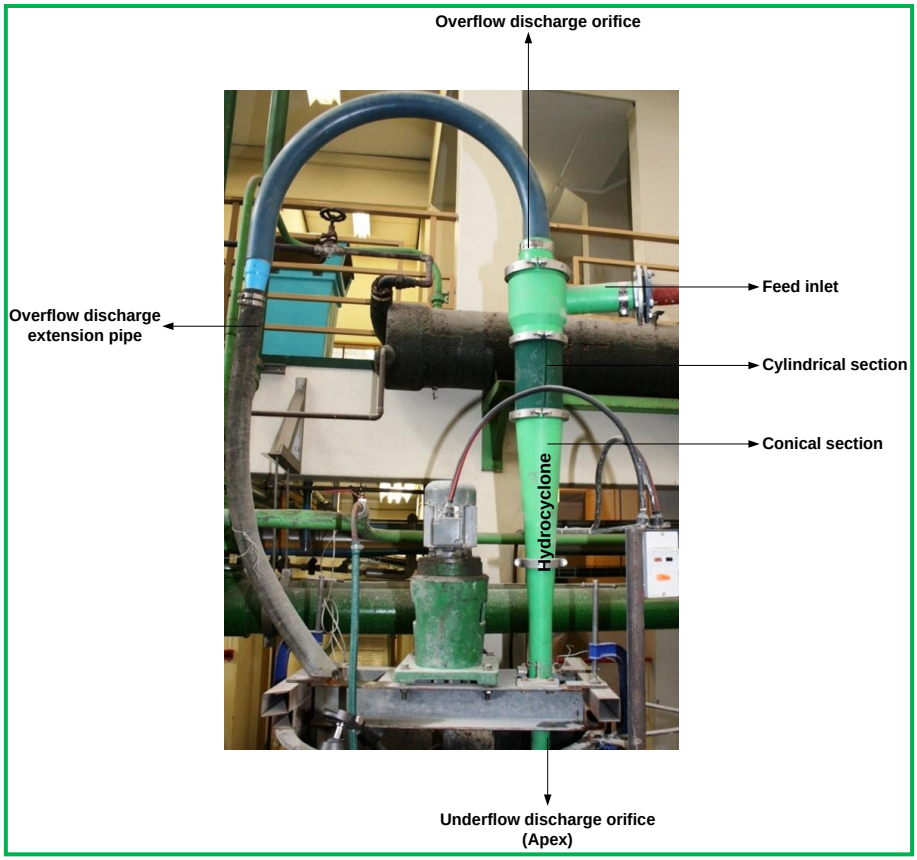

Figure 2-1: A digital image of a laboratory hydrocyclone showing its typical parts

In addition to a widely used and accepted conventional hydrocyclone illustrated above and other (Chu & Luo, 1994) hydrocyclone types, a new type of hydrocyclone referred to as an axial-flow hydrocyclone was made to address the issue of complex hydrocyclone inner flow behavior. This hydrocyclone functions similarly to the conventional one with the exception of

[2] The underflow is also referred to as an apex or spigot

a guided vane that causes a flow to rotate at high speed. Figure 2-2 illustrates the axial flow hydrocyclone as redrawn from Zhen-Bo *et al.* (2011).

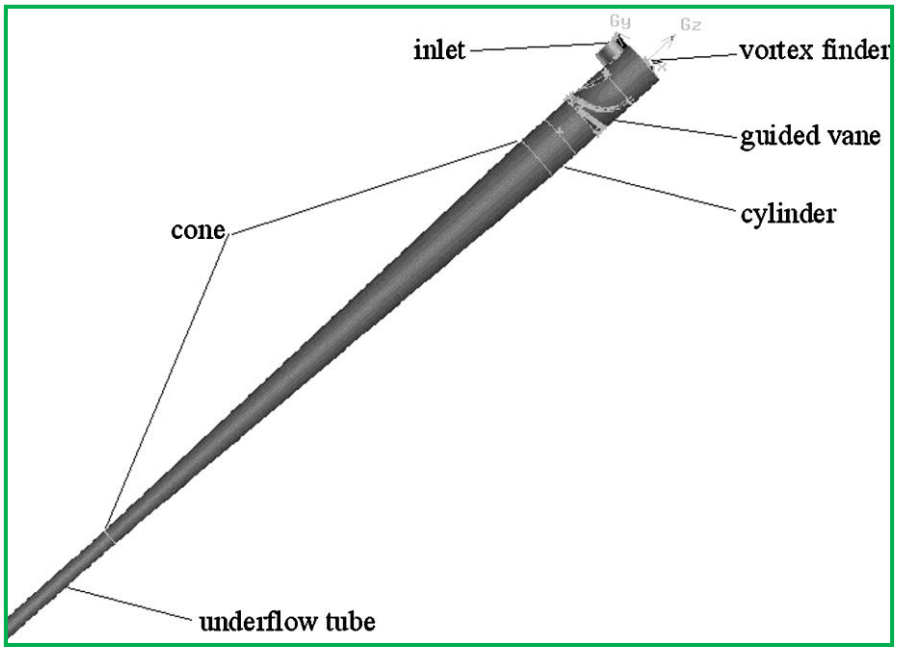

Figure 2-2: Typical structure of axial-flow hydrocyclone (Zhen-bo *et al.*, 2011)

2.3 Hydrocyclone operation and flow structure

There are no internal moving parts in a hydrocyclone. Thus, the centrifugal forces together with the feed flow rate promote the separation of the feed contents inside. The slurry is fed into the cyclone via a feed inlet, entering in a tangential flow that creates a spiral pattern. This flow creates a vortex, by the impact of a vortex finder, that prevents the short-circuiting of feed to the overflow and so achieves separation by size, density and shape (Wills, 1997; Svarovsky, 1984).

Separation of particles in the hydrocyclone is due to the flow pattern which is subjected to two forces; a centrifugal and drag force. The centrifugal force accelerates the particles, allowing them to separate according to different sizes and specific gravity. This force causes the faster settling particles to move outward to the lower velocity walls of the cyclone and eventually leave the hydrocyclone through the underflow orifice. On the contrary, the drag force causes the slower settling particles to move towards the low pressure zone across the cyclone axis (Wills & Napier-Munn, 2005; Bergstrom & Vomhoff, 2007). These particles are then carried upward via the vortex finder and exit the hydrocyclone through the overflow

orifice. Figure 2-3 illustrates the inward and outward forces acting on the particles in the hydrocyclone.

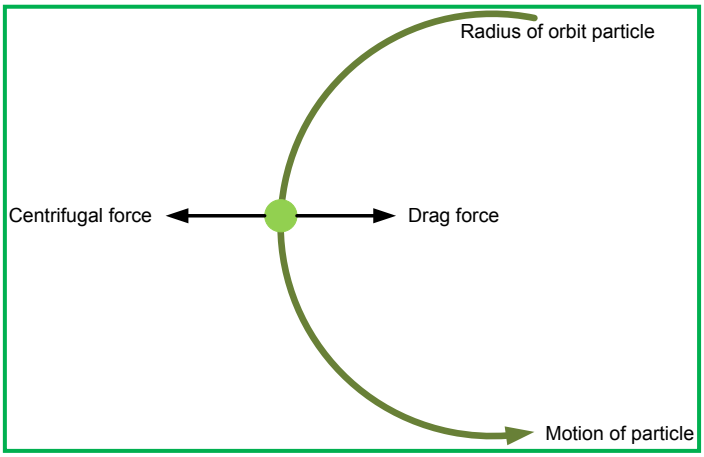

Figure 2-3: Forces acting on orbiting particle in hydrocyclone

An axial air core is another feature of flow structure according to which hydrocyclones operate (Napier-Munn *et al.*, 1996). The air core is formed in the center of the hydrocyclone due to a strong vortex motion of high pressured tangential feed. The air can also be sucked in through the spigot or introduced by bubbles in the feed (Hararah *et al.*, 2010; Neesse & Dueck, 2007a).

2.4 Hydrocyclone separation efficiency

Efficiency of hydrocyclone separation is associated with the type and/or design of hydrocyclone with its related application and how it is operated. Thus, it is not a characteristic of the hydrocyclone itself but a fractional efficiency (Rietema & Verver, 1961). The cyclone efficiency greatly depends on the particle size (Bradley, 1965; Svarovsky, 1984). It is commonly determined by the use of a partition or tromp curve. In a tromp curve, the weight percentage or fraction of each feed particle size is related to the same size fraction passing through an apex (Wills, 2006).

Hydrocyclone separation efficiency can be influenced by the ratio of underflow to throughput and may be improved by increasing the feed throughput and sustaining a steady flow.

2.5 Hydrocyclone operating state characteristics

As can be expected, the underflow characteristics of the hydrocyclone (the underflow width in particular), is influenced by the flow phenomena inside the hydrocyclone. Broadly speaking, a distinction can be made between dilute flow, transition flow and dense flow separation in the apparatus. Typical features that indicate these operating states are the sediment mass stored in the conical part of the hydrocyclone, the formation of the air core and the shape of the underflow discharge (Neesse *et al.*, 1991; Neesse *et al.*, 2004b). In the following subsections the characteristics of each operating state are detailed. Table 2-1 summarises the conditions found in each operating state whereas Figure 2-4 and Figure 2-5 visualise the various operating states, schematically and by digital images.

Table 2-1: Conditions of hydrocyclone operating state characteristics

Dilute Flow Separation	**Dense Flow Separation**	**Transition State (favored Separation)**
Continuous air core	Reduced air core length and oscillates rigorously	High solids recovery and solid content
Underflow discharge spray-shaped	Underflow discharge rope-shaped	
High solid recovery	More solid stored in the cone part-reduce solids recovery	
More fines to the underflow due to low solid concentration in feed		

2.5.1 Dilute state flow

The dilute flow state is the condition with low solids content in the feed. It displays a spray or umbrella-shaped discharge from the underflow. Figure 2-5B illustrates this flow state as viewed from the laboratory device.

In dilute flow separation air is sucked through the spigot to the center of the hydrocyclone forming a continuous air core towards the overflow. Very thin sediment is formed along the walls of the hydrocyclone and this allows for the formation of an extended air core. In addition, high particles content are recovered at the underflow including more fines that would otherwise report to the overflow (Wills, 2006).

2.5.2 Dense flow state

Changing the solids concentration in the hydrocyclone feed stream affects the density and viscosity of the internal slurry, which then alters the pressure drop, cut size and separation efficiency (Maurice *et al*., 2003).

At high feed solids concentration, sediment of solids is stored in the conical region of the hydrocyclone. These solids are partially forced upward to the overflow reducing the solids reporting to the underflow, thus increasing coarse particles recovered to the overflow. This is a negative effect known as the short-circuiting of the particles (Braun & Bohnet, 1990). The discharge size would be similar to that of the apex orifice and assumes rope-shaped flow due to the deposit of solids around the spigot (Neesse *et al.*, 1991). Figure 2-5C illustrates this flow state.

As the hydrocyclone continues to operate at dense flow, the air can no longer pass through the underflow. This causes the instability of the air core and/or eventually terminates it. When the air core is terminated, it has an undesirable effect on the separation efficiency because the solid particles short-circuit through the overflow. The extension of this operation can lead to system blockage. Dense flow state can be used to monitor the hydrocyclone operation as it indicates a problematic state.

2.5.3 Transition flow state

The transition flow state (Figure 2-5A) rapidly changes between rope and spray flow states and is thus described as a combined discharge. The air core keeps oscillating due to the sediment residue in the hydrocyclone; however it is at a favourable rate. The monitoring of this state is of interest since the separation effects during this operation state are desired. These include the advantages of high solid content in the underflow as well as high solids recovery.

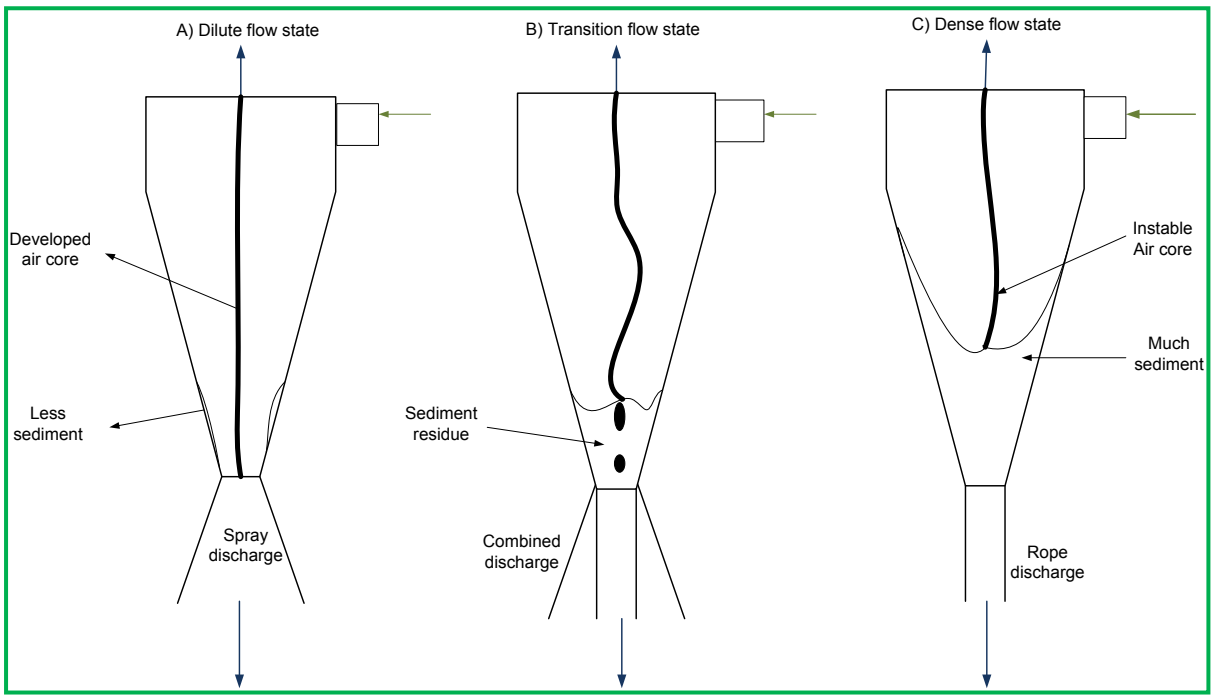

Figure 2-4: Schematic diagram of the operating states of the hydrocyclone (redrawn from Neesse et al. 2004)

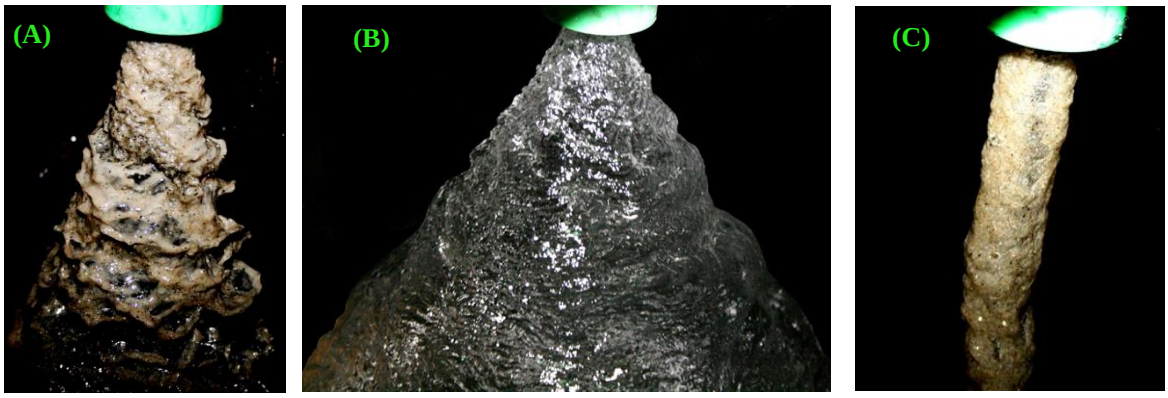

Figure 2-5: Underflow images showing the operating states, (A) combined or transition (B) spray-shaped & (C) rope-shaped discharges

Chapter Summary

The hydrocyclone is a classifying device that uses centrifugal forces to separate particles depending on dimension, shape and density. The centrifugal force causes the air core to be

formed at the centre of the hydrocyclone further complicating the flow within the cyclone and thus making it difficult to control its parameters. The performance of a hydrocyclone is strongly affected by design and operating variables. Operating variables include the fluid and particle properties, inlet pressure and flow rate, and the solid concentration of the feed. With these operating variables, the hydrocyclone may operate in either a dilute flow state, transition or dense flow state. Of these three, the transition state is desired whereas the dense flow state is seen as troublesome and should be avoided.

Chapter 3: Hydrocyclone Online Monitoring

Previous chapters highlighted the essential need for hydrocyclone monitoring and control. This chapter discusses some of the monitoring techniques studied. The methodology, utility, viability, application as well as the measured components of each technique are presented.

3.1 The importance of online monitoring

The condition of the hydrocyclone underflow discharge can be used as a visual indication of hydrocyclone operation. This can then be used heuristically to indicate the operating states. However, this is not a reliable monitoring method as a specific underflow discharge condition may be judged as different operating states by different people based on their individual observations. Therefore, it is necessary to automate the monitoring of plant equipment.

Online monitoring is one of the growing techniques in industry due to its effectiveness in measuring and giving current operation status information. Hydrocyclone online monitoring is one of the methods used to apply automated control in processes (Petersen, 1998). It is used to monitor cyclone operation in order to sustain the optimum conditions. A hydrocyclone is at its optimum level when it attains a minimum amount of fines going to the underflow while maximising the underflow solids recovery (Neesse *et al.*, 2004a).

The underflow is found to be the only externally visible feature of the hydrocyclone that can be measured (Petersen, 1998). Underflow discharge features are some of the best parameters used to monitor hydrocyclone operation conditions due to their relation to the internal flow of the hydrocyclone. They indicate the operation state of the cyclone (Gutiérrez *et al.*, 2000; Janse van Vuuren, 2011; Neesse *et al.*, 2004b; Petersen *et al.*, 1996; van Deventer *et al.*, 2003; Williams *et al.*, 1999). In addition, spray profile measurements can be used to determine the underflow rate and be related to hydrocyclone performance (van Deventer *et al.*, 2003).

3.2 Monitoring techniques

Multiple studies involving hydrocyclone sensor monitoring techniques have been conducted. These studies showed that monitoring of the cyclone states needs correct measurements to

obtain successful observations (Petersen *et al.*, 1996; Svarovsky, 1984; Neesse *et al.*, 2004a). For a technique to be judged as a good monitoring technique, the following requirements should be met (Neesse *et al.*, 2004b):

- Sensitivity
- Non-invasiveness
- Online sensing with sampling time less than 1 second
- Robustness
- Cost-effectiveness

In addition to the above mentioned requirements, a technique should be free of hazards from high energy radiation as well as capable of making rapid measurements in fast moving, dense slurries/powders (Williams *et al.*, 1992). Monitoring techniques should also require less maintenance and little modifications to the current set-ups (Janse van Vuuren, 2011).

Sensor techniques used to monitor hydrocyclones are applied to measure various operating conditions (Galvin & Smitham, 1994; Gutiérrez *et al.*, 2000; Hou *et al.*, 1998; Williams *et al.*, 1999). The following subsections summarise some of these studied techniques. Table 3-1 outlines these techniques with their respective sources and measured components. This table also provides the method sampling frequencies as well as some comments on the method application.

Table 3-1: Hydrocyclone monitoring techniques in summary

Monitoring technique used	Reference	Measured element	Sampling frequency	Comments
Mechanical detector	Hulbert, 1993	• Underflow discharge angle	-	• Exposed to mechanical wear • Frequent replacement required
Gravimetric method (Load cell)	Neesse et al., 2004	• Hydrocyclone weight (Mass of solids content)	-	• Gives direct & rapid determination of operating state • However, not recommended - signals superimposed due to flexible connections
Tomographic monitoring				
X-Ray	Galvin & Smitham, 1995	• Solids distribution within hydrocyclone	20 seconds exposure time	• Non-intrusive but procedure needs refinement and has • Too long exposure time
Ultrasound	Schlaberg et al., 2000	• Air core position and size	-	• Method implementation too complex • Sensor number limited to transducers & hydrocyclone size
Electrical Impedance Tomography	Williams et al., 1997 Gutiérrez et al., 2000	• Air core size and shape • Solids distribution within hydrocyclone	500 frames/sec	• Short sampling time • Good for on-line control, e.g. fault detection • Underflow discharge to maximize throughput
Electrical Resistance Tomography	Williams et al., 1999 Williams et al., 1999 Dyakowski & Williams, 1996 West at al., 2000	• Air core size, location and shape • Solids concentration within hydrocyclone	100-200 frames/sec	• Can successfully be applied and operated • Good for fault,& spigot wear detection • However, can be intrusive
Electrical Capacitance Tomography	Williams et al., 1995	• Underflow discharge shape	100 frames/sec	• Safe, rapid & low cost • Preferential for controlled cyclone series • High speed image
Acoustic monitoring	Williams et al., 1996 Hou et al., 1998 Hou et al., 2002 Neesse et al., 2004	• Feed pressure • Feed solids concentration • Underflow discharge oscillation	~2000 readings/sec	• Simple, effective, low cost, non-intrusive & non-invasive • Promising control & optimization for cyclone performance • However, not good for oscillation measurement
Ultrasound monitoring	Olson & Waterman., 2006	• Underflow discharge oscillation	-	• Effective method • Detects fault conditions of the hydrocyclone
Image analysis monitoring				
Videography	Petersen et al., 1996 Petersen, 1998 Castro et al., 1996 Janse van Vuuren, 2011	• Underflow discharge spray angle • Air core diameter • Underflow discharge width	~ 30 frames/sec	• Practical monitoring method • Good for on-line process control
Laser-optical	Neesse et al., 2004	• Underflow discharge shape	-	• An indirect non-intrusive method • Gives clear difference of discharge shapes
Digital processing	Krishna et al., 2010	• Air core diameter	-	• A robust, practical and non-intrusive method

3.2.1 Tomographic monitoring technique

"Tomographic techniques produce cross-sectional 'slice images' depicting the spatial variation in a physical parameter based on sets of boundary measurements" (Tapp *et al.*, 2003). They are advantageous in that, they non-invasively provide information from within the complex structure of a device (Dyakowski *et al.*, 2000). The following sections shortly present some of the tomographic techniques used in hydrocyclone monitoring.

i. X-ray monitoring

X-ray tomography, a non-intrusive radiographic technique was employed to determine magnetite-particles' concentration distribution in a dense medium cyclone (Galvin & Smitham, 1994). In this study, magnetite was used as a high density medium. The dense medium cyclone operates with manipulated densities by adding a medium to the feed (Janse van Vuuren, 2011).

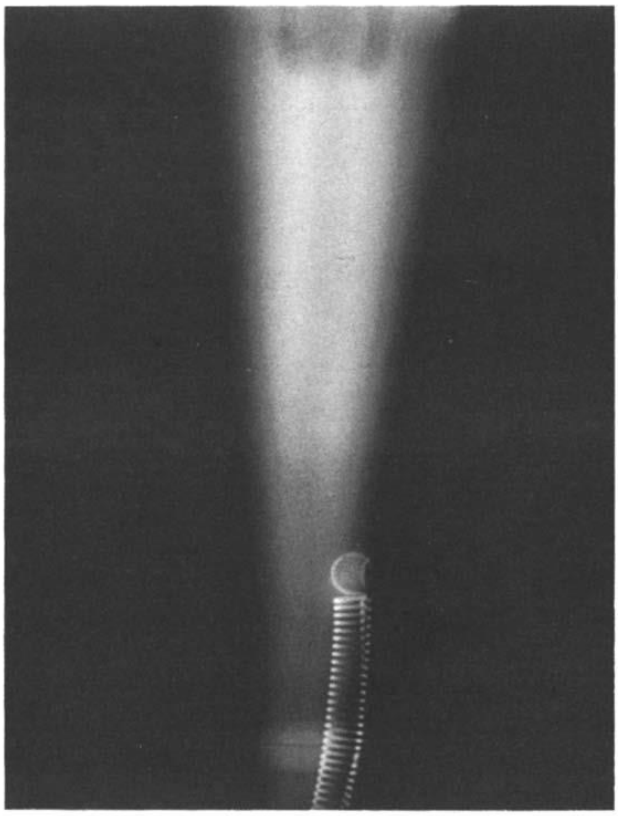

Figure 3-1: X-ray photograph of magnetite slurry with specific gravity of 1.6 (Galvin and Smitham, 1994), permission of reuse granted by Elsevier.

Galvin & Smitham (1994) highlighted some advantages of understanding the concentration distribution of operating cyclones. This includes its usefulness in device design and operating improvement, and it provides the ability to validate more complex CFD simulations. X-ray images of the cyclone were recorded at different feed density values. The set-up of Galvin & Smitham (1994) used an X-ray plate that was fastened behind the cyclone with a source focal distance of 750 mm from the cyclone. The images obtained were analyzed with a Quantimet Image Analyzer in order to determine the particle density across the cyclone diameter at three different locations. Figure 3-1 shows an X-ray image of a 30 mm diameter glass hydrocyclone.

Although the particle distribution was observed, the technique still requires some improvements because it focused only on magnetite particles. So, other components need to be tested as well. It further requires a long exposure time of 20s sampling time. The calibration method and signal-to-noise ratio also need improvement.

ii. Electrical impedance tomography

Electrical impedance tomography (EIT) is a technique that can measure hydrocyclone internal flow dynamics without being affected by the nature of the process environment (Gutiérrez *et al.*, 2000; Williams *et al.*, 1997). These authors used this method to measure the air core size and the solids concentration in the hydrocyclone, incorporating operating states monitoring as well.

The experimental set-up involved 16 plate electrodes externally attached to the outside of the hydrocyclone body in a single horizontal plane close to the feed inlet. Figure 3-2 illustrates the electrode location on the hydrocyclone. Images of the underflow discharge were captured to monitor the hydrocyclone operating states, hence correlating them to the EIT results.

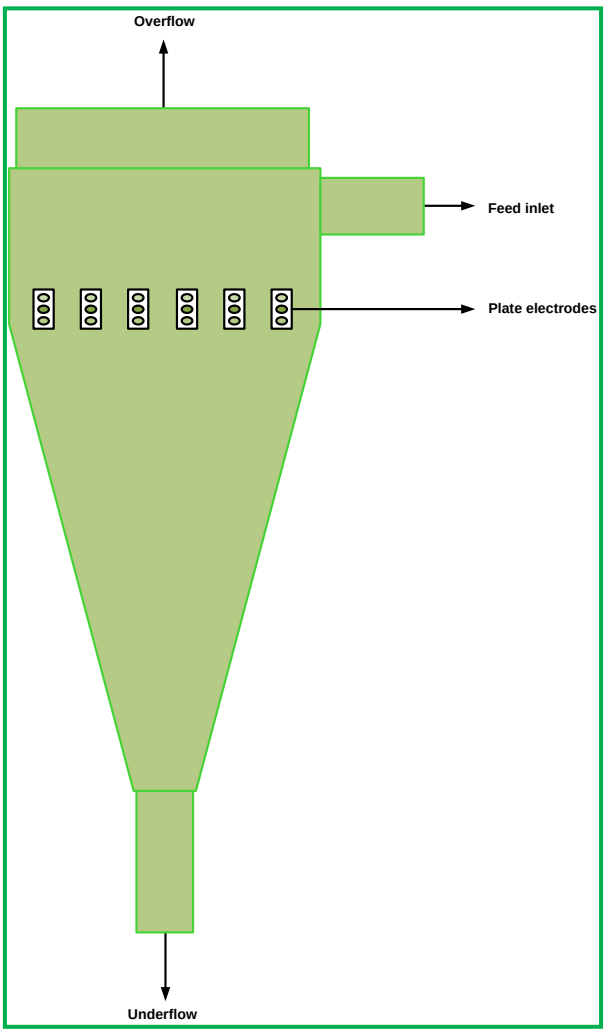

Figure 3-2: Location of the electrode plane on the hydrocyclone
(redrawn from Gutiérrez *et al*., 2000)

The results showed the expected outcomes (detailed in authors cited by Williams *et al*., 1995b) that the air core decreases with an increase in solids concentration. In terms of the operating states, it was observed that the air core size is related to the underflow discharge types. The spray discharge indicates the existence of the air core whereas the rope discharge shows the disappearance of the air core.

These observations thus suggest the viability of the EIT technique in hydrocyclone state monitoring. The EIT technique is non-intrusive and fast (taking measurements at a rate of one frame per 2 milliseconds). It is thus found to be suitable for fault detection and could be used in computer fluid dynamics (CFD) simulations making it fit for online control.

iii. Electrical resistance tomography

Electrical resistance tomography (ERT) is used for the electrical conductivity reconstruction of the internal part of a device and like other tomographic techniques; it is well suited to the monitoring of complex flow structures (Dyakowski *et al.*, 2000; West *et al.*, 2000; Williams *et al.*, 1995b; Williams *et al.*, 1999).

The above cited authors did a study using the ERT method to monitor the air core characteristics within a hydrocyclone. The experimental set-up was comprised of ERT sensors in 8 planes of 16 disc-shaped electrodes each (a single plane was used in the study of Williams et al., 1995). These experiments were performed in both laboratory and industrial hydrocyclones. The eight planes of disc shaped electrodes were fabricated into a resin mould, which Figure 3-3 (A) illustrates.

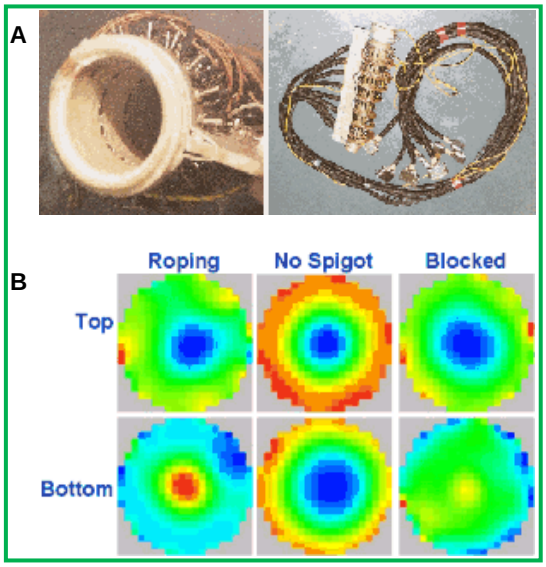

Figure 3-3: Illustrations of A- the sensor electrodes and B-the ERT images (reused from Willians *et al.*, 1995 with permission from Elsevier)

The findings of this technique showed that the technique was able to identify the conductivity distribution of the three different fault conditions. The fault conditions were set as roping discharge, spigot detachment and underflow blockage, refer to Figure 3-3 (B) for images.

Furthermore, these studies revealed that the ERT technique can be used to provide online information of the respective parameters. Like EIT, it is good for fault and spigot wear detection and can be successfully applied to the process. The ERT method is however intrusive as modification to the current device could be required depending on the installation

procedure of the technique. In regard to the air core measurements, results revealed that its values may be overestimated at times when the air core is at the center of the hydrocyclone.

iv. Electrical capacitance tomography

A brief discussion of electrical capacitance tomography (ECT) is given in Williams *et al.* (1995a) in which the performance of a dewatering hydrocyclone was measured by imaging the underflow discharge. In this experiment, a 12-electrode capacitance sensor was installed at two vertical planes in the underflow section. Figure 3-4 shows the planes, A-A and B-B.

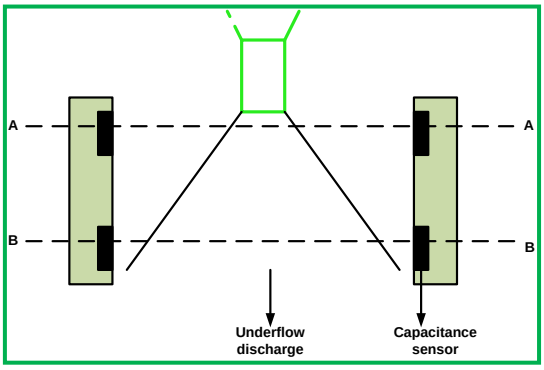

Figure 3-4: Electrical capacitance sensor mounted to hydrocyclone underflow (redrawn from (Williams *et al.*, 1995a))

The results were recorded as discharge profiles between the two electrodes of different sizes and shapes. From these profiles it was observed that it is possible to quantify the oscillation of the spray due to the high speed sampling rate of approximately 100 frames per second.

The ECT technique is shown to be portable, and suitable for harsh and realistic operating conditions (Williams *et al.*, 1995a). In addition to these advantages, the device can be used to detect problematic hydrocyclone conditions like underflow blockage. It is safe and has low cost which has made it the most used technique in hydrocyclone series monitoring. However, it requires further improvement in the area of background noise (Neesse *et al.*, 2004b).

v. Ultrasound tomography

An ultrasound tomography technique was employed by Schlaberg *et al.* (2000) and West *et al.* (2000) to monitor the air core formation, its size and location within the hydrocyclone. This was done by modifying the hydrocyclone and by fitting a ring of 16 ultrasonic transducers on its exterior top part. Figure 3-5 illustrates this set-up.

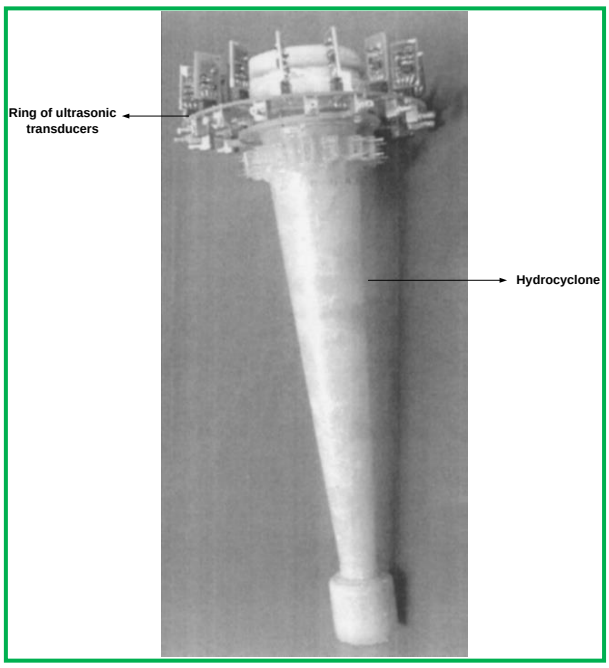

Figure 3-5: Modified hydrocyclone with attached ring of 16 ultrasonic transducers (reused from Williams *et al*., (1995) with permission from Elsevier)

The images obtained were of 50 X 50 pixels resolution and taken at the rate of six frames per second. From these images it was observed that the size and location of the air core can be ascertained.

The ultrasound tomography technique was shown to be a better monitor of the air core in harsh conditions in comparison to optical techniques. It is robust and can be improved by increasing the number of transducers used, depending on the size of the transducers and the hydrocyclone. The method was however found to be too complex for use in industrial operations.

3.2.2 Mechanical detector

The mechanical detector is a mechanical device that measures the shape of the hydrocyclone underflow discharge (Hulbert, 1993). Hulbert (1993) invented and patented this method in which a hydrocyclone was modified by mounting a pivoting arm near the apex. The pivoting arm was protected from rough discharges by an attached abrasion resistant tip. In addition, an angle detector was used to measure the angle of the attached tip that in turn indicates the angle of the underflow discharge. An experiment where this method was used was performed on an industrial milling circuit hydrocyclone.

The mechanical detection technique is one of the least studied methods of the hydrocyclone monitoring techniques outlined in this study. This could be due to its set-up that exposes it to extensive mechanical wear caused by its contact with the running discharges of the underflow (Hulbert, 2010 cited in Janse van Vuuren, 2011).

3.2.3 Gravimetric method

Accumulation of solids in a hydrocyclone depends on the amount of solid in the feed as well as the feed solids size distribution. The gravimetric method was studied by Neesse *et al.* (2004b) to determine the amount of solids accumulated inside the hydrocyclone. This set-up involved the installation of a load cell with the hydrocyclone attached to a feed distributor, and flexible connections used at the feed inlet and vortex finder. Figure 3-6 illustrates this.

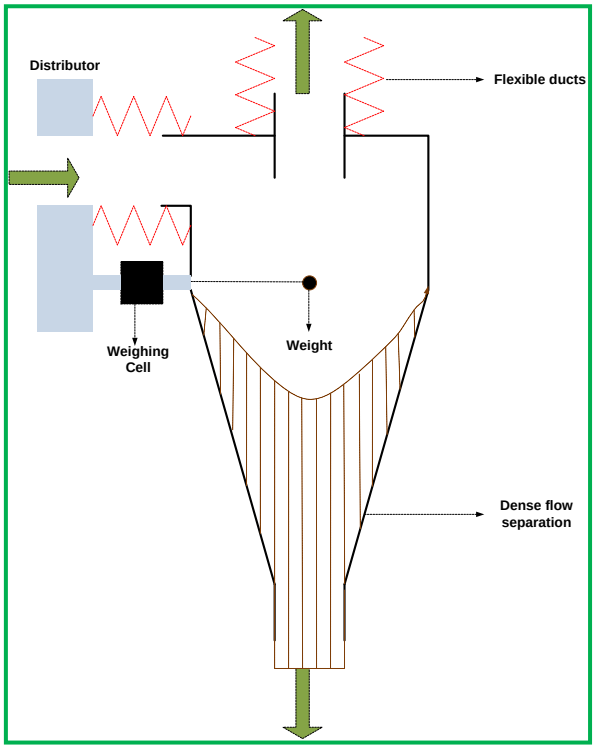

Figure 3-6: Hydrocyclone weight determination by using a weighing cell (redrawn from Neesse *et al.*, 2004b)

The gravimetric method provides a direct and fast determination of the operating state of the cyclone and it indicates the dependency of hydrocyclone weight on feed solids concentration. Despite the mentioned conclusions, this method still needs to be modified due to the problem

of signals being superimposed by disturbances caused by flexible connections. This problem can however be addressed by special computer software.

3.2.4 Acoustic monitoring

i. Acoustic emission monitoring to hydrocyclone conical section

Operating hydrocyclones vibrate, causing the flow structure inside the hydrocyclone to be more turbulent. This may be due to the eccentrical and unstable movement of the air core and discharged rope in dense flow separation, the impact of particles and the highly turbulent vortex motion inside the cyclone (Janse van Vuuren, 2011; Neesse & Dueck, 2007b; Neesse *et al.*, 2004b; Sripriya *et al.*, 2007).

A study by Hou *et al*. (2002) was done where a PC-based acoustic signal processing system was used to monitor hydrocyclone performance and feed properties. A similar study was also previously carried out by Hou *et al*. (1998). In their work, a single 190 KHz piezoelectric passive acoustic sensor was used to monitor fine silica slurries in a cyclone. This sensor was attached to the outside of the conical part of a 125 mm diameter hydrocyclone in a circulating circuit. The data was acquisitioned and processed in a 12-bit system equivalent to digital conversion card, comprised of a Pentium 133 MHz PC and signal processing and control software.

Results showed that various operating parameters respond differently, emitting distinctive acoustic signals. It further indicated that the acoustic technique can successfully be used for hydrocyclone fault detection, routine online performance monitoring and performance optimisation. This was determined based on a laboratory case study and the quantification of the relationships between different hydrocyclone operating parameters. The acoustic signal data was analysed by using multivariate statistical analysis techniques.

ii. Acoustic emission monitoring of hydrocyclone underflow discharge

Another study using acoustic emission monitoring was done by Neesse *et al*. (2004b) where the sensor attached to the outside of the hydrocyclone near the spigot was used to determine the underflow discharge shapes by measuring the hydrocyclone oscillation. The results obtained indicated that a rope-shaped discharge can be categorized as high amplitudes in low

frequency and are damped at higher frequencies. In contrast, spray-shaped discharges show vibrations at higher frequencies (100 – 600 Hz).

Major operating states could be identified from the acoustic spectrum. However, further research is required to better understand the acoustic signal emitted by the device. This research would include the installation of a robust set-up.

The acoustic emission sensor (AES) was found to be a non-intrusive, non-invasive, simple, operative, and low cost technique that can be used for online monitoring of hydrocyclone efficiency (Hou *et al.*, 2002). In addition, it is fast with the ability to take about 2000 readings per second. Therefore the AES technique seems practical and is a promising technique for hydrocyclone performance optimisation and control. However, this method still requires more investigation before it can be considered for industrial use.

3.2.5 Ultrasound monitoring

The ultrasound hydrocyclone monitoring technique is a newly studied method done and patented by Olson & Waterman (2006). In this study, "the ultrasonic sensor with a peak frequency response at approximately 40 kHz" (Olson & Waterman, 2006) was used. The sensor was attached to the splash skirt that was then fitted on the spigot of a hydrocyclone. This technique aimed to measure the shape of the underflow for the detection of roping conditions in the device.

The results obtained indicated that the operating states could be identified via a vibration monitor (Janse van Vuuren, 2011). Vibration amount was observed to reduce with a decrease in the size of the underflow discharge. Therefore ultrasound monitoring could be used as a control measure for hydrocyclone operating conditions.

3.2.6 Image analysis monitoring

Image analysis is mostly done by studying the pixel values of images, either as whole images or in fragments. The most used method is looking into statistics like mean, maximum and minimum pixel values. Eigenvalue decomposition methods like Principal Component Analysis (PCA) and texture analysis are also useful (Tapp *et al.*, 2003; Daniel, 2011).

The following sections outline some of the image analysis methods previously used to monitor the hydrocyclones.

i. Image analysis of the air core

A videography image analysis was employed to measure the hydrocyclone air core diameter in a pilot plant (Castro *et al.*, 1996). This involved the cyclone modification whereby the device was cut open at the top to fit in a light for air core visibility.

The outcome showed that using video to monitor the air core can be possible as the air core was clearly visible in the images obtained. By incorporating air core diameter; a semi-empirical model was set-up for the pilot plant.

ii. Image analysis of hydrocyclone underflow angle

The underflow discharge is an externally visible parameter that can be measured to monitor hydrocyclone operations and its angle can be used as control for the hydrocyclone operation conditions (Petersen *et al.*, 1996). This technique has been employed by the cited author where videographic image analysis was used to monitor the underflow discharge angle. The discharge angle can in turn be used for hydrocyclone feed condition monitoring.

The set-up of this study involved the digitisation of video images using a VHSC (Video Home System Camcorder) video camera. Images were processed on a personal computer (PC) installed with a frame grabber. The video camera was directed to the underflow at about 50 cm away to eliminate discharge splashes on the camera lens. Figure 3-7 illustrates the principle of imaging the hydrocyclone underflow as indicated by Petersen *et al*. (1996). The experiments were done in laboratory and industrial hydrocyclones.

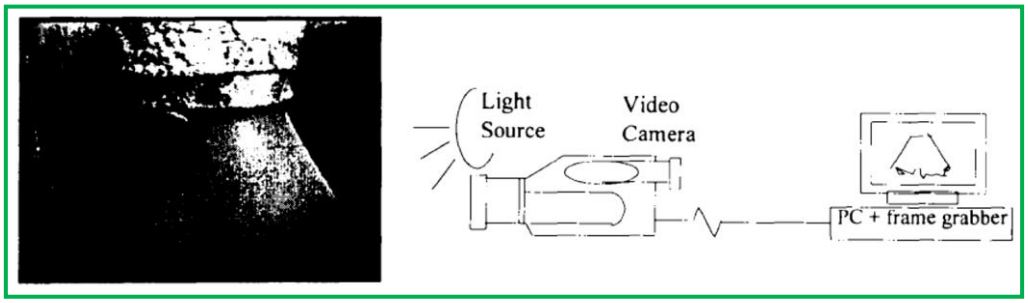

Figure 3-7: Illustration of hydrocyclone underflow videographic imaging (permission of use granted by Elsevier)

Van Deventer *et al*. (2003) did a follow-up study and combined the spray measurements with empirical and theoretical modelling to develop a soft sensor that could be used for the process parameter predictions.

The observations of this study showed that the spray angle profile can be used as an indicating tool for the operating parameters (flow rate, inlet pressure and particle cut size) of the hydrocyclone. It was further suggested that this technique can successfully be employed as the hydrocyclone online controller, proposing the possibility of a machine vision system at large as a viable online controller.

Although this technique was shown to be robust and viable for industrial process monitoring purposes, the author mentioned that it was computationally limited at the time of the study. Hence, the images were discretely analysed instead of using continuous data analysis.

iii. Image analysis of the discharge shape - Optical detection

In the work of Neesse *et al*. (2004b), a laser-optical device was used to obtain images of the discharge shapes of the hydrocyclone underflow. A two-dimensional laser beam was directed towards the underflow and the reflection of the beam recorded with a Charged Coupled Device (CCD) camera. Figure 3-8 illustrates this. The analysis of data was done with PC-supported pattern recognition.

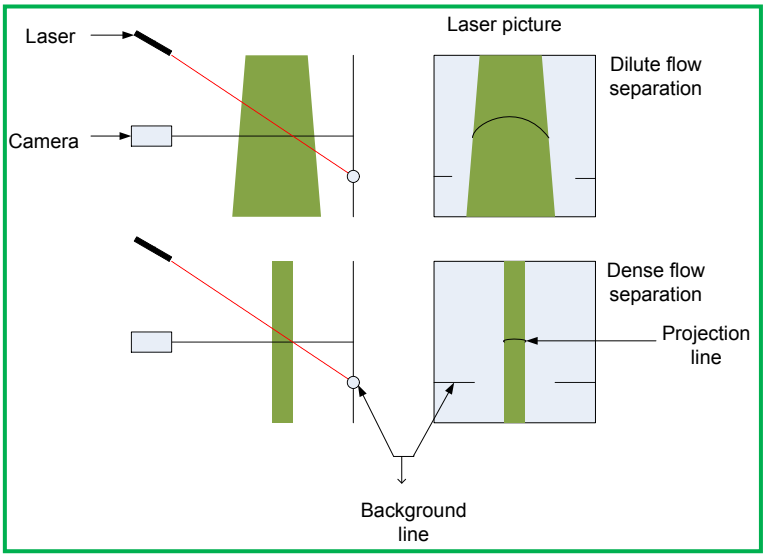

Figure 3-8: Laser optical detection monitoring set-up (redrawn from Neesse *et al*., 2004b)

The results showed that different laser segment lengths and background line distances indicated the discharge shapes as shown in Figure 3-8, making it possible for the dilute and dense flow separations to be identified.

Furthermore, advantages of this method were highlighted as being an indirect and non-invasive method, having the necessary hardware well formulated, being cost effective and being useful for rough operating conditions. It is therefore suggested that the laser-optical technique can be used as a remote sensing monitoring technique to address harsh condition operations.

iv. Image analysis based on digital processing technique

Krishna *et al*. (2010) did some recent work on image analysis (the digital signal sensor technique) in which a data acquisition card was used to identify and predict the hydrocyclone air core diameter from the online actual data.

A transparent Perspex hydrocyclone with a cylindro-conical structure was used for the experiment. To the conical section of the hydrocyclone, a central solid rod was inserted to eliminate the formation of the air core. Digital images of the formed air core were collected. This was made possible by the transparency of the hydrocyclone as shown in Figure 3-10. These images were processed in 'ImageJ' image processing software. The set-up includes a computer equipped with the National Instruments' data acquisition card that collects the live data from the pressure transmitter (a new type of online sensor). The pressure transmitter was connected to the overflow pipe, underflow pipe and central part of the hydrocyclone respectively, and it continuously measured the pressure.

Furthermore, the data collected was processed in MATLAB software to determine the formation of the air core within the hydrocyclone and to calculate the air core diameter. The illustration in Figure 3-9 shows a schematic diagram of the connection system of the data acquisition card as shown by Krishna *et al*. (2010). During data collection, the noise data was picked up and this was corrected by using the noise-average elimination method by smoothing the signals using an 'Immediate Trigger'.

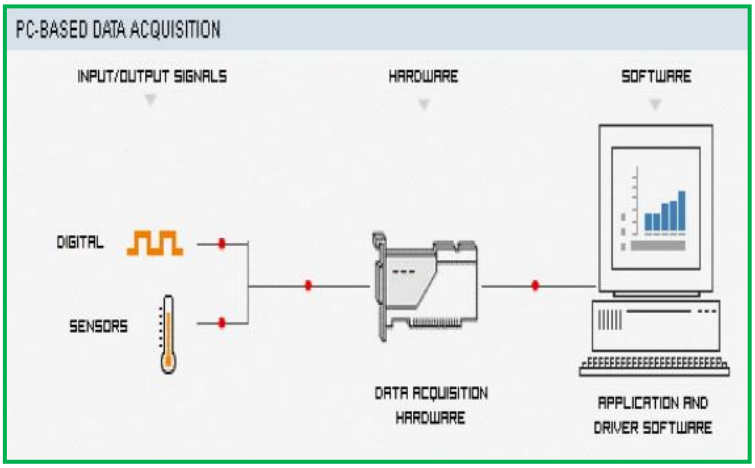

Figure 3-9: Illustration of online data collection via data acquisition card (Krishna *et al.*, 2010)

The results showed that the air core can be accurately identified and predicted using this technique. Figure 3-10 shows the well-developed air core as can be seen through the transparent hydrocyclone. An alarm that indicates the formation of the air core during the hydrocyclone operation was also developed in the MATLAB code. The pressure was found to vary at different hydrocyclone positions with the pressure measured at the center being the highest and that from the overflow being the least. It was stated that since some of the hydrocyclones might not have a spigot, the connection of the sensor to the overflow can then be considered.

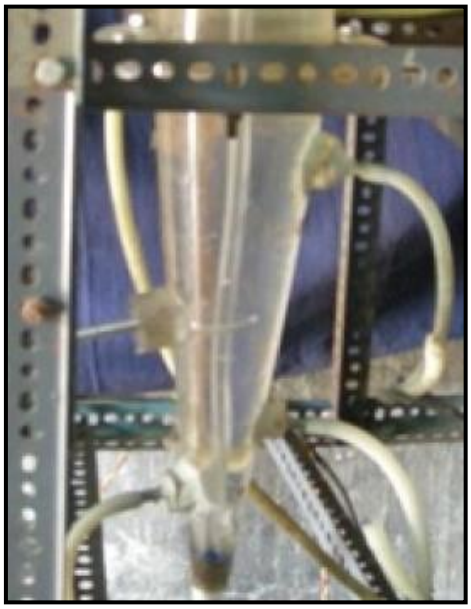

Figure 3-10: Transparent hydrocyclone showing a stable air core.
(Permission of re-use granted by Elsevier)

The predicted values of the air core diameter were in agreement with the experimental results. Therefore, it was suggested that this technique could be used in many mining and mineral processes as it was confirmed to be robust, practical and non-intrusive.

v. Image analysis of the underflow width

Another recent image analysis study conducted is that of Janse van Vuuren *et al*. (2011) that was an extension of the work of Petersen *et al*. (1996) and van Deventer *et al*. (2003). It was performed on a pilot plant hydrocyclone using a video camera to record the underflow discharge. This investigation focused on detecting the hydrocyclone operating conditions by monitoring the shapes of the underflow to infer the underflow width. The underflow width was determined from a horizontal line sliced across an image as shown in Figure 3-11.

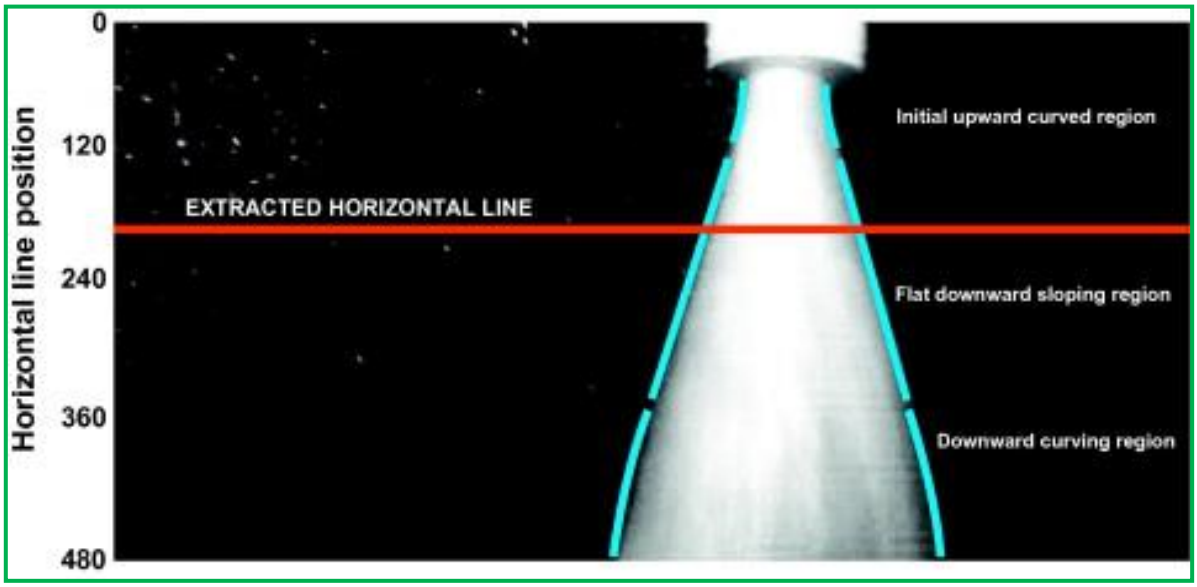

Figure 3-11: Illustration of the holizontal line used to determine the underflow width (Janse van Vuuren *et al.*, 2011)

The set-up of this experiment was similar to the set-up described in this thesis as the same unit was used (refer to section 4.2). The differences between the two set-ups were the additional light source and a video camera that was attached to the side of the mixing tank in the work of Janse van Vuuren *et al*. (2011).

The results showed that underflow width from videographic images could be used to identify different hydrocyclone operating conditions. Although some problems can arise in regard to the foreground noise, the technique proved to successfully address the issue of background and random noise, as well as system vibration. This could be done by performing image

enhancement and motion threshold. The observations further indicated that the technique can practically be applied in industrial processes as it is able to meet the requirements stipulated on page 168, with 30 frames per second sampling rate.

Further work is currently being done to study the possibility of this technique being used for measureable estimation of hydrocyclone performance. This includes the work described in this thesis which aims to further confirm the technique's viability and robustness.

3.3 Evaluation of monitoring techniques

A summary of the above mentioned monitoring techniques is presented here and Table 3-2 displays tabulated notes, highlighting the advantages and disadvantages of each specific technique as well as its practicability in industries.

Table 3-2: Hydrocyclone monitoring techniques evaluation

Monitoring technique	Comments		Use in industry	
	Advantages of the technique	Disadvantages of the technique	Practical	Limited
Mechanical detector		• Exposed to wear due to contact with underflow • Hydrocyclone modification required		X
Gravimetric method		• Method requires further investigation		X
Tomographic monitoring	• Advantageous in complex structures	• Complex installation for industrial use		
X-Ray	• Non-intrusive	• Limited study done • Long sampling time • Method needs further improvement		
Ultrasound	• Good in harsh operating environment	• Hydrocyclone modification required		
Electrical Impedance Tomography	• Not sensitive to process environment nature • Viable, fast and non-intrusive • Can be used as fault detector and in CFD simulations			X
Electrical Resistance Tomography	• Provides essential on-line information • Can be used as fault detector • Can successfully be applied	• Can be intrusive		
Electrical Capacitance Tomography	• Good in harsh operating environment • Can be used as fault detector • Portable, safe and cost effective	• Background noise recorded		
Acoustic monitoring	• Good fault detector and routine on-line performance monitor • Good for performance optimization • Non-intrusive, non-invasive, simple setup & effective method • Cost effective	• Further investigation required		X
Ultrasound monitoring	• Simple setup & data interpretation method • Fast sampling rate • Practicable method		X	
Image analysis monitoring	Robust, industrial suitable, non intrusive, economical			
Videography	• Viable, robust, • Can be used as on-line controller • Fast sampling rate	• Hydrocyclone modification required for air core monitoring	X	
Laser-optical	• Non-invasive and cost effective			
Digital processing	• Robust, practical and non-intrusive			

Though a mechanical detector could successfully identify the underflow shapes, its use in industry is limited by the extensive mechanical wear that is caused by its contact with the underflow discharge. Likewise, the gravimetric method's practicability in industrial use is limited since this technique still requires modification to minimise the disturbances caused by the flexible connections.

Tomographic techniques have many advantages as good monitoring techniques and meet most of the requirements as stipulated on page 16, with the exception of X-ray tomography that requires a lengthy exposure time. In regard to the operating states, West *et al*. (2000) have pointed out the complexity of setting up the tomographic monitoring methods in industrial hydrocyclones that decreases their application in industrial processes.

Although the acoustic monitoring techniques were found to be effective for hydrocyclone optimisation and control, they also need further investigation prior to their application in industry. Hence, they still remain experimental and the "expertise knowledge on the correct placement of the sensor determines the techniques' robustness" (Janse van Vuuren, 2011).

The ultrasound monitoring technique on the other hand seems viable. Although the splash skirt used in the experimental set-up explained in section 3.2.5 may be exposed to the underflow discharge, the sensor is effective and can be a good indicator of the faulty conditions in a process. The arrangement of this technique allows for simple data interpretation and set-up.

Image analysis in regard to air core determination is seen as ineffective as major modification to the hydrocyclone is required. However, the underflow discharge image analysis is identified as a potential technique for operating conditions monitoring. From the previous studies (Petersen *et al*., 1996, Neesse *et al*., 2004 and Janse van Vuuren *et al*., 2011) on the monitoring of hydrocyclone operating states by image analysis, practical monitoring systems were developed whereby these states could be successfully identified.

The ultrasound monitoring and image analysis techniques were identified as potential hydrocyclone monitoring techniques due to their insensitivity to harsh conditions and usefulness in fault detection. However, image analysis is given preference above the ultrasound monitoring technique as it assists in the visible observation of the underflow discharges. Image analysis is also advantageous in that a wide range of data sets can be

extracted because of the possibility of obtaining the whole image as an output (Janse van Vuuren, 2011).

From the above mentioned evaluation, the image analysis monitoring technique was proposed as the monitoring system to be used in the work of this thesis. Digital images were used to study the underflow particle sizes as a basis of underflow discharge monitoring, extending on the work done by Janse van Vuuren (2011).

Chapter Summary

Hydrocyclone monitoring provides real-time information that could be useful in the implementation of device control measures. This however requires that the monitoring techniques meet the requirements for better monitoring as outlined by Neesse *et al*. These requirements include that a technique should be sensitive, easy to use, non-invasive, cost effective, with a sampling time of less than 1 second, robust and accompanied by little modification to the current set-up. Most of the monitoring techniques were found to be somewhat unsuited to practical use as the past studies indicated that they do not meet the above requirements. Of the monitoring techniques evaluated in this chapter, the ultrasound monitoring technique and image analysis of the underflow discharge, were identified as those that could be of practical use in the harsh conditions of hydrocyclone operations. However, image analysis is given preference over the ultrasound technique due to its ability to visually observe the underflow and interpret these observations through analysis of the obtained image data. In this light, image analysis was proposed as a technique to be used in the work reported in this thesis to determine the underflow particle sizes.

Chapter 4: Experimental Methodology

To achieve the objective of this research project, experimental work was done as mentioned in chapter 1. This chapter describes the procedures followed as part of the experimental work. It includes safety & health aspects concerning the experiments that were carried out, the set-up of the laboratory equipment and plant-hydrocyclones, as well as the methodology used.

4.1 Health and safety aspects of the experimental work

Work that is completed at the expense of the health and/or safety of the worker can be regarded as unsuccessful. Hence, the safety and health of both the worker and instruments were given high priority in this project. The main safety concerns for both the laboratory and the plant were the elevated equipment and the rotating stirrer. The uncovered hydrocyclone outlet discharge boxes in the plant process also posed a fall hazard.

With regards to health issues, dust and noise in both the laboratory and the plant set-up were the main concerns. Chemical fumes resulting from high pressure discharge of slurry into the discharge boxes of the plant set-up also posed health hazards. In the laboratory, dust was generated during sample preparation and also during addition of ore to the mixing tank. The personal protective equipment (PPE) used to mitigate these hazards are listed below:

- Body protection (safety overalls)
- Safety goggles, safety boots, hand gloves and ear plugs
- Dust mask

The elevated experimental set-up increased the risk of falling for both the tools that were used and the operator. Since this set-up consisted of running machines, the pump and the stirrer, care was taken to prevent the trapping of tools in running machines, especially during sampling. In order to minimise risks proper housekeeping was carried out, which also contributed to data integrity and aided the successful completion of the entire project. This involved thorough cleaning of the equipment to prevent cross contamination between different ore types and particle sizes and to improve hydrocyclone performance.

4.2 Laboratory experimental set-up

The experiment was carried out using a general laboratory hydrocyclone set-up which involved a recirculation system; refer to appendix A.1, V for the equipment specifications. It consisted of a hydrocyclone suspended on a mixing tank so that both the overflow and the underflow streams discharged in the same mixing tank. The two streams were mixed by a stirrer and pumped back to the hydrocyclone inlet by a centrifugal pump. The only measurable parameter on this system was the inlet pressure that was 55-97 kPa for the first set of experiments and 145-159 kPa for the second set. The inlet pressure was dependent on the solid content into the system. The feed flow rate was reconstituted from the overflow and underflow sampling time since there was no flow meter. A schematic diagram in Figure 4-1 illustrates the hydrocyclone setup.

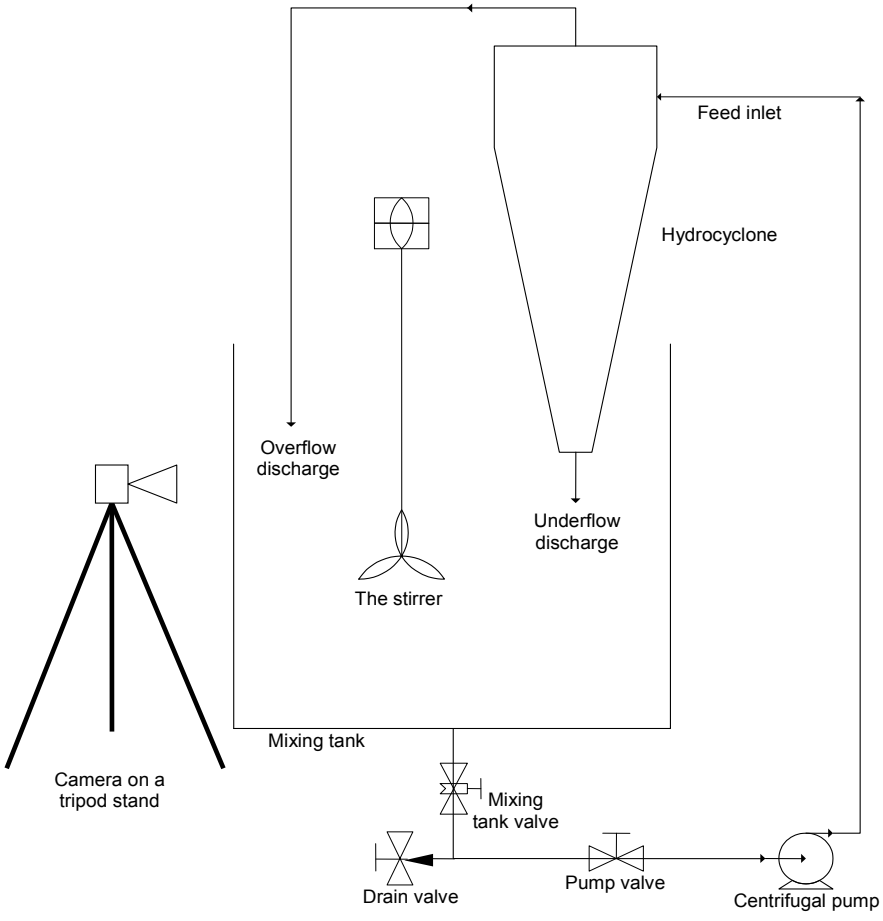

Figure 4-1: A schematic diagram of the hydrocyclone set-up

Digital images of the underflow discharge were captured with a Canon EOS 400D digital camera. Since the underflow discharges inside a mixing tank, the camera was positioned in such a way that it was not obstructed by the tank. Figure 4-2 shows the position of the camera stand and how the underflow was positioned in the mixing tank.

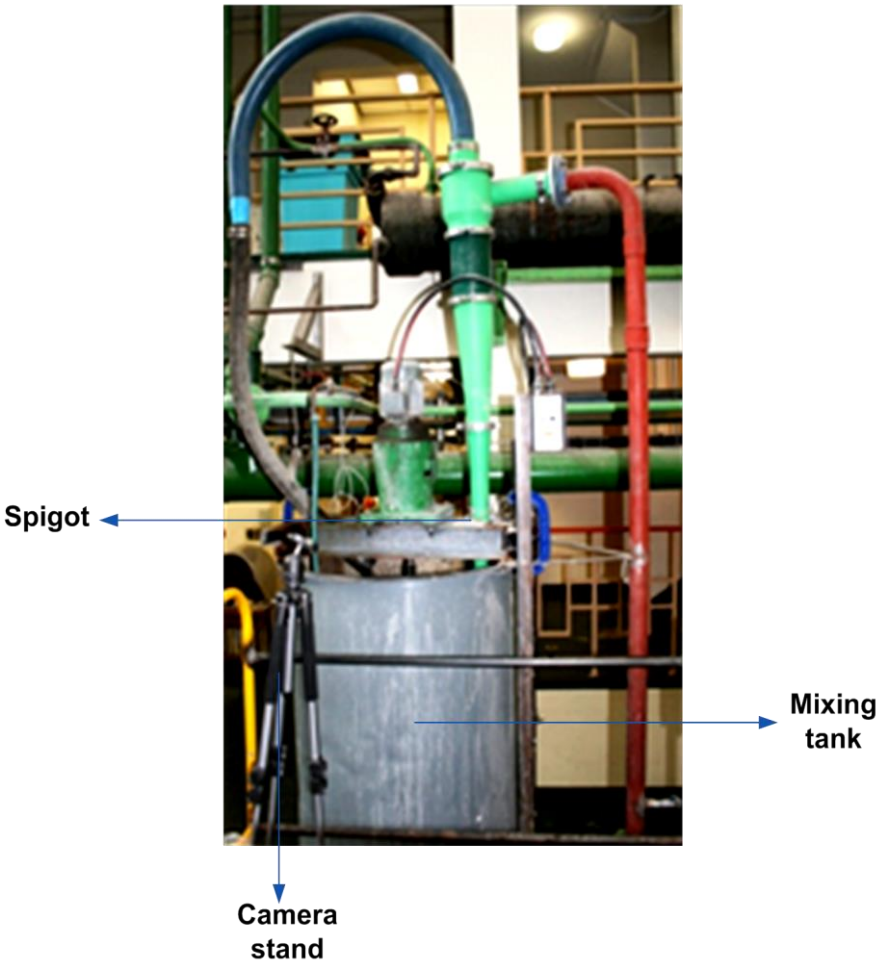

Figure 4-2: Illustration of the camera positioning

4.3 Laboratory experimental method

Description of case studies, equipment used, sample preparation as well as a detailed experimental procedure is presented in this section. Step-by-step methods of the experimental procedures are found in Appendix A.1.

4.3.1 Ore samples preparation and experiments description

The ore material used for the experiments was obtained from the Bushveld Igneous Complex which is a main source of platinum-group metals (PGM) in South Africa. These ores were

primarily extracted from the Upper Ground 2 (UG2) and Merensky mining horizons or reefs (Lidell *et al.*, 1986).

4.3.2 Equipment setting

The Canon EOS 400D camera settings were kept at the resolution of 1600 ISO (International Standard Organization) emulsion sensitivity. Images were captured in a raw mode as well as in Joint Photographic Experts Group (JPEG) format. A tripod was used to maintain a single position for the camera during the same run and to obtain better quality images which would have been a challenge if it was held by a person.

4.3.3 Equipment start-up procedure

The mixing tank was half-filled with water after which the system and the stirrer were activated. The flow of water was used as the system fault check and as maintenance of recirculation. For every different ore run, the system was run with pure water for about 5 minutes prior to addition of sample.

4.3.4 Experimental procedure

Although there were different experiments with varied conditions, as explained in the sample ore preparation section, the experimental set-up and procedure was the same for all experiments. The altered variables were the particle sizes and ore types only and each ore size material or type was run separately. The ore material was slowly added to the mixing tank to prevent choking the system as well as to assist in the agitation of the slurry. In total, 15 completely independent runs were conducted with the PGM slurries in the laboratory hydrocyclone. During each of these runs, the solids loading was increased in incremental steps. The table below shows the cyclone run conditions, runs 13 – 15 is a repetition of 10 – 12, carried out for the reason of increasing data.

Table 4-1: Experimental ore conditions per individual runs

Cyclone Test	Ore Type	Particle Size (50% feed passing) µm	Feed Solids Loading %
Run 1	Plat Reef	241	16.1
Run 2	Merensky Reef	300	16.3
Run 3	UG2	197	16.1
Run 4	Plat Reef	41	16.1
Run 5	Merensky Reef	59	16.3
Run 6	UG2	41	16.1
Run 7	Plat Reef	1189	13.0
Run 8	Merensky Reef	276	13.0
Run 9	UG2	251	13.0
Run 10	Merensky Reef	710	10.9
Run 11	Merensky Reef	210	10.6
Run 12	Merensky Reef	75	10.6
Run 13	Merensky Reef	710	10.9
Run 14	Merensky Reef	210	10.6
Run 15	Merensky Reef	75	10.6

The underflow discharges were visually observed for any variation between different feed states. Similarly, the physical appearances of the images were also noted prior to analysis of data via the image analysis technique.

The samples were collected from the underflow and overflow streams and were dried in the oven overnight. With each sample, the sampling time and mass (wet) were recorded. Solids percentage was thus determined and the PSD analysis was performed by using a Saturn DigiSizer Laser Particle Size Analyzer as well as sieve screens. The mean or median particle sizes of underflow discharge were calculated / extrapolated from the PSD results. This was in turn included as an input data set.

Underflow images were captured, and transferred to a standard PC. Image preprocessing was done by enhancing the image contrast and/or removing the background in the Microsoft office Picture Manager and then transferring it into MATLAB. Images were analysed on MATLAB Software using the image toolbox in order to extract the image features and then to determine the association between these features and the underflow particle sizes.

4.3.5 Equipment shut down procedure

A proper shut down procedure was followed at the end of every run. The slurry needed to be diluted before draining and a thorough water rinse through the system was done.

4.4 Industrial/Plant –based study

Investigations were done in an uranium ore processing plant (RUL mine) situated along the coastal area of western Namibia. This section is a description of the industrial case study. A layout of the hydrocyclone circuit and set-up in the plant is given including the explanation of the investigation procedure.

4.4.1 Motivation for the industrial case study

A plant-based case study was done in order to study the effectiveness of the underflow image analysis in a processing plant as well as to fill some gaps found in the laboratory cyclone study.

The gaps identified were:

- In the laboratory set-up, there was no changing in the ore running into the system; the industrial processing plant would always have undesirable materials that can contribute to the complexity of images taken.
- To apply image monitoring to the industrial hydrocyclone underflow discharges by carrying out an observational experiment.

4.4.2 RUL hydrocyclone circuit

Hydrocyclones in the RUL plant are found in the washing section of the plant. They are used to separate sands from the slimes that at this stage contain dissolved uranium in an acidic solution. The hydrocyclone underflow (sands > 210 μm) is washed in a two-stage procedure and then conveyed to tailings as waste. Alternatively, the cyclone overflow (slimes < 210 μm) is pumped to the counter current decantation (CCD) circuit. In the CCD section, more solids are removed from the slurry and the solution is further processed downstream. Figure 4-3 shows the process flow of the processing plant highlighting the circuit where the hydrocyclones are found (the block highlighted in blue).

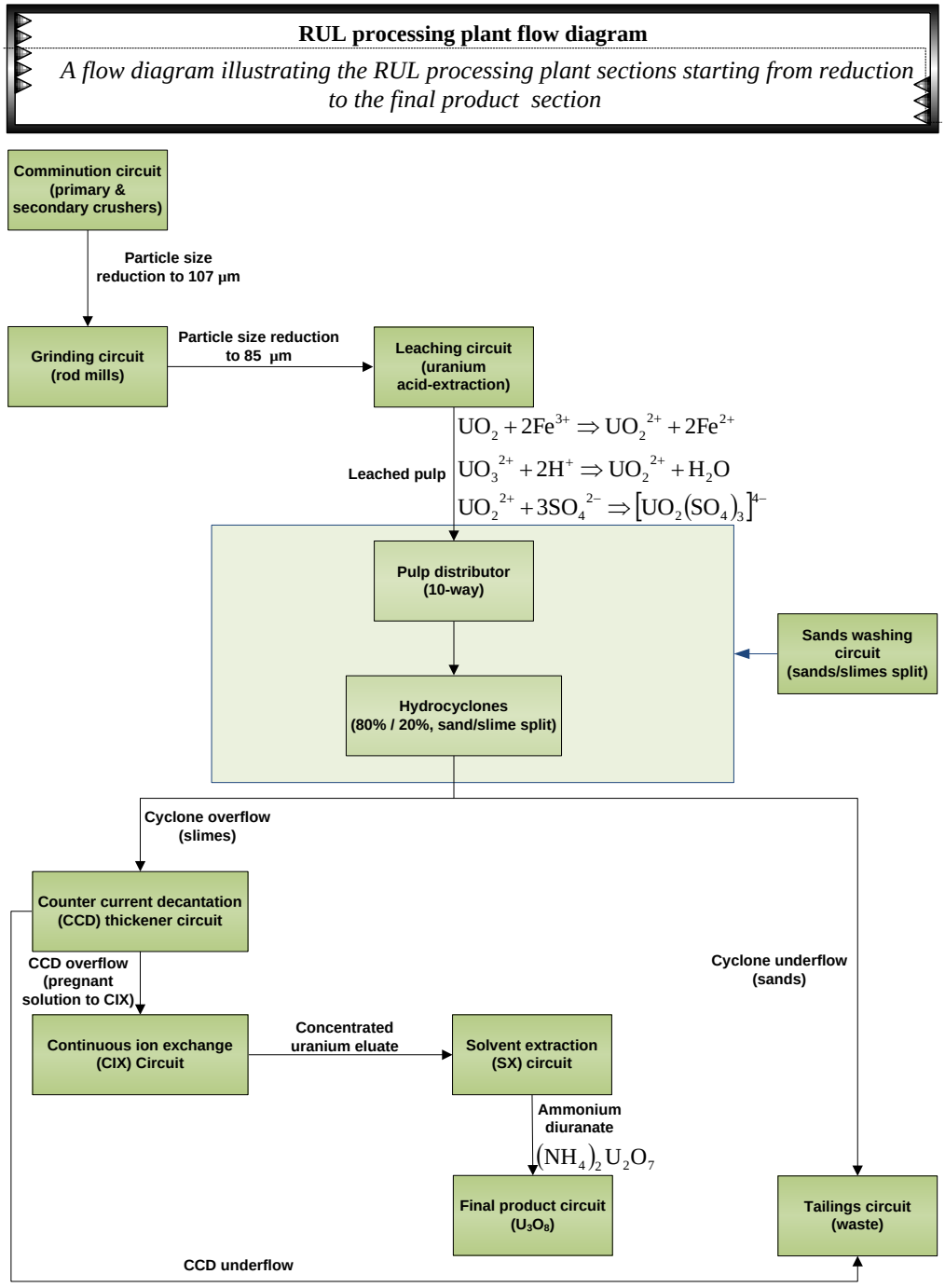

Figure 4-3: RUL processing plant flow diagram

a) Hydrocyclones set-up

There are two modules in this plant section. Each module comprises of ten hydrocyclones in parallel arranged in two rows of five each. Figure 4-4 illustrates this and also shows the first and last hydrocyclone in one row.

Figure 4-4: RUL hydrocyclones plant/circuit layout indicating the first and last cyclone in a sequence

The parallel arrangement of hydrocyclones aids in accommodating the amount of tonnages required for the operation. They receive the feed from a 10-way pulp distributor. This makes it impossible to isolate one cyclone and have it run on different conditions as done with the laboratory experiments. The cyclone layout is made in such a way that the feed (leached pulp) enters the hydrocyclone and discharges into the underflow and overflow discharge boxes (Rössing, 1995). These outlets are all discharging to different sections and there is no circulation of the material in the system. Figure 4-5 illustrates the layout described and Figure 4-4 shows the hydrocyclones arrangement in the RUL plant.

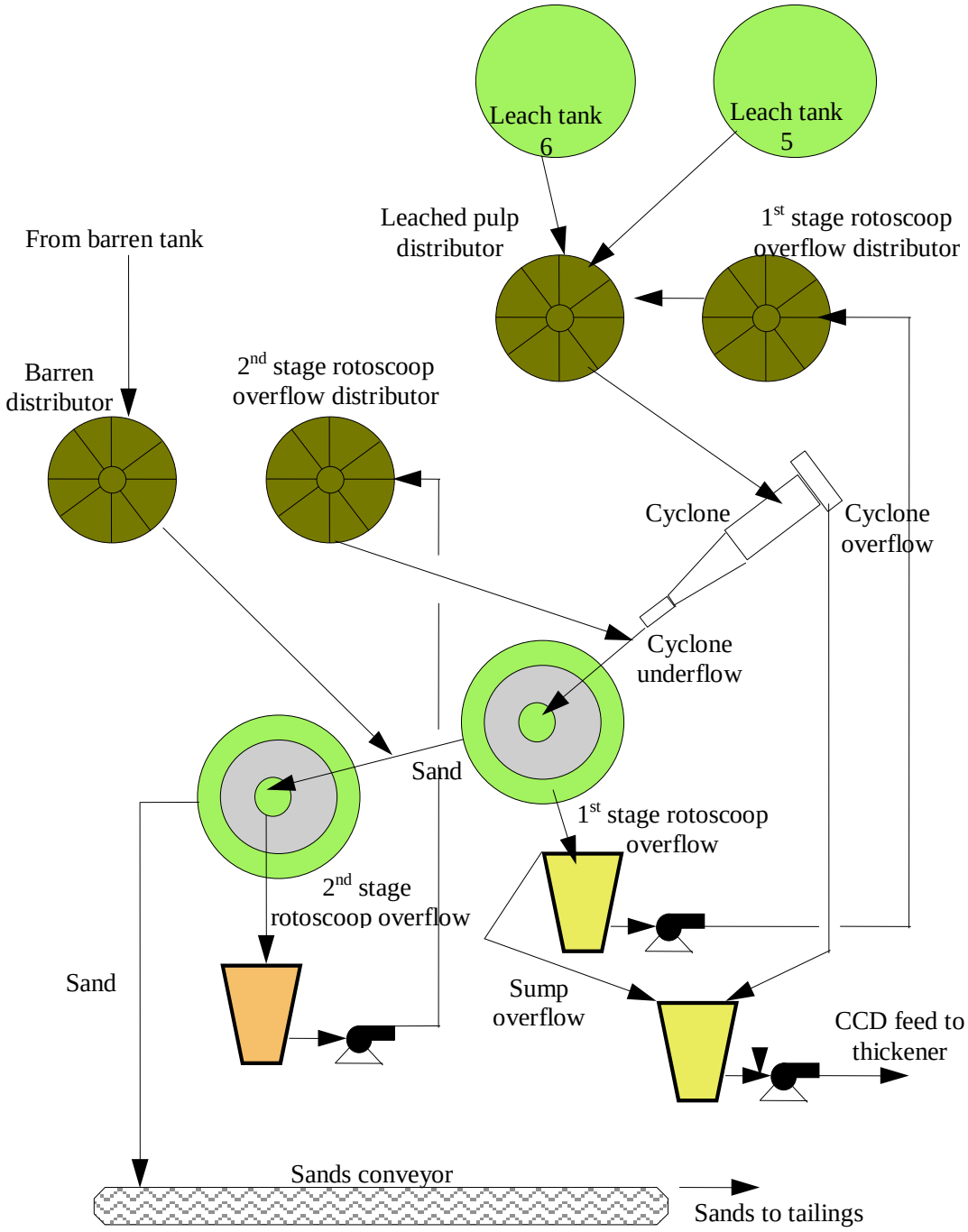

Figure 4-5: RUL hydrocyclones plant/circuit layout (redrawn from Rössing, 1995)

From Figure 4-5, the feed flow to the cyclones can be summarized in this manner: The leached slurry from the leaching section enters a leached slurry distributor where it meets with the washing solution and is pumped to the cyclones. In the hydrocyclones, the separation of slimes (product) and sands (waste) is performed; the overflow is pumped to the CCD circuit and then proceeds to the downstream sections. However, the hydrocyclone underflow

is further washed of the uranium-containing solution and then transported via sands conveyor to tailings as waste.

b) RUL hydrocyclone description

The hydrocyclones found in RUL are 660 mm big (refer to appendix A.2 for detailed dimensions). The maximum tonnages each module can receive is approximately 520 t/h and a barren wash rate of 20 m^3/min. The feed inlet pressure to each hydrocyclone is approximately 60 kPa to allow for normal cyclone operation. A project focused on improving the cyclone efficiency is currently being carried out and is partly addressing the issue of low pressure with big cyclones. For this study, all descriptions remained as such except for the mills throughput (tonnages) that was kept at 480 t/h for both cases. Figure 4-6 and Figure 4-7 show a typical hydrocyclone found in the RUL washing circuit.

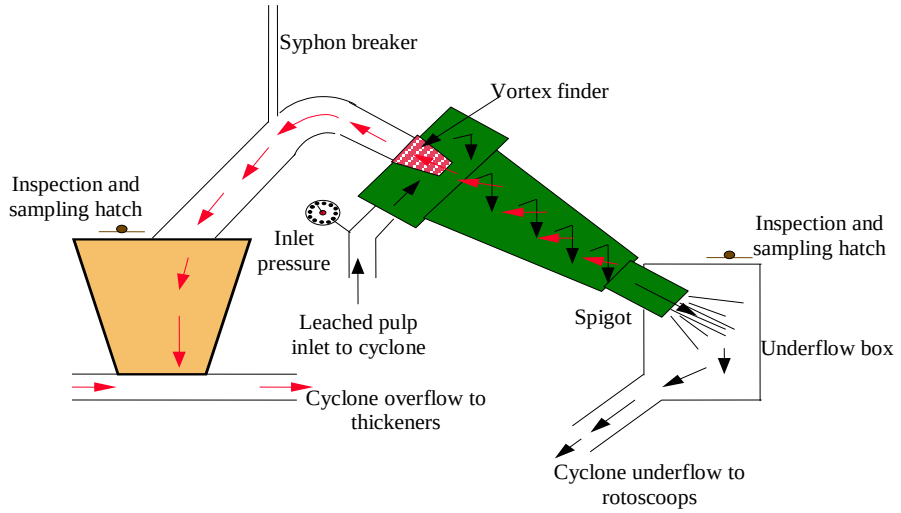

Figure 4-6: Illustration of a RUL hydrocyclone (redrawn from Rössing, 1995)

Figure 4-7: RUL hydrocyclones in a sequence as well as a zoomed-in individual cyclone

c) Monitoring the hydrocyclone

Inadequate monitoring of hydrocyclone operation such as those of RUL would lead to > 210 µm materials being sent to the CCD circuit and cause sanding of the thickeners that could result in inefficient operation. Roping conditions may occur due to solids sedimentation at the underflow section or high solids concentration in the cyclone feed. The effect of roping is that sand will report to the hydrocyclone overflow and be pumped to the CCD circuit resulting in the above mentioned negative effect. In addition, poor sand/slime split may result when the feed inlet pressure is not well monitored. Therefore, it is critical that hydrocyclones should be well monitored to prevent the mentioned unfavourable conditions.

4.4.3 Description of industrial/plant-based case study

Plant material was investigated by looking at the hydrocyclone underflow discharges as well as the underflow discharge image features. A more detailed explanation of how these were analysed is found in the next chapter. The investigation field of this study was the uranium mining plant (RUL plant) and two case studies were done. The study was conducted on the plant hydrocyclones as an in-line test and the cumulative 50% finer particle size for the cyclone feed was 63 µm and 80 µm respectively for the two case studies. From the PSD, it was shown that these data sets had different size distributions of finer particles, but a similar coarser size distribution.

4.4.4 Hydrocyclone underflow discharge manual sampling

The hydrocyclones were evaluated as to whether they were well conditioned based on spigot inspection and the appearance of their discharges. One of the best conditioned hydrocyclones was selected for sampling. From this hydrocyclone, two sets of data were collected in two days, one set for each day. These two sets could give slightly different results, but it was not expected to be too different because the same parameters were used for their normal process operation. The same hydrocyclone was used for the manual sampling and for the image collection.

Eight samples in total were taken from each stream (the underflow and overflow) of the hydrocyclone. For each sample the moisture analysis and sample screening for the PSD were performed. The solid concentration for each underflow discharge sample was determined by recording the wet (slurry) and dry mass of the samples obtained. The formula used was

$$\text{Solids } \% = \frac{\text{dry mass}}{\text{wet mass}} \text{ x } 100 \qquad (4\text{–}1)$$

The solids content in the underflow discharge was found to be in the range of 73% - 76% for RUL samples.

PSD analysis was used to determine the mean underflow particle sizes and in turn to predict the particle sizes in the regression model. PSD was analysed by using sieve screens as well as the laser particle size analyser and the results generated formed part of the dataset.

4.4.5 Hydrocyclone underflow image collection

After a proper camera set-up was established, the underflow discharge images were captured. These images were transferred to a standard PC and processed as described in section 4.3.4 and in detail in Chapter 1:.

The RUL hydrocyclone set-up posed some difficulties with image capturing. The major problems were identified as:

- *The discharging of hydrocyclones into the underflow boxes complicated the image taking since the spigot was inside the box.* In Figure 4-8, the fitting of the spigot into the discharging box (A and B) and the discharge box opening (C) are shown.

Figure 4-8: Illustration of fitting of; (A) the spigot onto the underflow box, (B) the underflow box opening and (C) the spigot seen from the opening

- *Difficulty positioning the camera:* As seen from Figure 4-8 (B), the opening of the underflow box was obstructing the vision to the spigot, thus the positioning of the

camera was made difficult. However, proper assessment of the area made the imaging possible.

- *Blurred image clarity:* The slurry enters the box at a high pressure and sometimes this creates a lot of fumes. The fumes cover the underflow discharge and blur the images as can be seen in Figure 4-9.

Figure 4-9: Fumes blurred the RUL hydrocyclone underflow discharge image

- *Ergonomics:* Due to the elevated underflow box and the size of the platform, there was a potential hazard of falling into the box or off the platform.
- *Camera safety:* The high pressured slurry entering the discharge box can lead to spillages (uranium-acidic content) over the camera and this could corrode and damage it. So, extra care was taken. There was also a real possibility of the camera falling into the uncovered box whilst in the process of setting it up, or of the camera falling off the platform to the ground.
- *Limited study time frame did not allow an excellent camera set-up to be established;* however the temporary improvements made were sufficient.

Although there were some shortcomings as mentioned above, the improvements that were made mitigated them and allowed the successful completion of the study.

4.5 Monitoring technique requirements

In Chapter 1: a number of monitoring techniques were evaluated and image analysis was indicated as one of the techniques that met the hydrocyclone monitoring requirements as shown by Petersen *et al*. (1996); Neesse *et al*. (2004b); Krishna *et al*. (2010) and Janse van Vuuren *et al*. (2011). This section outlines the specifications of the monitoring equipment used for this work with regards to the requirements of hydrocyclone monitoring.

For sensitivity the Canon EOS 400D camera was used at the resolution settings of 1600 ISO. To obtain clear high quality images and best shots, a Canon Speedlite 580EXII flash with 50 mm flash range was added. The camera takes images at a rate of 3 frames/sec.

The use of the tripod and the flash kept the camera at a distance away from the splashes yet allowed the camera to focus on the spigot by using its zooming ability. This monitoring system is non-intrusive as no modification was necessary to the existing hydrocyclone set-up. It is also robust and not sensitive to mechanical wear. Although a cyclone set-up may hinder the process of imaging as was observed with the RUL processing plant, little and inexpensive modifications may be effective to solve this problem. This monitoring system is also cost effective since the monitoring equipment is not expensive.

Chapter Summary

This chapter described the methodology used in this study. It has highlighted the importance of risk assessment prior to any test work. The major risks identified were the elevation of the hydrocyclones, housekeeping, dust, fumes and the ergonomics. The laboratory set-up involved a standard laboratory hydrocyclone with a recirculation system that allowed the underflow and overflow streams to discharge in a mixing tank to be used as feed for the hydrocyclone. The ore used for the experiments were PGM samples from a Bushveld Igneous Complex in South Africa. These were the Merensky, UG2 and Platinum reef materials of about 50 kg each per case study and 15 experimental case studies were carried out.

The plant investigation on the other hand used an in-line uranium material from a RUL processing plant in Namibia. Hydrocyclones at the RUL plant are found in a washing circuit and are used to separate waste sand from the slimes containing dissolved uranium. Hence their monitoring is critical to prevent loss of uranium along with the waste material. Two case studies were done with the aim of comparing the effectiveness of image analysis monitoring in an industrial operation to its application in laboratory cases. Though there were a few limitations associated with the underflow imaging procedure in the plant, small and inexpensive modifications could successfully mitigate them.

For both the laboratory and plant studies, the underflow samples were collected for the analysis of solids percentage and PSD. These analytical results formed part of a dataset in addition to the underflow image features. Image analysis was performed with the MATLAB image toolbox. The monitoring system used a Canon EOS 400D camera with a Canon Speedlite 580EXII flash that allowed for better quality images to be taken. The camera takes 3 frames per second and it is non-intrusive, robust, and cost effective. This makes it suitable as a good hydrocyclone monitoring device for an underflow monitoring system.

Chapter 5: Data Analysis

This section outlines the analysis of data obtained as explained in chapter 4. It gives an overview of the analytical methodology which covers the image processing and manual sample analysis. The chapter further presents the description of the data set and variables as well as the analysis methods used. In this document, underflow discharge images and underflow images are used interchangeably.

5.1 Analytical methodology

Regression and classification models were used to assess the relationship between the underflow image features and the mean particle size and solids content. The classification methods that were used included linear discriminant analysis (LDA) and multilayer perceptron neural networks. The classification analysis of data was performed in STATISTICA software, whereas the MATLAB NN toolbox software was used for the regression model.

Figure 5-1 gives an overview of the analytical methodology used. It shows the procedure followed to analyse the data obtained from the underflow samples as well as from the underflow images. A stepwise analytical procedure is found in Appendix A.1 - I.

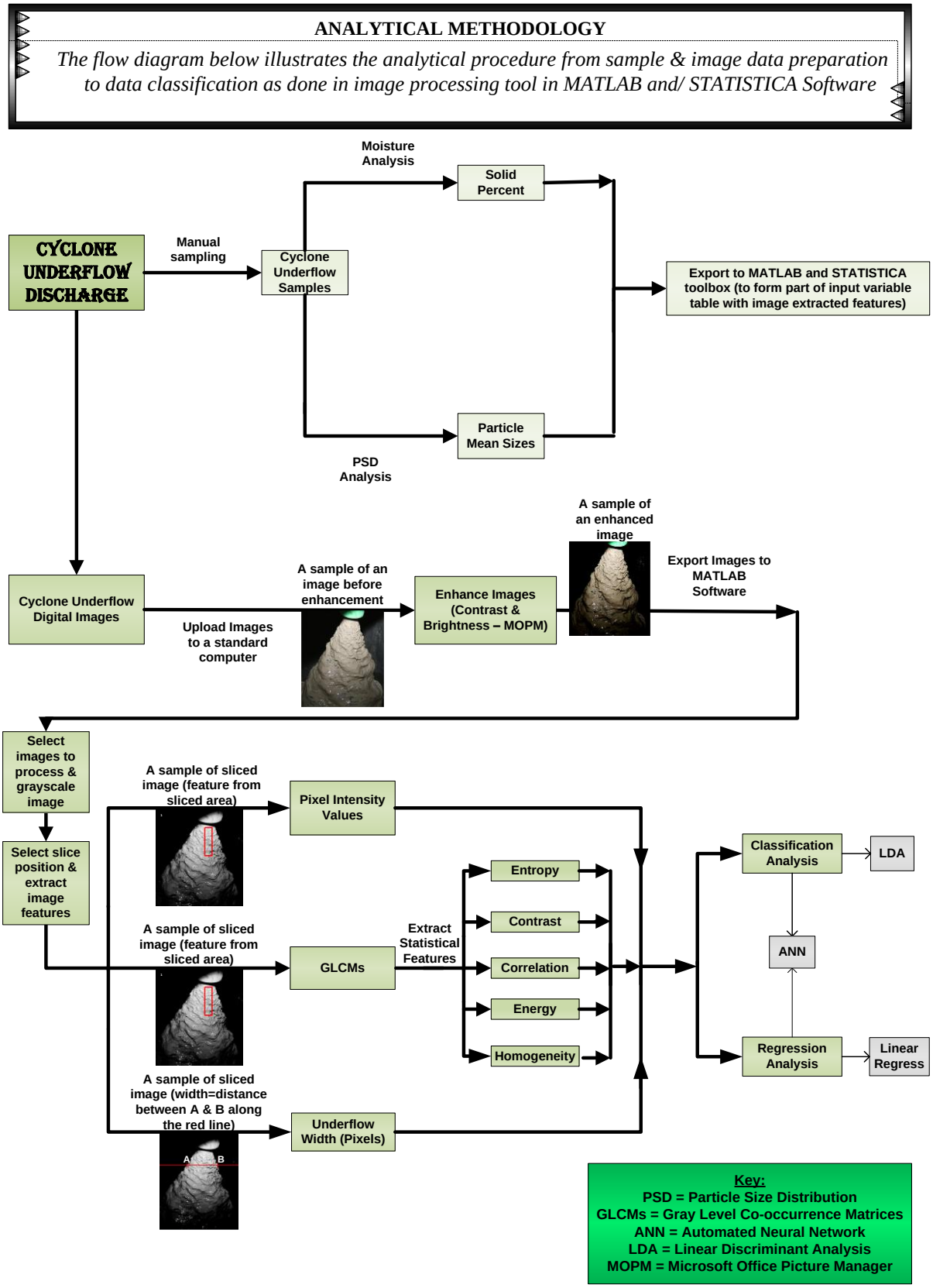

Figure 5-1: A flow diagram of the analytical methodology

5.2 Hydrocyclone underflow discharge image analysis

Image analysis is the way of obtaining useful information from an image based on different image properties (Prats-Montalbãn *et al.*, 2011). In this research, the image property used was mostly texture, where numerical values of the image features were extracted. The reason for a focus on textural features, was that the particle size and solids concentration in the slurry was observed to have an effect on the appearance of smoothness in the underflow. Colour on the other hand, appeared to be less reliable an indicator of the particle size of the flow, ore type. More work would be required to quantify these observations, which were not considered in-depth, as it fell beyond the scope of the present work.

Image processing begins with pre-processing to rid images of unwanted background and noise before the image analysis can be done successfully. For this work, hydrocyclone underflow discharge images of different feed conditions were processed with MATLAB, using an image processing tool as indicated in Figure 5-1. Appendix B: presents the MATLAB programming code used for explained image feature extraction.

The following sections describe the two methods used to extract numerical variables from the raw underflow images, namely image texture analysis and the underflow width extraction methods.

5.2.1 Underflow image texture analysis method

Among many definitions, image texture can be defined as a repeating pattern of local variation in image intensity which is characterized by spatial distribution of colours or intensities in an image (Berberoglu *et al.*, 2007; Bharati *et al.*, 2004; Tuceryan & Jain, 1998). The texture analysis method is used in a variety of applications like classification, segmentation and synthesis (Bharati *et al.*, 2004; Tuceryan & Jain, 1998; Prats-Montalbãn *et al.*, 2011). Although quite a number of textural features have been proposed, they are dependent on each other, as stated by Tomita & Tsuji (1990) cited in Tuceryan and Jain (1998). According to Bharati *et al*. (2004) and Prats-Montalbãn *et al*. (2011), texture analysis differs in approach depending on the method used. The method could be statistical, structural, model-based or transform-based.

In this research, the extracted image features were based on the statistical pattern recognition methods. These textural features were extracted using a grey level co-occurrence matrix (GLCM) and were in a numerical form.

a) Gray level co-occurrence matrix

"For an image, GLCM is a second order statistical method that distributes the co-occurring grey levels of two pixels at a given offset" (Aldrich *et al.*, 2010; Marais, 2010). It is broadly used to characterize the texture of images. The GLCM uses statistical measures and it is also widely accepted as an image feature extraction method (Rodriguez-Galiano *et al.*, 2012). A variety of statistical measures extracted from the GLCM can give unique information about spatial relationships of pixels in an image as well as the neighbouring grey level dependence matrix (Aldrich *et al.*, 2010; Marais, 2010).

The GLCMs were calculated from a rectangular slice of an image as shown in Figure 5-2, see appendix B.2 for the MATLAB code used to extract the numerical data for these features. Red rectangles in this figure represent the area of interest from which the image textural features were extracted. The slices were taken from the inside area of the discharge for noise reduction purposes. This was determined in such a way that they do not lie in the downward curving region where the image starts changing features. Slicing of images was done at different image settings after the images went through the contrast and brightness enhancements. These include RGB, grey scale and threshold image settings as illustrated in Figure 5-2 A, B and C respectively.

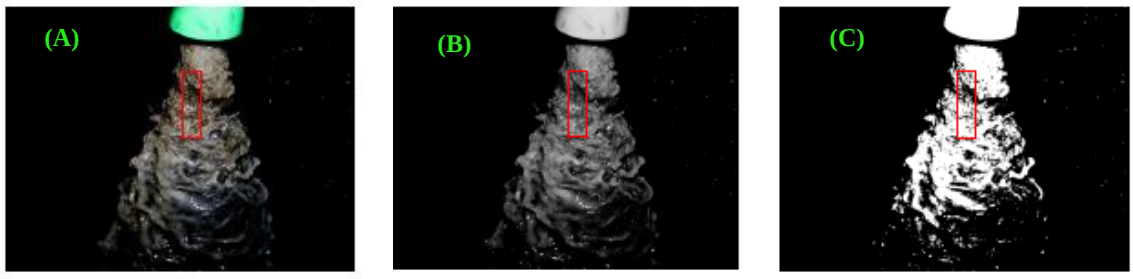

Figure 5-2: Image settings where GLCMs were extracted, (A) RGB image, (B) gray-scale image, (C) threshold image

From the three image settings, the analysis showed that only the grey-scaled settings could be used due to the complexity of working with colour (RGB) and threshold images. The colour

images use three values for one pixel which then complicates the analysis unlike one value in grey-scaled images. Threshold application generates too extreme values, either zeros (white) or ones (black), which caused complexity in further analysis. This could be due to some inconsistency in the lighting of images, and was observed more with the RUL images. With the above limiting factors in RGB and threshold, it was decided to rather make use of grey-scaled image settings.

b) Gray level co-occurrence matrix statistical measures

The GLCM statistical measures used were entropy, energy, homogeneity, contrast and correlation. The calculations were done with a built-in function in the MATLAB software. In all the GLCM statistics formulas the *i*,j is the co-occurring pair, P_{ij} is the co-occurring probability of the *i,j* elements in GLCM and *N* is the number of grey levels in the image.

i. Entropy

In a GLCM, entropy measures the local deviations of values, thus reflecting how repeatable grey level pairs are in an image (Clausi & Zhao, 2002). An image with a higher degree of repetition amongst the grey level pairs tend to have high entropy values and this is mostly found within the fine particle images, with a few exceptions dependent on the particle size ranges. The following formula calculates the entropy feature.

$$Entropy = \sum_{i,j=0}^{N-1} -\ln(P_{ij})P_{ij} \quad \text{(Correlation, 2012)} \qquad (5\text{–}1)$$

ii. Contrast

The contrast feature is calculated using the formula (5–2) and it measures the brightness difference between a pixel and its neighbour across the image, it also measures texture smoothness.

$$Contrast = \sum_{i,j=0}^{N-1} P_{ij}(i-j)^2 \qquad (5\text{–}2)$$

iii. Correlation

In a correlation feature, linear dependency of grey level in an image is measured (Marais, 2010). It shows how correlated a pixel is to its neighbour and is calculated by:

$$Correlation = \sum_{i,j=0}^{N-1} P_{ij} \frac{(i-\mu)(j-\mu)}{\sigma^2}$$, whereby (5–3)

$$\mu = \sum_{i,j=0}^{N-1} iP_{ij} \quad (5–4)$$

$$\sigma^2 = \sum_{i,j=0}^{N-1} P_{ij}(i-\mu)^2 \quad (5–5)$$

μ = the GLCM mean (being an estimate of the intensity of all pixels in the relationships that contributed to the GLCM)

σ^2 = the variance of the intensities of all reference pixels in the relationships that contributed to the GLCM

iv. Energy

The energy features measure the evenness or uniformity of an image and its value is small for non-uniform images. It is calculated using the following formula:

$$Energy = \sum_{i,j=0}^{N-1} (P_{ij})^2 \quad (5–6)$$

v. Homogeneity

Lastly, the homogeneity statistics measures the closeness of the elements in the GLCM to the GLCM diagonal. The following formula calculates homogeneity.

$$Homogeneity = \sum_{i,j=0}^{N-1} \frac{P_{ij}}{1+(i-j)^2} \quad (5–7)$$

5.2.2 Underflow width extraction method

The underflow width is the number of pixels between the underflow edges along the horizontal line within the interval search limits (Janse van Vuuren, 2011). An appropriate horizontal line was sliced for each image as shown in Figure 5-3.

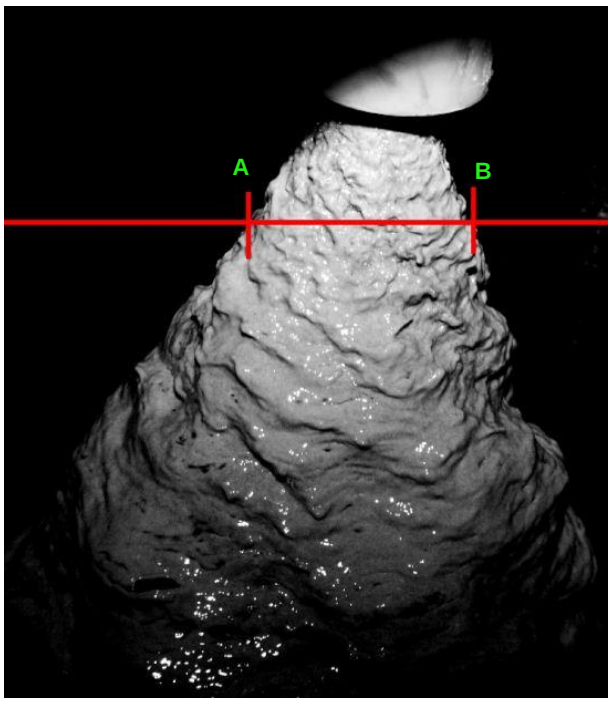

Figure 5-3: Illustration of the underflow width extraction method

A certain underflow width was determined in such a way that after slicing a horizontal line, a data cursor was used to get the pixel numbers between the underflow edges (A to B points as illustrated in Figure 5-3). The horizontal line was determined using a theoretical spray profile such that the line lies in the region of flat downward sloping. This area is between the initial upward curved region and the downward curving regions. For more details on this, Janse van Vuuren *et al*. (2011) can be consulted.

The values obtained from the underflow width were combined with other extracted features to form a dataset and were further analysed.

5.3 Description of the data set and variables

The numerical variables from sample analysis and the underflow image features are defined here. The data values for all variables were normalized so that they ranged between 0 and 1.

The consolidated data set for this research comprised 10 variables and 340 observations, as indicated in Appendix A.3.II. The data set was made up of combined data from the calculated hydrocyclone underflow PSD (mean particles size) and solids content, and the cyclone underflow image features. The data obtained from experimental work on the industrial plant have also been included in the consolidated data set (designated by *Ore Type* = RUL), but these data were analyzed separately, as conditions between the laboratory and industrial setups were not comparable.

The variables that were used for analysis and modeling are summarized in Table 5-1. They consisted of one categorical and two continuous response variables, as well as seven predictor variables. The categorical response variable represented the ore type and could assume any of the four values *Merensky*, *Platreef*, *UG2* or *RUL* (where in the case of the industrial data). The two continuous response variables were the mean particle size (MPS) and the solids content of the underflow slurries. The seven predictor variables were derived from the images of the underflow and were the underflow width, homogeneity, entropy, correlation, standard deviation of the pixel intensities, energy and contrast, as previously described in more detail.

Table 5-1: Variables used in data analysis of the PGM ores.

Variable Type		**Variable**	**Range**
Response	Categorical	Ore Type	Merensky, Platreef, UG2 (RUL)
	Continuous	MPS (μm)	97-1400
		Solids (%)	6-32
Continuous Predictor		Underflow Width (pixels)	332-936
		Homogeneity	0.84-0.95
		Entropy	0.27-1.00
		Correlation	0.86-0.97
		St Dev Pixel Intensity	22-76
		Energy	0.07-0.41
		Contrast	0.10-0.44

5.4 Classification analysis

Classification models were built with the categorical response variable as output and the seven continuous predictor variables as input. For this purpose, Fisher's linear discriminant

analysis (Nagpaul, 2009) and (nonlinear) neural network models were used. Generally, a non-linear method is observed to have an advantage over the linear method due to its ability to separate closely spaced data (Khashei *et al.*, 2012; Kone and Karwan, 2011). These two approaches are described in more detail below.

5.4.1 Linear discriminant analysis method

The LDA method is a widely applied supervised classification method that is simple in use and very effective. It is used to determine a variable that can distinguish two or more groups as well as to predict the classification cases with regard to the mean of a variable (STATISTICA, 2012). The basic idea is to project the variables onto a lower-dimensional plane, so that separation of the different groups in the data is maximized on the projection plane. Classification is then done by identifying the boundaries between the different groups in the discriminant score space. In this investigation, linear functions were used to do this.

Linear discriminant analysis reduces classification problems to linear identification constituents by transforming them into discriminant functions that separate data into classes. It further estimates the coefficients of these functions. A discriminant function minimizes the misclassification rate according to the training data set and classifies new observations. For a certain problem, the effectiveness of the classification process depends on the performance of its discriminant function (Khashei *et al.*, 2012).

5.4.2 Automated Neural Network analysis method

Neural networks are non-parametric or weakly parametric models that can identify complex relationships between variables. Multilayer perceptron neural networks comprise and input layer of process units or neurons that distribute the data to one or more hidden layers and finally an output layer. Each of these layers consists of process units or neurons with weighted incoming connections. Each neuron is also associated with a simple activation function (typically sigmoidal), that transforms the data before it is passed on to the next layer or presented as the output of the network. Adjustment of the weights is done by means of a training process and essentially the network can be seen as a set of weighted basis functions that are fitted to the data (Muhamad and Deravi, 1994; STATISTICA, 2012). Figure 5-4 shows a typical layout of the neural network showing an input, a single hidden and an output layer.

Neural networks and multilayer perceptrons in particular, are widely applied techniques and it has been successfully used in many fields (Khashei *et al.*, 2012). In classification problems, a neural network model assigns a class to a certain set of input variable (Berberoglu *et al.*, 2007) and during training its weights are adjusted iteratively until the misclassification of the training data is minimized.

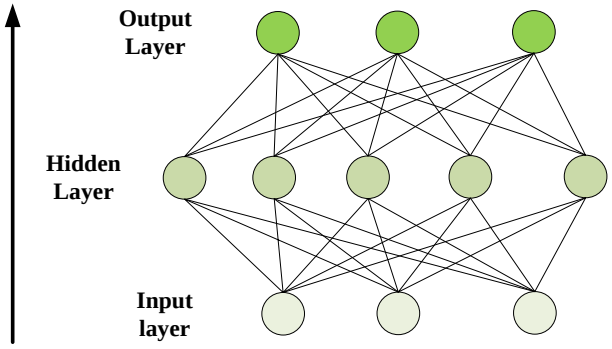

Figure 5-4: A schematic diagram of a neural network with three inputs, five hidden neurons and three outputs.

An example of the use of neural networks as classifiers was the content-based image classification that was constructed for various image features by using a NN back-propagation learning algorithm (Park *et al.*, 2004). These authors used the images on the internet and found that neural networks have the potential to be used as an automatic classification system for images of this type. In their work, textural image features were extracted by wavelet transform and sliding window-based feature extraction. These textural features included contrast, diagonal moment, energy, entropy, homogeneity, second diagonal moment and uniformity. The overall classification rate for this experiment was 79.2% correct.

5.5 Regression analysis

Regression is defined as a statistical tool for the investigation of best relationships between variables. A commonly used regression technique is multiple regression analysis whereby a single variable is related to a set of variables. “Multiple regression allows additional factors to separately enter the analysis and estimate the effect of each factor. It is valuable for quantifying the impact of various simultaneous influences upon a single dependent variable” (Sykes, n/a).

In a regression equation, a dependent variable is estimated as a function of a number of independent variables, an error term, as well as corresponding parameters (Bello, 1995; Sykes, n/a; Um *et al.*, 2011). The equations (5–8) and (5–9) for the linear (multiple regression) and the non-linear regression methods respectively have mathematical forms

$$Y^* = \beta x_1 + \beta_2 x_2 + ... + \beta_k x_k + \mu \qquad (5–8)$$

$$Y_i = f(x_i, \varpi) + \in_i \qquad i = 1,..., n \qquad (5–9)$$

In equation (5–8), the symbols Y^*, β, μ, and x represents the vectors of observations of dependent variable (n x 1), parameter (k x 1), disturbance terms (n x 1) and the (n x k) matrix of observations of independent variables. n is the number of observations (Constantinides & Mostoufi, 2000).

The definitions of the symbols in equation (5–8) are; Y_i as the responses, f is a known function of the covariate vector $x_1 = (x_{1\,1}, \ldots, x_{1\,k})^T$ and the parameter vector ϖ $(\theta_1, \ldots, \theta p)^T$, and $\in_i$ are random errors (Smyth, 2002).

Two approaches towards predicting the continuous response variables (MPS and solids %) from the set of predictor variables were considered, namely multiple linear regression analysis and neural networks. Refer to sections 5.5.1 and 5.4.2 for a brief explanation of these methods respectively.

5.5.1 Multiple linear regression analysis method

Multiple linear regression (MLR) method is used to model the linear relationship between a dependent variable and one or more independent variables. It predicts the values of a dependent variable given a set of explanatory variables. In MLR it is assumed that Y is directly related to a linear combination of the explanatory variables, hence it models the linear relationship. This analysis is based on least squares where the model is fit such that the sum-of-squares of differences of observed and predicted values is minimized (Tranmer & Elliot, 1998).

5.5.2 Neural Network (NN) regression analysis method

In terms of regression problems, the NN method can be used to relate a number of input variables with a set of target variables. It was therefore used to predict the underflow particle mean sizes using the observed dependent variable data. For the interpretation of results, the mean squared error (MSE) and R^2 were assessed. The MSE is the mean of the squared deviation between the actual and the estimated values which accounts for the bias as well as the error difference. R^2 evaluates the variation percentage of the actual data that is explained by the predicted data. Thus, knowing the MSE and R^2, the model performance can be evaluated.

A Neural Network method is applied in many regression problems. An investigation similar to this study was carried out by Ko & Shang (2011) and it focused on the determination of particle size distribution using a Neural Network-based soft sensor to model the image uniformity. The outcome from this investigation indicated that the proposed methodology can provide reliable particle size calculation, and could be used for online measurement of particle size. This procedure together with the resulting neural network-based soft sensor that uses particle images was shown to be applicable to mineral processing operations for analysis, monitoring and control (Ko & Shang, 2011).

In this report, the NN analysis was performed using an automatically MATLAB software GUI generated script with modifications. A 3-fold cross validation was executed and the best performer of the three networks was selected to run the model using the independent test data. This was defined as the network with the highest performance rate and least error values. The MATLAB scripts used for the analysis are given in appendices B.3 and B.4.

Chapter Summary

The data was analysed by classification and regression methods. The regression analysis formed only a basis for further research in this field due to the nature of the work that was done and the scope of this work. Therefore, the major conclusions are made based on the classification analysis results. The methods used to classify data were the LDA and NN

methods, whereas MLR and NN were the regression methods. In both the classification and the regression analyses the non-linear and linear model results were compared.

Additionally, the variables were a combination of categorical classes, the calculated values from the underflow samples and the underflow image features in numerical values. The categorical classes were the ore types and the particle size classes, whereas the calculated data was the MPS plus solids content. The categorical variables were used in classifying the data, and the calculated data were used in predicting the particle sizes. Furthermore, the image features variables were the underflow width, pixel intensity values and the GLCM statistics. The statistics included the energy, entropy, contrast, correlation and homogeneity. For the regression model, the input variables used were the underflow width, pixel intensity values and the GLCM statistics.

Chapter 6: Results and Discussion

The previous two sections explained the experimental and analytical methodologies of this research. In this chapter the results obtained thereof are presented and discussed. These include the findings from the exploratory analysis, the classification of data and the prediction of the hydrocyclone underflow particle sizes distribution.

6.1 Classifying underflow image features

Classification models were built to assess the ability of the image features to discriminate between the different platinum ore systems. These could not easily be distinguished by observation, as the ores could not be differentiated by colour. In addition, the data obtained in industry were also analysed, this time to distinguish between mean particle sizes. In this case, classification was almost trivial (100% classification could be obtained), owing to the differences in the operating conditions between the two classes of particle size data.

6.1.1 LDA models

The classification rate for the laboratory data set when grouped per ore type was 61% accurate overall. This is a relatively poor classification rate, but nonetheless better than what would be obtained with a random classifier. Figure 6-1 illustrates these results on a scatter plot of canonical roots. As it can be seen from this graph, there is considerable overlap between the scores associated with the different classes. This showed similar observation to that made by physical assessment of the underflow.

Furthermore, the data set from the industrial hydrocyclone system was separately classified according to the underflow particle size classes. The two sets of data differed in median particle size as they were collected on different days, which meant that process conditions could not be controlled completely. Hence, for classification purposes, the data sets were divided into (212 μm) and (318 μm) size classes. Due to the time limit and difficulty capturing the cyclone underflow images, this data set consisted of 20 observations (images) for each set only. The rest of the image frames could not be used.

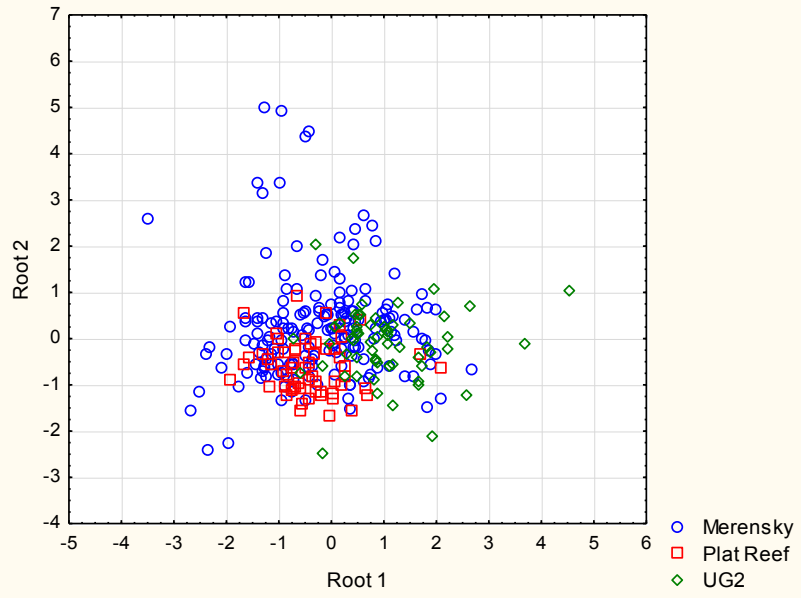

Figure 6-1: A graph of canonical roots illustrating the classification of the laboratory hydrocyclone data set according to the ore type category

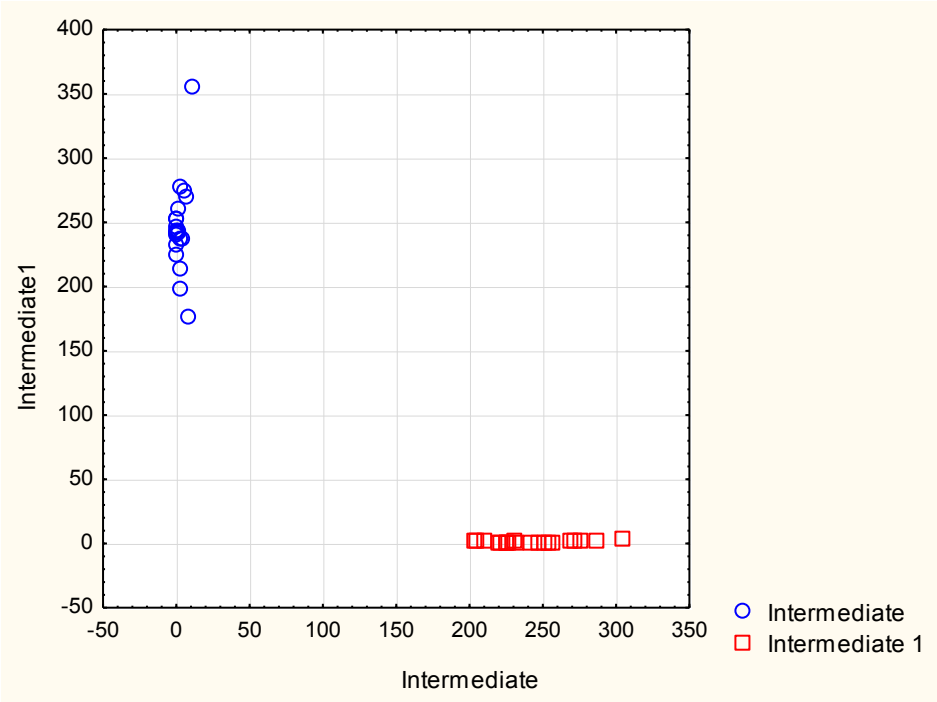

Figure 6-2: Scatterplot of Intermediate1 (212 µm) against Intermediate (318 µm) as categorized by Observed Squared Mahalanobis Distances from industrial hydrocyclone system data set

As mentioned previously, the classification results indicated that there was clear distinction between the two data sets with a 100% classification success rate, as indicated in Figure 6-2.

Even so, more experimental work would be required to draw more general conclusions with regard to the application of the methodology in the specific industrial setup.

6.1.2 Neural network classification models

For the comparison of the linear classification model with the non-linear model, the results from the neural network analysis are presented here. These outcomes are reported in the same order as the LDA results in the previous section.

The error function for the NN classification analysis was kept as the sum of squares. In addition, the training algorithm used was the Broyden-Fletcher-Goldfarb-Shanno (BFGS) technique (its parameters are given in the tables of presented results). Furthermore, the network employed various hidden neurons like hyperbolic tangent (tanh) or identity and the output neurons were mostly the softmax activation function. Other (logistic sigmoid and exponential for hidden nodes; identity, tanh and exponential for output nodes) activation functions also attained favourable outcomes. A specific summary of networks are given for each set of results in its respective results table.

The best neural networks which were selected out of the five active networks for each analysis are highlighted in all the tables of results presented. Table 6-1 shows the networks and the respective analysis performance for the laboratory data ore type category. The table shows the optimal structures of the single hidden layer multilayer perceptrons (all with seven input nodes and three output nodes), the error function that yielded the optimal model, as well as the activation functions of the hidden nodes of the neural networks.

Table 6-1: The view of networks retained from the laboratory cyclone data classification analysis with NN method, categorized by ore type. The best and selected network is highlighted

Index	Net. name	Training perf.	Test perf.	Validation perf.	Training algorithm	Error *f*	Hidden activation	Output activation
1	MLP 7-9-3	64.3	68.9	62.2	BFGS 16	Entropy	Exponential	Softmax
2	MLP 7-8-3	80.5	77.8	62.2	BFGS 37	Entropy	Logistic	Softmax
3	MLP 7-12-3	90.0	77.8	60.0	BFGS 69	Entropy	Tanh	Softmax
4	MLP 7-4-3	68.1	51.1	66.7	BFGS 0	Entropy	Exponential	Softmax
5	MLP 7-6-3	67.6	57.8	60.0	BFGS 0	Entropy	Tanh	Softmax

Categorising the laboratory cyclone data set by the ore types showed that the total classification rate was 62.2% on average based on the validation data. This is similar to what

could be obtained with the linear discriminant model. The Merensky ore type could be distinguished more readily from the other two ore types, as indicated by the data in Table 6-2.

Table 6-2: Summary of the laboratory cyclone data classification categorised by ore types, total percent classified highlighted

Net. name		*Merensky*	*Plat Reef*	*UG2*	*All data*
3. MLP 7-12-3	Total	180.0	60.0	60.0	300.0
	Correct	164.0	41.0	46.0	251.0
	Incorrect	16.0	19.0	14.0	49.0
	Correct (%)	91.1	68.3	76.7	83.7
	Incorrect (%)	8.9	31.7	23.3	16.3

6.2 Predicting the particle size and solids % of the underflow images

The results of multiple linear regression (MLR) and non-linear regression analyses with multilayer perceptrons were evaluated to determine the relationship of the underflow image features to the underflow particle sizes and solids loading. This was done for the laboratory hydrocyclone system only. The industrial system data set could not be modelled efficiently due to insufficient data (only two values for the response variable). As a consequence, industrial data analysis was excluded from this modelling.

6.2.1 Linear regression

The results from the MLR model showed that R^2 statistics values of approximately 0.558 and 0.403 was obtained for the laboratory system as predicted by the mean particle size (MPS) and solids content respectively. This indicated a poor fit of data to the model and the use of linear regression models was not considered further.

6.2.2 Neural network models

The network employed was comprised of the linear transfer function (purelin), and as a predictor function, the linear output nodes. A total of 300 image frames were used for this analysis; 240 images trained the data by a 3-fold cross validation analysis and 60 images were used as the independent test data. The output variables were the MPS and solids % or content which were predicted from these image features: underflow width and standard deviation of the pixel intensity values as well as the GLCM statistical features (entropy, energy, homogeneity, contrast and correlation).

A feed forward multilayer perceptron (MLP) network with 7-10-3 architecture was the optimized network used to predict the discharge particles after having run a number of trials with the training data. MLP is able to use different activation functions and to efficiently train them to any function. Thus it can be applied to both linear and non-linearly separable data. To the contrary, a single unit perceptron can only be applied to patterns that can be linearly separated. Therefore, the MLP architecture was used in this analysis since it was not known a priory in which type of data relationship these image features were. This prevented the risk of applying a linear architecture to non-linear data which would result in an unsuccessful data fit.

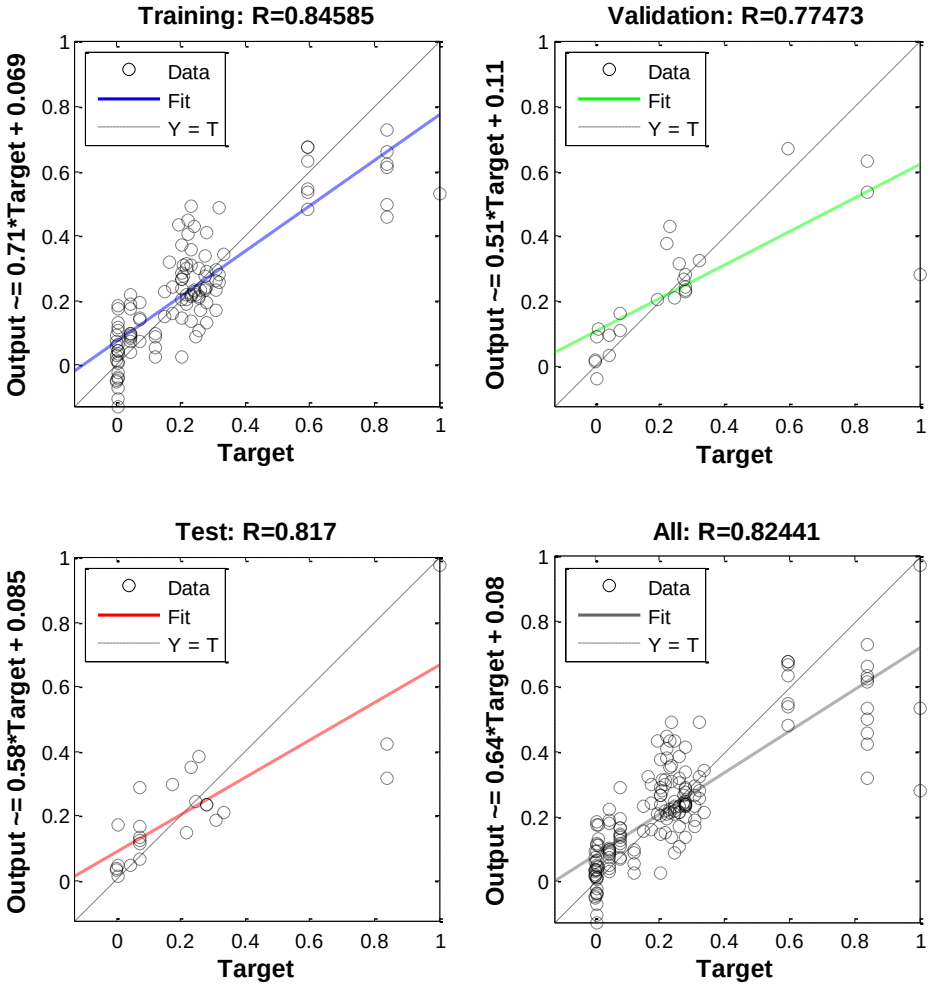

Figure 6-3: The Neural Network Regression-Fit for the laboraratory hydrocyclone system data, with the mean particle sizes as the predictor

The findings of the optimized MLP on the test data used for the prediction of the output variables indicated that the R values were 0.817 and 0.673 for the MPS and solids content respectively. The closer the value of R is to 1, the better the model (the predicted and the

observed variables have a closer relationship). Refer to Figure 6-3 and Figure 6-4 test graphs. The R^2 values for the MPS and solids content were 0.667 and 0.453 respectively. From these results, it is clear that the laboratory data poorly fit the NN model with both the mean PS and with the solids content output variables. With both predictors the results were poor, with the MPS showing a better outcome than the solids content.

Therefore, it could be concluded that it was more difficult to predict the solids content than to predict the MPS, using the laboratory data presented in this thesis.

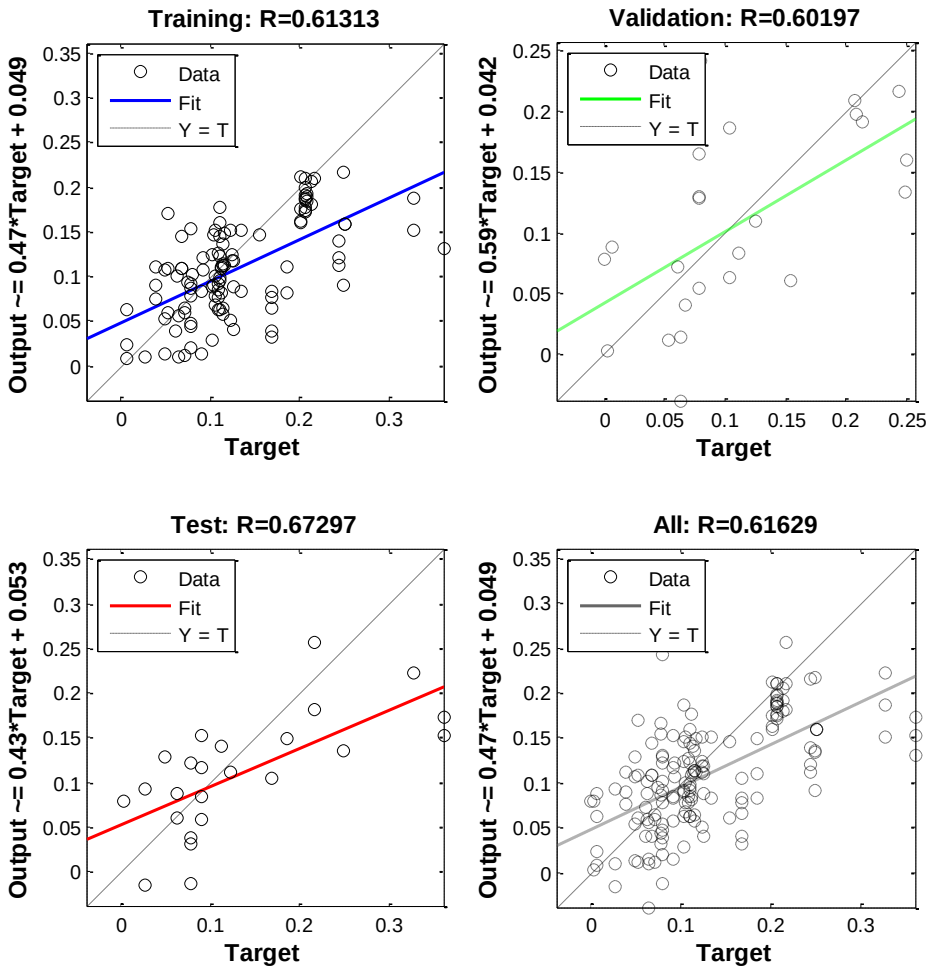

Figure 6-4: The Neural Network Regression-Fit for the laboraratory hydrocyclone system data, with solids loading as the predictor

To further evaluate the goodness of fit to the models, the predicted and observed values for the two output variables, mean particle size (mean PS) and solids %, were compared. The results indicated that the predicted values of the mean PS were closer to the experimental values in comparison to the solids loading. Refer to Figure 6-5 for the comparison plots of predicted versus observed values for the mean PS and solids % validation data of the laboratory cyclone systems.

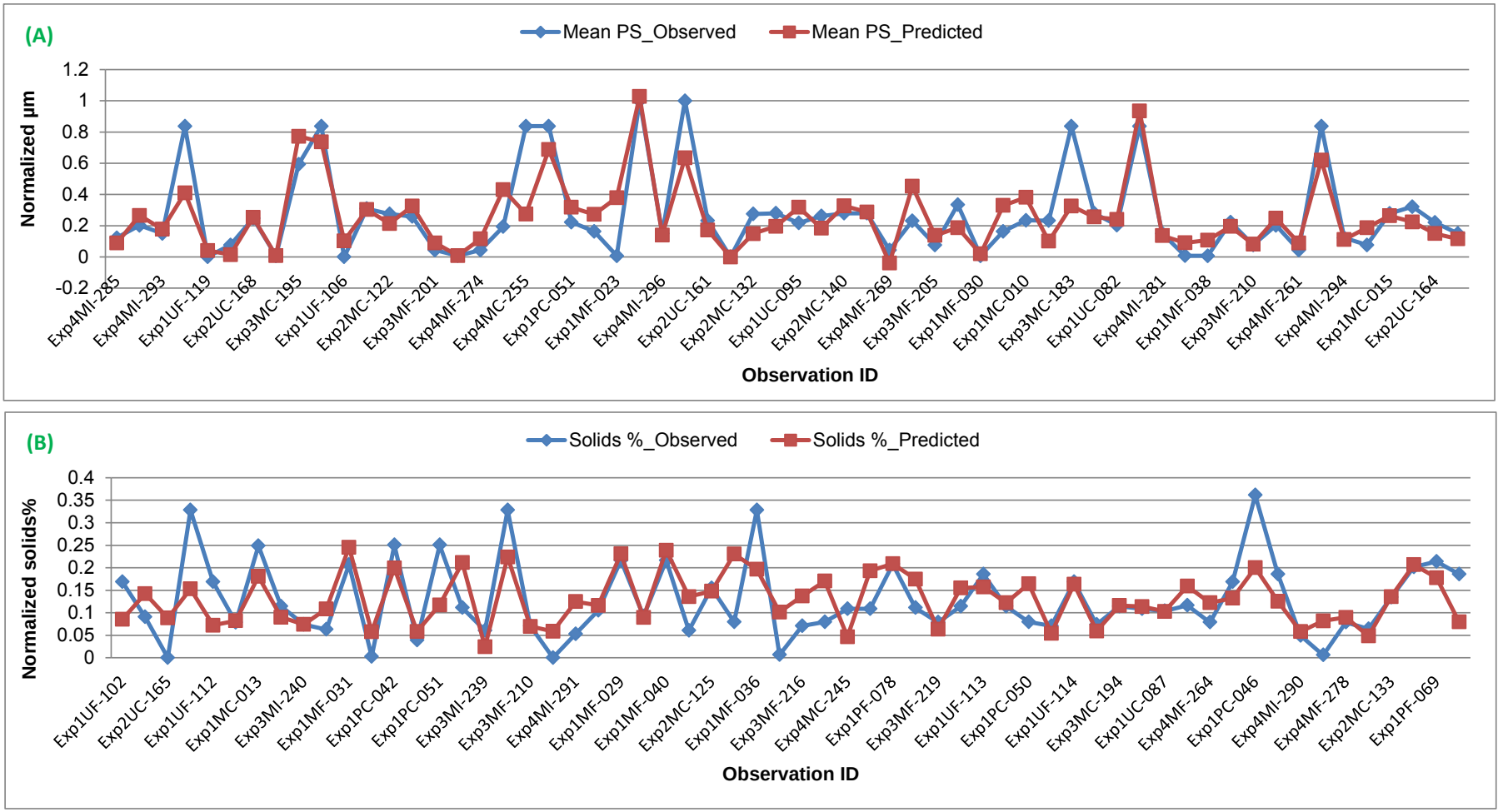

Figure 6-5: Illustration of the observed values versus predicted values of the mean particle sizes (A) and solids loading (B) as obtained from the laboratory hydrocyclone system

The model performance was compared to the data and it showed that both output variables were closely correlated with the average standard deviation of ±0.0736 and ±0.0355 for the mean PS and solids content respectively. Figure 6-6 presents this correlation.

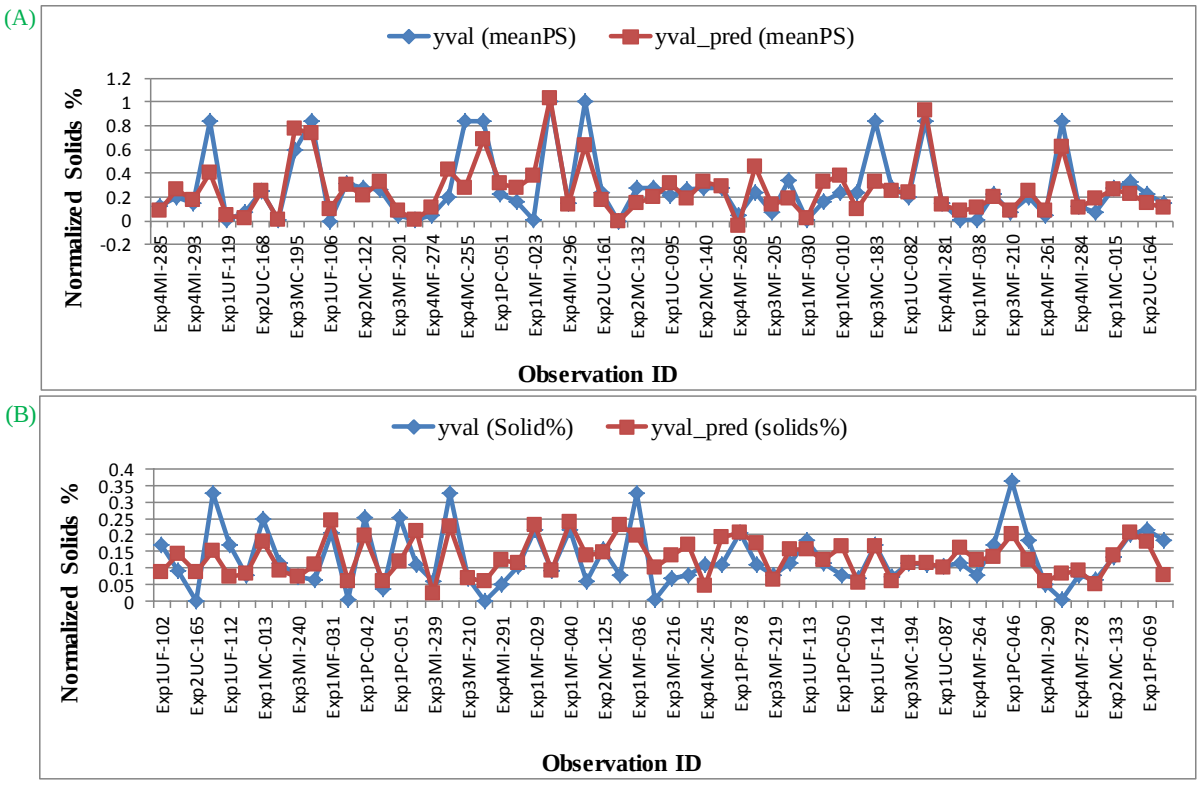

Figure 6-6: Illustration of the correlation between the y-validation predicted and y-data for mean PS (A) and solids content (B)

Chapter Summary

Visual observation and underflow image pixel intensity values were used for the exploratory study. It was used to test the sub-hypothesis which stated that different particle sizes of the hydrocyclone underflow discharges can be distinguished. The results proved this statement correct as the particle sizes was correctly classified. These results set the basis for further investigations carried out during the rest of the study described in this thesis.

The laboratory data categorisation results obtained by performing the linear (LDA) and non-linear (NN) models showed similar results. However, the outcomes of NN classification analysis were slightly better than with the LDA. The successful classification rate from the

NN model was 84% and 92% for the ore type and particle size class categories. In contrast, LDA outcomes were 61% and 79% respectively. A linear model would therefore be sufficient to correctly discriminate between the particles of different sizes. However, ore types could only be non-linearly distinguished.

The industrial data was only classified according to the particle size classes since the ore type was the same (uranium ore type) and a 100% classification rate was achieved. This outcome suggests that a feasibility image analysis study could be conducted on industrial cyclone systems.

With regard to the underflow particles prediction, only laboratory data was analysed due to the insufficiency of industrial data. The results thereof showed that the particles information could hardly be explained in both linear and non-linear models. In the linear model, the predictors (Y) only explained the input variables by about 56% and 40% with mean PS and solids content respectively. Besides, non-linear models yielded a % variance of 67 and 45 respectively. However, the non-linear model performed better in comparison to the linear model. The test R^2 values attained were 0.667 and 0.453 with the mean PS and solids content output variables for the non-linear and linear methods respectively. This is an improved performance of model fit from linear to non-linear model.

Ultimately, the conclusion made is that, although the non-linear model obtained better results in comparison to the linear model, the cyclone underflow particles could not successfully be correlated to the underflow image features. Furthermore, extensive research is required to gain a good understanding of the influence that this monitoring system could have in the industrial environment. This is however outside the scope of the work described in this thesis. The aim for the industrial-based study was only to establish a feasibility study of image analysis to RUL cyclones. This can be conducted with a few modifications to the current hydrocyclone set-up.

Chapter 7: Conclusions

The previous chapter presented and discussed the observations made from the investigations of the research. In this chapter the conclusions from these findings are reported. These conclusions were made in the light of the objectives of the project and knowledge obtained from the literature in this study field. The recommendations for future work are also reported.

7.1 Results

7.1.1 Classification of cyclone underflow particles

As the prior chapters have highlighted, the main focus of this research was to use image features of the underflow from the hydrocyclone to predict ore type, particle sizes and solids loadings of the underflow. Linear (LDA, ML) as well as nonlinear (NN) models were used for this purpose.

a) Laboratory cyclone system

The LDA results showed that the ore type could be classified approximately 61% correctly. All image feature variables contributed to these analyses, except for the underflow width. The overall conclusion here is that discrimination between the different ores was only partially successful, as could be expected for these ores that had a similar appearance.

b) Industrial hydrocyclone system

The industrial data which was only classified by particle size achieved a 100% correct classification rate with both the LDA and NN models. However, these data were too few to allow any conclusions to be drawn from these results.

7.1.2 Predicting the cyclone underflow particles

Quantitative prediction of the mean particle size and solids content of the underflow of the hydrocyclone was likewise moderately successful, if the response variable variance explained by the models is considered as the criterion.

Linear models could explain 56% and 40% of the variance in the mean particles size and solids content respectively. In contrast, the nonlinear models (neural network) could explain 0.67 and 0.45 of the variance of the mean particle size and solids content in the underflow of the hydrocyclone.

These results are not definitive, and further studying would be required to better evaluate the hypothesis that image variables could be used to characterize the mean particle size (or cut size) and solids concentration in the underflow. This could be done by deriving more informative image variables in the first place, as the grey level dependence matrix methods may not necessarily have been the most suitable approach to extracting features from the image data, despite its comparatively widespread use in other mineral processing applications.

7.2 Possible practical limitations of the cyclone underflow image capturing

There were some physical constraints related to the image capturing during the industrial study and the major ones identified include:

- Discharging of the hydrocyclone underflow inside a discharge box. A camera needs to be situated at an appropriate location such that it takes images of the underflow discharge at an angle suitable for better and quality image capturing. This can be obstructed if the hydrocyclone does not discharge to the open, as in the case of RUL cyclones.
- Variability in ore type and color: The influence of the differences in the types and color of the ore was identified as one of the major problems. This is problematic as it can be difficult to make immediate corrections while the plant is in operation due to the feed on a stock pile. In addition, dark/black colored ore types are difficult to analyze due to the edges of the underflow not clearly distinct from the background. Depending on the image features extracted from the underflow images, these features can be interrelated as shown in the global sensitivity (NN) and variable correlation values of R^2 (LDA) and could influence the classification outcome.

7.3 Recommendations

In chapter 4, some negative conditions were highlighted while conducting the industrial study cases including the obstruction of vision to the hydrocyclone spigot. It is thus recommended that the opening of the discharge box/sump be big and well positioned to allow for the best location of the camera.

More data from an industrial hydrocyclone set-up need to be collected to gain a better understanding of the constant changes in the operation states that are experienced during hydrocyclone operation. In addition, having more data would improve the model which would assist in a better understanding of the hydrocyclone underflow particles and image analysis. Additionally, more measurable parameters (inlet and outlet stream parameters) could improve the fit of data to the model.

Sampling of the underflow discharges and taking underflow images simultaneously would yield information on the same discharged particles. Hence underflow images would be compared with the exactly corresponding samples. The current set-up did not allow for this modification to be made.

Lastly, it is suggested that a set-up that automatically captures images at a set frequency should be used as this would result in a better study of subsequent images.

References

Aldrich, C., Marais, C., Shean, B. J. & Cilliers, J. J. 2010. Online monitoring and control of froth flotation systems with machine vision: A review. *International Journal of Mineral Processing,* 96**:** 1-13.

Bello, A. L. 1995. Imputation techniques in regression analysis: Looking closely at their implementation. *Computational Statistics & Data Analysis,* 20**:** 45-57.

Berberoglu, S., Curran, P. J., Lloyd, C. D. & Atkinson, P. M. 2007. Texture classification of Mediterranean land cover. *International Journal of Applied Earth Observation and Geoinformation,* 9**:** 322-334.

Bergstrom, J. & Vomhoff, H. 2007. Experimental hydrocyclone flow field studies. *Separation and Purification Technology,* 53**:** 8-20.

Bharati, M. H., Liu, J. J. & MacGregor, J. F. 2004. Image texture analysis: methods and comparisons. *Chemometrics and Intelligent Laboratory Systems,* 72**:** 57-71.

Bradley, D (ed.). 1965. *The Hydrocyclone.* Oxford: Pergamon Press Limited.

Braun, T. & Bohnet, M. 1990. Influence of feed solids concentration on the performance of hydrocyclones. *Chemical Engineering and Technology,* 13**:** 15-20.

Castro, O., Concha, F., Montero, J., Miranda, J., Castro, J. & Urizer, D. 1996. Air core modelling for an industrial hydrocyclone. In *Hydrocyclones 96.* London: Mechanical Engineering Publications Limited, 229-240.

Chu, L.Y. & Luo, Q. 1994. Hydrocyclone with high sharpness of separation. *Filtration & Separation,* 31**:** 733-720.

Clausi, D. A. & Zhao, Y. 2002. Rapid extraction of image texture by co-occurrence using a hybrid data structure. *Computers & Geosciences,* 28**:** 763-774.

Constantinides, A. & Mostoufi, N. 2000. Statistical Terminology used in Regression Analysis. In *Numerical Methods for Chemical Engineers with MATLAB Application.* USA: Prentice-Hall Inc.

Correlation. 2012. [Online]. Available: http://support.echoview.com/WebHelp/Reference/Algorithms/Operators/GLCM_textures/Correlation.html [2012, May 2].

Daniel, H. 2011. Methods for automatic control, observation, and optimization in mineral processing plants. *Journal of Process Control,* 21**:** 211-225.

Dyakowski, T. & Williams, R. A. 1993. Modelling turbulent flow within a small-diameter hydrocyclone. *Chemical Engineering Science,* 48**:** 1143-1152.

Dyakowski, T. & Williams, R. A. 1996. Prediction of high solids concentration regions within a hydrocyclone. *Powder Technology,* 87**:** 43-47.

Dyakowski, T., Jeanmeure, L. F. C. & Jaworski, A. J. 2000. Applications of electrical tomography for gas-solids and liquid-solids flows: a review. *Powder Technology*, 112(3): 174-192.

Galvin, K. P. & Smitham, J. B. 1994. Use of X-rays to determine the distribution of particles in an operating cyclone. *Minerals Engineering,* 7**:** 1269-1280.

Gutiérrez, J. A., Dyakowski, T., Beck, M. S. & Williams, R. A. 2000. Using electrical impedance tomography for controlling hydrocyclone underflow discharge. *Powder Technology*, 108**:** 180-184.

Hararah, M. A., Endres, E., Dueck, J., Minkov, L. & Neesse, T. 2010. Flow conditions in the air core of the hydrocyclone. *Minerals Engineering,* 23: 295-300.

Hou, R., Hunt, A. & Williams, R. A. 1998. Acoustic monitoring of hydrocyclone performance. *Minerals Engineering,* 11**:** 1047-1059.

Hou, R., Hunt, A. & Williams, R. A. 2002. Acoustic monitoring of hydrocyclones. *Powder Technology,* 124**:** 176-187.

Hsieh, K. T. & Rajamani, R. K. 1991. Mathematical model of the hydrocyclone based on physics of fluid flow. *AIChE Journal*, 37 (5): 735–746.

Hulbert, D. G. 1993. *Measurement methods and apparatus for hydrocyclones*. Pat EP0522215A3, Randburg.

Janse van Vuuren, M. J. 2011. Online monitoring of hydrocyclones by use of image analysis. Unpublished master's thesis. Stellenbosch: Stellenbosch University.

Janse van Vuuren, M. J., Aldrich, C. & Auret, L. 2011. Detecting changes in the operational states of hydrocyclones. *Minerals Engineering,* 24**:** 1532-1544.

Kawatra, S. K., Eisele, T. C. & Walqui, H. J. 2002. Optimization of Comminution Circuit Throughput and product Size Distribution by Simulation and Control. USA: Michigan Techological University.

Khashei, M., Zeinal Hamadani, A. & Bijari, M. 2012. A novel hybrid classification model of artificial neural networks and multiple linear regression models. *Expert Systems with Applications,* 39**:** 2606-2620.

Ko, Y.-D. & Shang, H. 2011. A neural network-based soft sensor for particle size distribution using image analysis. *Powder Technology,* 212**:** 359-366.

Kone, E. R. S. & Karwan, M. H. 2011. Combining a new data classification technique and regression analysis to predict the Cost-To-Serve new customers. *Computers & Industrial Engineering,* 61**:** 184-197.

Kraipech, W., Chen, W., Dyakowski, T. & Nowakowski, A. 2006. The performance of the empirical models on industrial hydrocyclone design. *International Journal of Mineral Processing,* 80**:** 100-115.

Krishna, V., Sripriya, R., Kumar, V., Chakraborty, S. & Meikap, B. C. 2010. Identification and prediction of air core diameter in a hydrocyclone by a novel online sensor based on digital signal processing technique. *Chemical Engineering and Processing: Process Intensification,* 49**:** 165-176.

Lidell, K. S., McRae, L. B. & Dunne, R. C. 1986. Process routes for beneficiation of noble metals from Merensky and UG-2 ores. *Mintek Review,* 4: 33-44.

Lynch, A. J. & Rao, T. C. 1968. Studies on the operating characteristics of the hydrocyclone classifiers. *Indian Journal of Technology,* 6**:** 106-114.

Lynch, A.J. & Rao, T.C. 1975. Modelling and Scale-Up of Hydrocyclone Classifiers. Unpublished paper delivered at the 11th International Mineral Processing Congress. 20-26 April, Cagliari.

Machado, A. 1992. The role of hydrocyclones in mineral processing. *Filtration & Separation,* 29**:** 479.

Marais, C. 2010. Estimation of concentrate grade in platinum floatation based on froth image analysis. Unpublished master's thesis. Stellenbosch: Stellenbosch University.

Maurice, C., Fuerstenau, C. & Kenneth, N. H. (eds.). 2003. *Principles of Mineral Processing.* USA: Society for Mining, Metallurgy, and Exploration Inc.

Muhamad, A. K. & Deravi, F. 1994. Neural networks for the classification of image texture. *Engineering Applications of Artificial Intelligence,* 7**:** 381-393.

Nageswararao, K., 1995. A generalised model for hydrocyclone classifiers. *Proceedings of Australasian Institute of Mining and Metallurgy,* 300 (2), 21.

Nageswararao, K., Wiseman, D. M. & Napier-Munn, T. J. 2004. Two empirical hydrocyclone models revisited. *Minerals Engineering,* 17**:** 671-687.

Nagpaul, P. S. 2009. *Guide to Advanced Data Analysis using IDAMS Software: 5.1 Multiple Classification Analysis* [Online]. Available: http://www.unesco.org/webworld/idams/advguide/Chapt5_3.htm [2012, November 18].

Napier-Munn, T. J., Morrel, S., Morrison, R. D. and Kojovic, T. 1996. *Mineral Comminution Circuits - Their operation and optimisation.* Indooroopilly: University of Queensland (JKMRC).

Neesse, T., Schubert, H. & Graichen, K. 1991. Practical and Theoretical Aspects of Dense-Flow Classification. *Aufbereitungstechnik,* 32**:** 459-472.

Neesse, T., Golyk, V., Kaniut, P. & Reinsch, V. 2004a. Hydrocyclone control in grinding circuits. *Minerals Engineering,* 17: 1237-1240.

Neesse, T., Schneider, M., Golyk, V. & Tiefel, H. 2004b. Measuring the operating state of the hydrocyclone. *Minerals Engineering*, 17: 697-703.

Neesse, T. & Dueck, J. 2007a. Air core formation in the hydrocyclone. *Minerals Engineering*, 20**:** 349-354.

Neesse, T. & Dueck, J. 2007b. Dynamic modelling of the hydrocyclone. *Minerals Engineering*, 20**:** 380-386.

Olson, T. J. & Waterman, R. J. 2006. *Hydrocyclone Roping Detector and Method*. Pat US6983850B2, Tuscon.

Park, S. B., Lee, J. W. & Kim, S. K. 2004. Content-based image classification using a neural network. *Pattern Recognition Letters*, 25**:** 287-300.

Petersen, K. R. P., Aldrich, C., Van Deventer, J. S. J., McInnes, C. & Stange, W. W. 1996. Hydrocyclone underflow monitoring using image processing methods. *Minerals Engineering*, 9: 301-315.

Petersen, K. R. P. 1998. The monitoring of the hydrocyclone underflows and mill feed systems using image processing techniques. Unpublished master's thesis. Stellenbosch: Stellenbosch University

Plitt, L. R. 1976. A Mathematical Modelling of the Hydrocyclone Classifier. *CIM Bulletin*, 69 (776), 114-123.

Prats-Montalbãn, J. M., de Juan, A. & Ferrer, A. 2011. Multivariate image analysis: A review with applications. *Chemometrics and Intelligent Laboratory Systems*, 107**:** 1-23.

Rodriguez-Galiano, V. F., Chica-Olmo, M., Abarca-Hernandez, F., Atkinson, P. M. & Jeganathan, C. 2012. Random Forest classification of Mediterranean land cover using multi-seasonal imagery and multi-seasonal texture. *Remote Sensing of Environment*, 121**:** 93-107.

Rietema, K. & Verver, C. G. 1961. *Cyclones in Industry*. New York: Elsevier Publishing Company.

Rössing, T. T. (ed.). 1995. *Rotoscoops Operations Training Manual: Revision 1995*. Swakopmund: Rossing Uranium.

Schlaberg, H. I. Á., Podd, F. J. W. & Hoyle, B. S. 2000. Ultrasound process tomography system for hydrocyclones. *Ultrasonics*, 38: 813-816.

Smyth, G. K. 2002. *Nonlinear regression.* Chichester: John Wiley & Sons, Ltd. [Online]. Available: http://www.statsci.org/smyth/pubs/eoe_nr.pdf [2012, November 18].

Sripriya, R., Kaulaskar, M. D., Chakraborty, S. & Meikap, B. C. 2007. Studies on the performance of a hydrocyclone and modelling for flow characterization in the presence and absence of air core. *Chemical Engineering Science*, 62**:** 6391-6402.

STATISTICA. 2012. STATISTICA Software Electronic Manual.

Svarovsky, L. 1984. *Hydrocyclones.* London: Holt, Rinehart and Winston Ltd.

Svarovsky, L. 2001. Hydrocyclones. In *Solid-Liquid Separation (Fourth Edition)*. Oxford: Butterworth-Heinemann, 191-245

Sykes, A. O. *An Introduction to Regression Analysis* [Online]. Available: http://www.law.uchicago.edu/files/files/20.Sykes_.Regression.pdf [2013, March 4].

Tapp, H. S., Peyton, A. J., Kemsley, E. K. & Wilson, R. H. 2003. Chemical engineering applications of electrical process tomography. *Sensors and Actuators B: Chemical,* 92**:** 17-24.

Tranmer, M. & Elliot, M. 1998. *Multiple Linear Regression* [Online]. Available: http://www.ccsr.ac.uk/publications/teaching/mlr.pdf [2012, November 19].

Tuceryan, M. & Jain, A. K. 1998. Texture Analysis, in Chen, C. H., Pau, L. F. & Wang, P. S. P. (eds.). *Handbook of Pattern Recognition and Computer Vision.* Singapore: World Scientific, 235–276.

Um, M.-J., Yun, H., Jeong, C.-S. & Heo, J.-H. 2011. Factor analysis and multiple regression between topography and precipitation on Jeju Island, Korea. *Journal of Hydrology,* 410**:** 189-203.

van Deventer, J. S. J., Feng, D., Petersen, K. R. P. & Aldrich, C. 2003. Modelling of hydrocyclone performance based on spray profile analysis. *International Journal of Mineral Processing,* 70**:** 183-203.

West, R. M., Jia, X. & Williams, R. A. 2000. Parametric modelling in industrial process tomography. *Chemical Engineering Journal,* 77**:** 31-36.

Williams, R. A., Dickin, F. J., Dyakowski, T., Ilyas, O. M., Abdullah, Z. & Beck, M. S. 1992. Looking into mineral process plant? *Minerals Engineering,* 5**:** 867-881.

Williams, R. A., Dyakowski, T., Xie, C. G., Luke, S. P., Gregory, P. J., Edwards, R. B. & Gate, L. F. 1995a. Industrial measurement and control of particulate processes using electrical tomography. In *Process Tomography - Implementation for Industrial Processes.* Manchester: University of Manchester, 3-5.

Williams, R. A., Ilyas, O. M., Dyakowski, T., Dickin, F. J., Gutierrez, J. A., Wang, M., Beck, M. S., Shah, C. & Rushton, A. 1995b. Air core imaging in cyclonic separators: implications for separator design and modelling. *The Chemical Engineering Journal and the Biochemical Engineering Journal,* 56**:** 135-141.

Williams, R.A., Peng, S.J., Brown, D., Parkinson, N., Jannes, P. 1996. On-line measurement of hydrocyclone performance using acoustic emission. In *Hydrocyclones 96*. London: Mechanical Engineering Publications Limited, 241-252.

Williams, R. A., Dickin, F. J., Gutiérrez, J. A., Dyakowski, T. & Beck, M. S. 1997. Using electrical impedance tomography for controlling hydrocyclone underflow discharge. *Control Engineering Practice,* 5**:** 253-256.

Williams, R. A., Jia, X., West, R. M., Wang, M., Cullivan, J. C., Bond, J., Faulks, I., Dyakowski, T., Wang, S. J., Climpson, N., Kostuch, J. A. & Payton, D. 1999. Industrial monitoring of hydrocyclone operation using electrical resistance tomography. *Minerals Engineering*, 12**:** 1245-1252.

Wills, B. A. 1997. *Mineral Processing Technology 6th edition, An Introduction to the Practical Aspects of Ore Treatment and Mineral Recovery*. Oxford: Butterworth-Heinemann.

Wills, B. A. & Napier-Munn, T. 2005. Classification, in Wills, B.A. (ed.). *Wills' Mineral Processing Technology (Seventh Edition).* Oxford: Butterworth-Heinemann. 203-224.

Wills, B. A. 2006. *Wills' Mineral Processing Technology 7th Edition, An introduction to the Practical Aspects of Ore Treatment and Mineral Processing.* Oxford: Butterworth-Heinemann.

Zhen-bo, W., Yi, M. & You-hai, J. 2011. Simulation and experiment of flow field in axial-flow hydrocyclone. *Chemical Engineering Research and Design*, 89**:** 603-610.

Appendix A: Experimental Details

A.1 Experimental procedure

This part consists of the step-by-step procedures of experimental methods.

I. Experimental set-up and sample preparation

A stepwise procedure of the sample preparation is shown below:

1. Obtain an ample quantity of sample to be prepared.
2. Ensure that the sieve machine is functional and insert an 850 µm sieve plate.
3. Sieve sample.
4. Change sieve plate to 100 µm.
5. Using the sample prepared in step 2, sieve the samples through a sieve machine.
6. Collect both the oversize (+100) and undersize (-100) material.
7. Mix both samples thoroughly.
8. Sample a portion from the oversize sample.
9. Using a rotary splitter, split sample from step 7 to at least a sample of 200g.
10. Do a sub-sieve test for the sample prepared in step 8, to have an idea of what material is to be fed into the hydrocyclone.
11. Put the rest of the sample in step 8 back into the bulk sample.
12. From each sample prepared in step 5, weigh out a sample to be used to run the experiment (in this case, 40kg and 33kg for first and second experiments respectively).
13. The samples are ready to be used.

The following is a step-by-step procedure for using the camera:

1. Set up the tripod in the direction of the spigot.
2. Attach the camera on the tripod and adjust it to clearly view the spigot.
3. Set the camera to the programmed settings (ISO 1600 and Large and Raw images).
4. Attach the additional flash to the camera.
5. By taking test pictures, zoom in and out to capture closer and clear images as well as to locate the best shot angle of the underflow discharge.
6. If step 5 is showing satisfactory results, delete the testing images.

7. The camera is ready, start the photo session.

II. Start-up procedure

1. Ensure that the mixing tank valve is closed before filling the tank with water.
2. Turn on the stirrer of the mixing tank. The stirring motion will aid in maintaining particle suspension in the water.
3. To allow the circulation of water through the system, close the drain valve, while opening the pump- and mixing tank valves. Switch the pump on immediately after this, to avoid the pump running dry.

III. Operating procedure

1. Allow the water to circulate for 5 minutes in order to attain steady state.
2. Take pictures of the underflow discharge.
3. Add the ore to the circulating fluid by slowly emptying the bucket into the mixing tank. Excessive splashing is minimised in this manner.
4. Allow an extra 10 minutes for the system to reach steady state.
5. During the course of the experiment, minimise physical movement on the structure on which the set-up is mounted. Any movement on the structure causes excessive vibration of the hydrocyclone and the digital camera. The camera may fall or the pictures could be blurred.
6. Take pictures of the slurry underflow discharge, taking a time period of about 20 minutes. After the picture session, take samples of both the overflow and the underflow discharge streams.
7. Each run follows the same procedure from sample preparation to shut-down procedure.

IV. Shut-down procedure

1. On completion of the last run, disband the digital camera set-up and put it away.
2. Commence with cleaning the hydrocyclone system. While cleaning the system, the ore may settle in the piping and cause blockages. To reduce the likelihood of blockages, dilute the circulating fluid with water.
3. When the fluid is sufficiently dilute, start emptying the mixing tank by opening the drain valve. Continue to add water to the mixing tank.

4. Collect the fluid in a large container to allow the settling of the ore particles. This also permits the overflow of water to the floor drain.
5. Once the majority of particles are flushed from the system, switch off the pump.
6. Hose the remainder of the particles from the mixing tank. Close the mixing tank valve when the tank is completely clean and empty.
7. Flush the pump and piping system through the openings adjacent to the drain valve.
8. Close the drain valve on completion of washing.
9. Clean the floor area of the experiment.

V. Laboratory hydrocyclone specifications

The laboratory cyclone dimensions are provided in this section:

- Cyclone diameter: 76 mm
- Vortex finder diameter: 75 mm
- Feed inlet diameter: 53 mm
- Spigot diameter: 32 mm
- Cyclone length: 130 mm

A.2 RUL hydrocyclone specification

The RUL hydrocyclone dimensions are:

Hydrocyclone diameter: 660 mm
Spigot diameter: 150 mm
Vortex finder: 250 mm
Feed inlet diameter: 115 mm
Hydrocyclone length: 482mm

A.3 Data analysis

I. Analytical methodology

The following section outlines a stepwise procedure for data analysis (image processing and sample analysis) from the sampling point and/or image capturing.

a) Manual sampling

1. Take underflow discharge samples, note the sampling time.
2. Weigh wet samples, note the mass and dry the samples.
3. Weigh dried samples and calculate the wet content to get the solid percentage.
4. Do a sieve test to get the PSD of the samples.
5. Compile a table of solid percentages and PSD data and combine this with image features to run the classification analyses.

b) Cyclone underflow digital images

1. Capture the underflow discharge images using the high speed camera (400D Canon camera used for this research).
2. Upload images to a standard computer (PC).
3. By using suitable image software, enhance the images to attain similar brightness and contrast settings. The Microsoft Office Picture Manager was used in this work.
4. Export images to MATLAB Software for further processing.
5. Select images to be processed.
6. By the use of the MATLAB Image Processing Tool, convert images to grayscale.
7. Select the area of interest from the images where the features would be extracted. Different slice positions were selected for different experiments or cyclone runs due to slight changes in them which may complicate image processing.
8. Extract image features, such as pixel intensity values, gray level co-occurrence matrix (GLCM) and underflow width.
9. From GLCMs, further extract the statistical features which are: entropy, contrast, correlation, energy and homogeneity.
10. Export the statistical features extracted in step 9 together with pixel intensity values and underflow width to the table of data created in a).

11. Use the data in the table that is now comprised of sample data and image features data to do a classification analysis. Do this after the data is normalised or standardised to have values in a similar scale.
12. In STATISTICA / MATLAB Software, run classification analysis using LDA and Automated Neural Network methods.
13. Similarly, using MATLAB Toolbox / STATISTICA Software, run a regression analysis with Neural Network methods.

II. Consolidated Data Set

Table A-1: Consolidated Data Set with Data Normalized between 0 and 1.

Sample ID (observations)	Response Variables			Predictor Variables						
	Discrete	Continuous								
	Ore Type	Mean PS	Solid %	Homo-geneity	Under-flow Width	Entropy	Correla-tion	Pixel Intensity STDDEV	Energy	Contrast
Exp1MC-001	MER	0.2348	0.2487	0.4166	0.3167	0.8035	0.8318	0.5872	0.1271	0.4355
Exp1MC-002	MER	0.3217	0.2015	0.6337	0.4240	0.9521	0.6433	0.2946	0.4038	0.2416
Exp1MC-003	MER	0.2782	0.2436	0.7450	0.3677	0.9913	0.8076	0.3723	0.4106	0.1629
Exp1MC-004	MER	0.2348	0.2487	0.5975	0.3115	0.9757	0.9137	0.6119	0.1421	0.2655
Exp1MC-005	MER	0.3217	0.2015	0.6365	0.3104	0.9961	0.8844	0.5383	0.2101	0.2411
Exp1MC-006	MER	0.2782	0.2436	0.5019	0.3292	0.9649	0.8964	0.6280	0.1265	0.3257
Exp1MC-007	MER	0.2348	0.2487	0.5730	0.3552	0.9521	0.7265	0.3759	0.3315	0.2809
Exp1MC-008	MER	0.3217	0.2015	1.0000	0.3667	1.0000	0.8204	0.2648	0.7927	0.0000
Exp1MC-009	MER	0.2782	0.2436	0.5856	0.3104	0.9649	0.8896	0.5737	0.2135	0.2756
Exp1MC-010	MER	0.2348	0.2487	0.3835	0.2479	0.8570	0.8949	0.7028	0.0804	0.4398
Exp1MC-011	MER	0.3217	0.2015	0.6721	0.3667	0.9521	0.7273	0.3515	0.3545	0.2224
Exp1MC-012	MER	0.2782	0.2436	0.6100	0.2927	0.9649	0.9065	0.6037	0.2363	0.2703
Exp1MC-013	MER	0.2348	0.2487	0.6597	0.3292	0.8803	0.9153	0.5934	0.2437	0.2422
Exp1MC-014	MER	0.3217	0.2015	0.6594	0.3854	0.9521	0.9280	0.6203	0.2165	0.2305
Exp1MC-015	MER	0.2782	0.2436	0.4961	0.3354	0.7050	0.9439	0.7486	0.1243	0.3476
Exp1MC-016	MER	0.2348	0.2487	0.6258	0.2167	0.9757	0.8930	0.5620	0.2574	0.2462
Exp1MC-017	MER	0.3217	0.2015	0.4183	0.2229	0.6261	0.9413	0.8111	0.0954	0.4301
Exp1MC-018	MER	0.2782	0.2487	0.5432	0.1938	0.8803	0.8023	0.4831	0.3904	0.3215
Exp1MC-019	MER	0.2348	0.2015	0.6954	0.2917	0.9757	0.7546	0.3627	0.4636	0.2047
Exp1MC-020	MER	0.3217	0.2436	0.7644	0.2854	0.9913	0.8233	0.4089	0.5711	0.1521
Exp1MF-021	MER	0.0065	0.3282	0.6646	0.5167	0.9373	0.6505	0.2872	0.4546	0.2335
Exp1MF-022	MER	0.0064	0.2071	0.7259	0.5125	0.9961	0.7248	0.3326	0.4693	0.2160
Exp1MF-023	MER	0.0071	0.2163	0.8360	0.3167	0.9845	0.8173	0.3548	0.5407	0.1213
Exp1MF-024	MER	0.0065	0.3282	0.7642	0.4917	0.9990	0.7763	0.3564	0.4616	0.1709
Exp1MF-025	MER	0.0064	0.2071	0.7854	0.5083	0.9913	0.7492	0.3267	0.4460	0.1638
Exp1MF-026	MER	0.0071	0.2163	0.9194	0.4375	0.9521	0.6533	0.1734	0.7331	0.0474
Exp1MF-027	MER	0.0065	0.3282	0.8080	0.4958	0.9961	0.8230	0.3796	0.4799	0.1489
Exp1MF-028	MER	0.0064	0.2071	0.8080	0.4802	1.0000	0.8170	0.3380	0.4679	0.1285
Exp1MF-029	MER	0.0071	0.2163	0.8113	0.4823	0.9521	0.7787	0.3332	0.5662	0.1391
Exp1MF-030	MER	0.0065	0.3282	0.7354	0.4500	0.9845	0.7737	0.3790	0.4575	0.2109
Exp1MF-031	MER	0.0064	0.2071	0.7829	0.5094	0.9990	0.7404	0.3150	0.6028	0.1605
Exp1MF-032	MER	0.0071	0.2163	0.6960	0.5083	0.9961	0.7705	0.3688	0.4433	0.2071
Exp1MF-033	MER	0.0065	0.3282	0.8071	0.5500	0.9961	0.7620	0.3332	0.5173	0.1587
Exp1MF-034	MER	0.0064	0.2071	0.8432	0.4760	0.9961	0.7730	0.3248	0.7909	0.1167
Exp1MF-035	MER	0.0071	0.2163	0.8017	0.4500	1.0000	0.7686	0.3447	0.5933	0.1600
Exp1MF-036	MER	0.0065	0.3282	0.8580	0.4083	0.9845	0.7479	0.2748	0.5900	0.1004
Exp1MF-037	MER	0.0064	0.2071	0.7241	0.4625	0.9649	0.7941	0.3792	0.3860	0.1857
Exp1MF-038	MER	0.0071	0.3282	0.7755	0.4250	0.9961	0.7536	0.3226	0.4789	0.1540

Exp1MF-039	MER	0.0065	0.2071	0.6731	0.5042	0.9913	0.6896	0.3199	0.4725	0.2307
Exp1MF-040	MER	0.0064	0.2163	0.7910	0.4958	0.9961	0.7663	0.3339	0.5560	0.1530
Exp1PC-041	PLAT	0.2588	0.0796	0.7108	0.3208	0.9204	0.9036	0.5362	0.2048	0.2010
Exp1PC-042	PLAT	0.2225	0.2505	0.4380	0.3542	0.8314	0.9050	0.7036	0.1053	0.4120
Exp1PC-043	PLAT	0.2447	0.3610	0.5219	0.3083	0.8803	0.8780	0.5987	0.1320	0.3401
Exp1PC-044	PLAT	0.2588	0.0796	0.1479	0.2958	0.2419	0.9265	0.9477	0.0175	0.6978
Exp1PC-045	PLAT	0.2225	0.2505	0.7374	0.3000	0.8803	0.9796	0.7133	0.2819	0.1885
Exp1PC-046	PLAT	0.2447	0.3610	0.2396	0.3917	0.6670	0.8998	0.7965	0.0434	0.5669
Exp1PC-047	PLAT	0.2588	0.0796	0.4141	0.3302	0.7404	0.9222	0.7648	0.0584	0.4367
Exp1PC-048	PLAT	0.2225	0.2505	0.2880	0.2833	0.6261	0.9406	0.8816	0.0222	0.5303
Exp1PC-049	PLAT	0.2447	0.3610	0.5020	0.2844	0.7732	0.9582	0.8034	0.0823	0.3591
Exp1PC-050	PLAT	0.2588	0.0796	0.6873	0.3125	0.9204	0.8347	0.4494	0.3283	0.2205
Exp1PC-051	PLAT	0.2225	0.2505	0.2457	0.3260	0.4304	0.8639	0.7437	0.0563	0.6142
Exp1PC-052	PLAT	0.2447	0.3610	0.2811	0.3708	0.6670	0.8979	0.7856	0.0498	0.5593
Exp1PC-053	PLAT	0.2588	0.0796	0.5529	0.3427	0.8570	0.9072	0.6632	0.2323	0.3315
Exp1PC-054	PLAT	0.2225	0.2505	0.5173	0.3458	0.9015	0.8782	0.5924	0.1714	0.3297
Exp1PC-055	PLAT	0.2447	0.3610	0.5199	0.3708	0.9373	0.8288	0.5251	0.2148	0.3323
Exp1PC-056	PLAT	0.2588	0.0796	0.3504	0.2938	0.7050	0.8796	0.7015	0.1163	0.4857
Exp1PC-057	PLAT	0.2225	0.2505	0.2273	0.3042	0.6261	0.8366	0.6916	0.0597	0.6020
Exp1PC-058	PLAT	0.2447	0.0796	0.7879	0.3583	1.0000	0.7682	0.3318	0.5161	0.1365
Exp1PC-059	PLAT	0.2588	0.2505	0.3532	0.3583	0.6261	0.9071	0.7542	0.0788	0.4782
Exp1PC-060	PLAT	0.2225	0.3610	0.7204	0.2625	0.9913	0.8547	0.4477	0.3716	0.1828
Exp1PF-061	PLAT	0.0076	0.2077	0.9378	0.4250	0.9913	0.7509	0.2387	0.6031	0.0337
Exp1PF-062	PLAT	0.0054	0.2065	0.8184	0.4865	0.9990	0.8551	0.3919	0.4216	0.1137
Exp1PF-063	PLAT	0.0095	0.2137	0.8534	0.5458	0.9757	0.8592	0.3774	0.4697	0.0977
Exp1PF-064	PLAT	0.0076	0.2077	0.8585	0.5667	0.9990	0.8361	0.3611	0.4579	0.0858
Exp1PF-065	PLAT	0.0054	0.2065	0.8488	0.4573	0.9913	0.8187	0.3347	0.4782	0.0913
Exp1PF-066	PLAT	0.0095	0.2137	0.9435	0.4375	0.9521	0.7001	0.1944	0.6147	0.0291
Exp1PF-067	PLAT	0.0076	0.2077	0.8619	0.4625	0.9521	0.7880	0.3047	0.4683	0.0842
Exp1PF-068	PLAT	0.0054	0.2065	0.8809	0.4708	0.9990	0.8881	0.4022	0.3949	0.0729
Exp1PF-069	PLAT	0.0095	0.2137	0.8310	0.4250	0.9990	0.7642	0.2958	0.4785	0.1056
Exp1PF-070	PLAT	0.0076	0.2077	0.9084	0.5083	0.9757	0.8376	0.3285	0.4731	0.0545
Exp1PF-071	PLAT	0.0054	0.2065	0.8947	0.4625	0.9757	0.8356	0.3407	0.4501	0.0682
Exp1PF-072	PLAT	0.0095	0.2137	0.8693	0.4417	0.9990	0.8703	0.3890	0.4192	0.0802
Exp1PF-073	PLAT	0.0076	0.2077	0.9162	0.4542	0.9845	0.8183	0.2883	0.4685	0.0480
Exp1PF-074	PLAT	0.0054	0.2065	0.8809	0.4542	0.9913	0.8198	0.3200	0.4906	0.0713
Exp1PF-075	PLAT	0.0095	0.2137	0.9391	0.4990	0.9649	0.7651	0.2384	0.5979	0.0329
Exp1PF-076	PLAT	0.0076	0.2077	0.8861	0.4719	0.9961	0.8814	0.3904	0.4629	0.0691
Exp1PF-077	PLAT	0.0054	0.2065	0.8033	0.4375	0.9913	0.8637	0.4205	0.4130	0.1208
Exp1PF-078	PLAT	0.0095	0.2077	0.9082	0.4448	0.9845	0.9013	0.4047	0.4277	0.0536
Exp1PF-079	PLAT	0.0076	0.2065	0.9352	0.4917	0.9961	0.8167	0.2868	0.4988	0.0372
Exp1PF-080	PLAT	0.0054	0.2137	0.8940	0.4667	0.9649	0.7650	0.2565	0.5822	0.0643
Exp1UC-081	UG2	0.2020	0.1038	0.3111	0.3167	0.7404	0.8427	0.6611	0.0844	0.5265
Exp1UC-082	UG2	0.2037	0.1052	0.4585	0.3083	0.8570	0.7726	0.4909	0.1958	0.3914
Exp1UC-083	UG2	0.2177	0.1253	0.3308	0.3958	0.6670	0.8719	0.7105	0.0818	0.5212
Exp1UC-084	UG2	0.2020	0.1038	0.7533	0.4458	0.9961	0.8161	0.3851	0.3865	0.1606
Exp1UC-085	UG2	0.2037	0.1052	0.0000	0.3208	0.1686	0.7952	0.8127	0.0161	1.0000
Exp1UC-086	UG2	0.2177	0.1253	0.1659	0.3667	0.3722	0.8607	0.8020	0.0295	0.7259
Exp1UC-087	UG2	0.2020	0.1038	0.6131	0.4292	0.4846	0.8853	0.6001	0.3888	0.3132
Exp1UC-088	UG2	0.2037	0.1052	0.5815	0.3708	0.7732	0.6051	0.3260	0.3740	0.3301
Exp1UC-089	UG2	0.2177	0.1253	0.1801	0.3375	0.0000	0.8604	0.8220	0.0275	0.7659
Exp1UC-090	UG2	0.2020	0.1038	0.4509	0.3917	0.5822	0.8734	0.6693	0.1022	0.4480
Exp1UC-091	UG2	0.2037	0.1052	0.2522	0.3792	0.3096	0.7649	0.5923	0.1300	0.6090
Exp1UC-092	UG2	0.2177	0.1253	0.4229	0.4042	0.6670	0.6895	0.4467	0.2251	0.4505
Exp1UC-093	UG2	0.2020	0.1038	0.2100	0.3083	0.3722	0.7617	0.6246	0.0918	0.6720
Exp1UC-094	UG2	0.2037	0.1052	0.4817	0.3542	0.8314	0.7838	0.5096	0.1955	0.4086
Exp1UC-095	UG2	0.2177	0.1253	0.2440	0.3125	0.3096	0.8600	0.7905	0.0545	0.7051
Exp1UC-096	UG2	0.2020	0.1038	0.5056	0.3833	0.7050	0.7355	0.4733	0.2709	0.4220
Exp1UC-097	UG2	0.2037	0.1052	0.3377	0.3583	0.5351	0.8423	0.6862	0.0807	0.5754
Exp1UC-098	UG2	0.2177	0.1038	0.5620	0.3542	0.7404	0.8475	0.5744	0.1838	0.3731
Exp1UC-099	UG2	0.2020	0.1052	0.3356	0.2875	0.0885	0.9229	0.9163	0.0845	0.6606

Exp1UC-100	UG2	0.2037	0.1253	0.3104	0.3292	0.5822	0.7793	0.6096	0.1297	0.6027
Exp1UF-101	UG2	0.0013	0.1855	0.7347	0.4833	1.0000	0.7756	0.3845	0.3811	0.2099
Exp1UF-102	UG2	0.0009	0.1685	0.6126	0.4500	0.9649	0.7827	0.4570	0.2642	0.3210
Exp1UF-103	UG2	0.0000	0.1685	0.6182	0.5375	1.0000	0.8549	0.5340	0.2125	0.2951
Exp1UF-104	UG2	0.0013	0.1855	0.7266	0.4958	0.9913	0.9401	0.6144	0.1780	0.2029
Exp1UF-105	UG2	0.0009	0.1685	0.5945	0.5167	0.9990	0.7980	0.4708	0.2261	0.3138
Exp1UF-106	UG2	0.0000	0.1685	0.7194	0.5208	0.9913	0.9585	0.6581	0.1549	0.1959
Exp1UF-107	UG2	0.0013	0.1855	0.7251	0.4667	1.0000	0.8206	0.4346	0.3507	0.2085
Exp1UF-108	UG2	0.0009	0.1685	0.6522	0.5333	0.9757	0.8921	0.5609	0.1877	0.2549
Exp1UF-109	UG2	0.0000	0.1685	0.6706	0.5250	0.9961	0.8553	0.4957	0.2741	0.2447
Exp1UF-110	UG2	0.0013	0.1855	0.6358	0.4917	0.9990	0.8075	0.4615	0.2621	0.2793
Exp1UF-111	UG2	0.0009	0.1685	0.6376	0.4750	0.9845	0.8780	0.5567	0.2118	0.2780
Exp1UF-112	UG2	0.0000	0.1685	0.7154	0.5458	0.9757	0.8400	0.4519	0.2415	0.2184
Exp1UF-113	UG2	0.0013	0.1855	0.5895	0.5542	0.9521	0.9630	0.7694	0.1014	0.3024
Exp1UF-114	UG2	0.0009	0.1685	0.6328	0.5167	0.9913	0.8177	0.4688	0.2928	0.2677
Exp1UF-115	UG2	0.0000	0.1685	0.6122	0.5625	0.9990	0.8011	0.4757	0.2722	0.3187
Exp1UF-116	UG2	0.0013	0.1855	0.6252	0.5167	0.9015	0.8141	0.4792	0.2546	0.2875
Exp1UF-117	UG2	0.0009	0.1685	0.5535	0.4667	0.9757	0.8403	0.5337	0.1736	0.3291
Exp1UF-118	UG2	0.0000	0.1855	0.6354	0.5292	0.9649	0.8422	0.4828	0.2746	0.2507
Exp1UF-119	UG2	0.0013	0.1685	0.5566	0.5375	0.9649	0.8148	0.5159	0.2099	0.3485
Exp1UF-120	UG2	0.0009	0.1685	0.6104	0.5083	0.8314	0.8630	0.5379	0.1774	0.2858
Exp2MC-121	MER	0.3092	0.1236	0.3814	0.3000	0.8803	0.7986	0.5645	0.1246	0.4673
Exp2MC-122	MER	0.2748	0.1111	0.3187	0.3917	0.8035	0.8259	0.6617	0.0734	0.5746
Exp2MC-123	MER	0.2589	0.1341	0.0934	0.2583	0.8803	0.8503	0.8466	0.0107	0.8394
Exp2MC-124	MER	0.2618	0.1119	0.2152	0.3083	0.8035	0.8443	0.7189	0.0490	0.6517
Exp2MC-125	MER	0.2796	0.1548	0.1962	0.4083	0.8570	0.8195	0.7371	0.0455	0.7177
Exp2MC-126	MER	0.3092	0.1236	0.3871	0.4229	0.7732	0.7448	0.5102	0.1676	0.5039
Exp2MC-127	MER	0.2748	0.1111	0.2123	0.2625	0.9521	0.8126	0.6665	0.0605	0.5995
Exp2MC-128	MER	0.2589	0.1341	0.3345	0.2667	0.8035	0.6312	0.4582	0.2046	0.6017
Exp2MC-129	MER	0.2618	0.1119	0.3420	0.3333	0.8314	0.6417	0.4502	0.1983	0.5494
Exp2MC-130	MER	0.2796	0.1548	0.5264	0.2500	0.9204	0.7170	0.4262	0.2555	0.3694
Exp2MC-131	MER	0.3092	0.1236	0.3619	0.2375	0.8570	0.7046	0.4572	0.1925	0.4491
Exp2MC-132	MER	0.2748	0.1111	0.5361	0.3500	0.9015	0.8862	0.6123	0.1850	0.3317
Exp2MC-133	MER	0.2589	0.1341	0.3252	0.2333	0.9015	0.6364	0.4099	0.2061	0.4698
Exp2MC-134	MER	0.2618	0.1119	0.4007	0.3292	0.7732	0.6746	0.4341	0.2167	0.4530
Exp2MC-135	MER	0.2796	0.1548	0.4729	0.2917	0.8035	0.9258	0.7322	0.1383	0.3864
Exp2MC-136	MER	0.3092	0.1236	0.4182	0.3167	0.9757	0.7615	0.5018	0.1900	0.4391
Exp2MC-137	MER	0.2748	0.1111	0.1220	0.2594	0.7050	0.7729	0.6197	0.0774	0.6353
Exp2MC-138	MER	0.2589	0.1341	0.3722	0.2375	0.8035	0.7501	0.5122	0.1786	0.4749
Exp2MC-139	MER	0.2618	0.1119	0.5153	0.3625	0.9521	0.8049	0.5174	0.1762	0.3664
Exp2MC-140	MER	0.2796	0.1548	0.5992	0.3292	0.9015	0.9246	0.6627	0.1444	0.2960
Exp2PC-141	PLAT	0.1939	0.1164	0.4844	0.3625	0.7732	0.8213	0.5526	0.1676	0.3947
Exp2PC-142	PLAT	0.1635	0.1022	0.2451	0.2073	0.7050	0.7429	0.5807	0.1277	0.6320
Exp2PC-143	PLAT	0.2314	0.1125	0.4058	0.1875	0.7732	0.7452	0.5238	0.2097	0.4999
Exp2PC-144	PLAT	0.1730	0.0923	0.4205	0.3542	0.6670	0.8171	0.5820	0.1791	0.4657
Exp2PC-145	PLAT	0.2100	0.1107	0.3718	0.2000	0.4304	0.7556	0.5390	0.1686	0.5227
Exp2PC-146	PLAT	0.1939	0.1164	0.3826	0.2219	0.8035	0.8543	0.6407	0.1054	0.4604
Exp2PC-147	PLAT	0.1635	0.1022	0.3808	0.3000	0.2419	0.8637	0.7331	0.1013	0.5901
Exp2PC-148	PLAT	0.2314	0.1125	0.5305	0.3635	0.8035	0.8584	0.5950	0.1581	0.3742
Exp2PC-149	PLAT	0.1730	0.0923	0.2396	0.4031	0.3722	0.8579	0.7713	0.0486	0.6794
Exp2PC-150	PLAT	0.2100	0.1107	0.2338	0.3115	0.5822	0.8496	0.7145	0.0548	0.6014
Exp2PC-151	PLAT	0.1939	0.1164	0.3865	0.2219	0.8570	0.8507	0.6228	0.1014	0.4378
Exp2PC-152	PLAT	0.1635	0.1022	0.1645	0.2260	0.5822	0.7766	0.6537	0.1013	0.6995
Exp2PC-153	PLAT	0.2314	0.1125	0.6654	0.3802	0.8314	0.7707	0.3869	0.2972	0.2390
Exp2PC-154	PLAT	0.1730	0.0923	0.3949	0.3458	0.7732	0.7710	0.5534	0.1978	0.5211
Exp2PC-155	PLAT	0.2100	0.1107	0.7012	0.3719	0.9649	0.8958	0.5304	0.2007	0.2068
Exp2PC-156	PLAT	0.1939	0.1164	0.5636	0.2010	0.9373	0.7603	0.4193	0.2379	0.3000
Exp2PC-157	PLAT	0.1635	0.1022	0.3434	0.2802	0.5822	0.9607	0.9109	0.1192	0.4972
Exp2PC-158	PLAT	0.2314	0.1125	0.4154	0.2542	0.7050	0.9279	0.7885	0.0693	0.4645
Exp2PC-159	PLAT	0.1730	0.0923	0.3569	0.4281	0.5822	0.9054	0.7575	0.0597	0.4935
Exp2PC-160	PLAT	0.2100	0.1107	0.5757	0.3792	0.9204	0.8593	0.5602	0.1517	0.3270

Exp2UC-161	UG2	0.2322	0.0066	0.3617	0.4740	0.8035	0.7881	0.5903	0.1394	0.5418
Exp2UC-162	UG2	0.3091	0.0271	0.3526	0.4177	0.3722	0.8763	0.7620	0.0599	0.5949
Exp2UC-163	UG2	0.2473	0.0027	0.6357	0.4677	0.9204	0.7661	0.4166	0.2781	0.2872
Exp2UC-164	UG2	0.2204	0.0058	0.4219	0.4542	0.5822	0.6701	0.4377	0.2105	0.4715
Exp2UC-165	UG2	0.1818	0.0000	0.4013	0.4750	0.6261	0.8240	0.5864	0.1373	0.4498
Exp2UC-166	UG2	0.2322	0.0066	0.5693	0.3917	0.5351	0.9474	0.7797	0.0811	0.3760
Exp2UC-167	UG2	0.3091	0.0271	0.2912	0.3583	0.5351	0.8312	0.6807	0.1358	0.5975
Exp2UC-168	UG2	0.2473	0.0027	0.4631	0.4000	0.6261	0.8709	0.6657	0.1033	0.4519
Exp2UC-169	UG2	0.2204	0.0058	0.3770	0.4667	0.5351	0.7580	0.5810	0.1579	0.5975
Exp2UC-170	UG2	0.2322	0.0000	0.3331	0.4885	0.4846	0.7320	0.5457	0.1540	0.5836
Exp2UC-171	UG2	0.3091	0.0066	0.1873	0.4469	0.5351	0.8352	0.7275	0.0469	0.6764
Exp2UC-172	UG2	0.2473	0.0271	0.3324	0.4969	0.2419	0.8386	0.6552	0.1115	0.5423
Exp2UC-173	UG2	0.2204	0.0027	0.1938	0.4135	0.2419	0.7606	0.7083	0.1021	0.8803
Exp2UC-174	UG2	0.2322	0.0058	0.5629	0.4625	0.8035	0.6260	0.3480	0.3461	0.3476
Exp2UC-175	UG2	0.3091	0.0000	0.2197	0.4344	0.8035	0.8077	0.6541	0.0812	0.6191
Exp2UC-176	UG2	0.2473	0.0066	0.4444	0.4292	0.4304	0.8667	0.6799	0.1279	0.4969
Exp2UC-177	UG2	0.2204	0.0271	0.5831	0.4417	0.4846	0.8019	0.5325	0.1830	0.4078
Exp2UC-178	UG2	0.2322	0.0027	0.3938	0.4875	0.6261	0.6860	0.4825	0.1981	0.5325
Exp2UC-179	UG2	0.3091	0.0058	0.4909	0.4094	0.5351	0.8726	0.6473	0.1326	0.4290
Exp2UC-180	UG2	0.2473	0.0000	0.3652	0.4750	0.5822	0.7829	0.5742	0.1405	0.5299
Exp3MC-181	MER	0.8374	0.0782	0.1758	0.2375	0.1686	0.9293	0.9450	0.0000	0.6861
Exp3MC-182	MER	0.5936	0.1101	0.3262	0.0542	0.2419	0.8559	0.7526	0.1294	0.6602
Exp3MC-183	MER	0.8374	0.1227	0.6735	0.3667	0.8035	0.8601	0.5252	0.1946	0.2750
Exp3MC-184	MER	0.5936	0.1143	0.6438	0.1927	0.9015	0.9204	0.6263	0.1560	0.2620
Exp3MC-185	MER	0.5936	0.1092	0.6200	0.2833	0.0885	1.0000	0.9410	0.1310	0.3301
Exp3MC-186	MER	0.8374	0.0782	0.5243	0.3177	0.5822	0.9431	0.7494	0.0816	0.3475
Exp3MC-187	MER	0.5936	0.1101	0.5953	0.2083	0.5822	0.7522	0.4138	0.2583	0.3021
Exp3MC-188	MER	0.8374	0.1227	0.6276	0.2250	0.8035	0.8486	0.5227	0.2077	0.2921
Exp3MC-189	MER	0.5936	0.1143	0.5781	0.2292	0.7404	0.9023	0.6126	0.1918	0.3006
Exp3MC-190	MER	0.5936	0.1092	0.3042	0.1688	0.2419	0.9525	1.0000	0.0423	0.6472
Exp3MC-191	MER	0.8374	0.0782	0.3994	0.1260	0.5822	0.9155	0.7631	0.0543	0.4567
Exp3MC-192	MER	0.5936	0.1101	0.2906	0.1958	0.4304	0.8707	0.7686	0.0758	0.6349
Exp3MC-193	MER	0.8374	0.1227	0.3200	0.1094	0.6261	0.9732	0.9736	0.0448	0.5315
Exp3MC-194	MER	0.5936	0.1143	0.3073	0.1000	0.5351	0.9166	0.8011	0.0335	0.5220
Exp3MC-195	MER	0.5936	0.1092	0.4790	0.0510	0.4846	0.9813	0.9670	0.0809	0.4533
Exp3MC-196	MER	0.8374	0.0782	0.4444	0.2292	0.7050	0.8943	0.7198	0.0790	0.4704
Exp3MC-197	MER	0.5936	0.1101	0.4099	0.1958	0.8803	0.8004	0.5434	0.1405	0.4259
Exp3MC-198	MER	0.8374	0.1227	0.5512	0.0927	0.8570	0.8799	0.5808	0.1818	0.3111
Exp3MC-199	MER	0.5936	0.1143	0.3871	0.0458	0.4846	0.8401	0.6797	0.1245	0.5661
Exp3MC-200	MER	0.5936	0.1092	0.3429	0.0000	0.5822	0.8135	0.6427	0.1437	0.5737
Exp3MF-201	MER	0.0438	0.0707	0.4843	0.4792	0.8803	0.7917	0.5087	0.1946	0.3836
Exp3MF-202	MER	0.0763	0.0787	0.5465	0.4927	0.8035	0.7287	0.4286	0.2582	0.3647
Exp3MF-203	MER	0.0763	0.0670	0.5054	0.5635	0.9521	0.5624	0.3115	0.3419	0.3557
Exp3MF-204	MER	0.0763	0.0707	0.5961	0.4760	0.9649	0.7392	0.4030	0.2991	0.3023
Exp3MF-205	MER	0.0763	0.0787	0.5840	0.4135	0.8803	0.7815	0.4572	0.2375	0.3216
Exp3MF-206	MER	0.0438	0.0670	0.7618	0.4927	0.9990	0.8996	0.4878	0.2402	0.1518
Exp3MF-207	MER	0.0763	0.0707	0.4163	0.4802	0.8570	0.7309	0.4868	0.1740	0.4641
Exp3MF-208	MER	0.0763	0.0787	0.5188	0.4417	0.9649	0.6349	0.3527	0.3128	0.3516
Exp3MF-209	MER	0.0763	0.0670	0.5398	0.5208	0.9757	0.7434	0.4280	0.2428	0.3315
Exp3MF-210	MER	0.0763	0.0707	0.5744	0.4625	0.6261	0.7457	0.4386	0.3312	0.3451
Exp3MF-211	MER	0.0438	0.0787	0.5995	0.5167	0.9757	0.6381	0.3231	0.3844	0.2916
Exp3MF-212	MER	0.0763	0.0670	0.5962	0.5292	0.8570	0.8004	0.4598	0.3266	0.2965
Exp3MF-213	MER	0.0763	0.0707	0.4808	0.4583	0.9015	0.6990	0.4188	0.2458	0.3893
Exp3MF-214	MER	0.0763	0.0787	0.6710	0.5083	0.9521	0.4504	0.2061	0.5288	0.2402
Exp3MF-215	MER	0.0763	0.0670	0.4993	0.5125	0.8314	0.8874	0.6440	0.1474	0.3852
Exp3MF-216	MER	0.0438	0.0707	0.5060	0.4375	0.9015	0.7831	0.4816	0.2121	0.3553
Exp3MF-217	MER	0.0763	0.0787	0.4814	0.4406	0.6670	0.8792	0.6531	0.1521	0.4146
Exp3MF-218	MER	0.0763	0.0707	0.2972	0.5375	0.4304	0.7908	0.6048	0.1034	0.5669
Exp3MF-219	MER	0.0763	0.0787	0.5040	0.4083	0.7732	0.8241	0.5734	0.1715	0.4330
Exp3MF-220	MER	0.0763	0.0670	0.5072	0.4292	0.6670	0.8064	0.5405	0.1695	0.4166
Exp3MI-221	MER	0.3349	0.0785	0.4233	0.3542	0.3722	0.9132	0.7792	0.0775	0.5005

Exp3MI-222	MER	0.2795	0.0773	0.3323	0.4458	0.4846	0.9628	0.9985	0.0113	0.5962
Exp3MI-223	MER	0.2795	0.0908	0.3445	0.4344	0.4304	0.8778	0.7485	0.0592	0.5738
Exp3MI-224	MER	0.2795	0.0604	0.3095	0.4385	0.7050	0.8209	0.6241	0.0961	0.5216
Exp3MI-225	MER	0.2795	0.0738	0.2979	0.4667	0.6670	0.7727	0.5985	0.1201	0.5967
Exp3MI-226	MER	0.3349	0.0785	0.5277	0.4385	0.8570	0.7247	0.4202	0.2457	0.3489
Exp3MI-227	MER	0.2795	0.0773	0.5392	0.3885	0.8035	0.8911	0.6330	0.1338	0.3528
Exp3MI-228	MER	0.2795	0.0908	0.3803	0.3813	0.6261	0.8374	0.6164	0.1113	0.4693
Exp3MI-229	MER	0.2795	0.0604	0.2833	0.4917	0.3722	0.8156	0.6773	0.0793	0.6408
Exp3MI-230	MER	0.2795	0.0738	0.3793	0.5083	0.5822	0.8885	0.7488	0.0668	0.5320
Exp3MI-231	MER	0.3349	0.0785	0.3962	0.3792	0.7404	0.8684	0.6601	0.1130	0.4550
Exp3MI-232	MER	0.2795	0.0773	0.2767	0.5042	0.3722	0.7769	0.5973	0.1170	0.5804
Exp3MI-233	MER	0.2795	0.0908	0.4095	0.4292	0.4846	0.8490	0.6479	0.1093	0.4916
Exp3MI-234	MER	0.2795	0.0604	0.6312	0.5000	0.9373	0.8511	0.5168	0.2040	0.2849
Exp3MI-235	MER	0.2795	0.0738	0.7379	0.5177	0.9845	0.7845	0.3699	0.3213	0.1785
Exp3MI-236	MER	0.3349	0.0785	0.3639	0.4417	0.6261	0.9639	0.9636	0.0204	0.5401
Exp3MI-237	MER	0.2795	0.0773	0.5394	0.5125	0.4304	0.7665	0.4673	0.2064	0.3616
Exp3MI-238	MER	0.2795	0.0908	0.2972	0.5458	0.8035	0.7745	0.5891	0.1103	0.5712
Exp3MI-239	MER	0.2795	0.0604	0.4434	0.4792	0.5822	0.8755	0.6876	0.0948	0.4832
Exp3MI-240	MER	0.2795	0.0738	0.4832	0.4344	0.5822	0.8995	0.6494	0.0928	0.3584
Exp4MC-241	MER	1.0000	0.1142	0.7579	0.0906	0.8570	0.9256	0.5620	0.2815	0.1828
Exp4MC-242	MER	0.8374	0.1088	0.8394	0.2208	0.9961	0.9190	0.4796	0.2831	0.1113
Exp4MC-243	MER	0.8374	0.0904	0.7185	0.3208	0.9373	0.9555	0.6584	0.1929	0.2117
Exp4MC-244	MER	1.0000	0.1142	0.6424	0.3813	0.9015	0.9276	0.6415	0.1324	0.2642
Exp4MC-245	MER	0.8374	0.1088	0.7844	0.2802	0.8314	0.9097	0.5209	0.2270	0.1700
Exp4MC-246	MER	0.8374	0.0904	0.6886	0.2667	0.8035	0.9393	0.6622	0.1412	0.2495
Exp4MC-247	MER	1.0000	0.1142	0.7113	0.2594	0.9649	0.8672	0.4881	0.2675	0.2114
Exp4MC-248	MER	0.8374	0.1088	0.6958	0.2458	0.9204	0.7967	0.4274	0.2873	0.2444
Exp4MC-249	MER	0.8374	0.0904	0.8743	0.2917	0.9913	0.8134	0.3244	0.4407	0.0915
Exp4MC-250	MER	1.0000	0.1142	0.7472	0.2750	0.9845	0.6721	0.2837	0.4255	0.1987
Exp4MC-251	MER	0.8374	0.1088	0.5058	0.3333	0.8570	0.9825	0.8971	0.0385	0.3690
Exp4MC-252	MER	0.8374	0.0904	0.6229	0.1792	0.5822	0.8644	0.5821	0.1985	0.3489
Exp4MC-253	MER	1.0000	0.1142	0.7051	0.1042	0.6261	0.9131	0.5985	0.1720	0.2591
Exp4MC-254	MER	0.8374	0.1088	0.7755	0.1906	0.9204	0.8016	0.3791	0.3525	0.1678
Exp4MC-255	MER	0.8374	0.0904	0.7272	0.3458	0.7732	0.7905	0.3935	0.3755	0.2172
Exp4MC-256	MER	1.0000	0.1142	0.8304	0.3333	1.0000	0.7616	0.2965	0.4256	0.1116
Exp4MC-257	MER	0.8374	0.1088	0.6852	0.2542	0.8803	0.9373	0.6409	0.1609	0.2372
Exp4MC-258	MER	1.0000	0.1142	0.7414	0.1469	0.9204	0.8603	0.4674	0.2746	0.2034
Exp4MC-259	MER	0.8374	0.1088	0.7835	0.2375	0.9649	0.5014	0.1974	0.8204	0.1654
Exp4MC-260	MER	0.8374	0.0904	0.6424	0.3042	0.8314	0.8816	0.5542	0.2527	0.2715
Exp4MF-261	MER	0.0438	0.0787	0.6213	0.4750	0.9521	0.7578	0.4114	0.2613	0.2797
Exp4MF-262	MER	0.0438	0.0640	0.6557	0.5010	0.9015	0.7112	0.3709	0.3310	0.2747
Exp4MF-263	MER	0.0438	0.0628	0.5525	0.4844	0.7404	0.8236	0.5404	0.3093	0.3769
Exp4MF-264	MER	0.0438	0.0787	0.6015	0.4583	0.9649	0.7788	0.4422	0.2827	0.3019
Exp4MF-265	MER	0.0438	0.0640	0.6694	0.6167	0.9990	0.6116	0.2876	0.4182	0.2530
Exp4MF-266	MER	0.0438	0.0628	0.6459	0.4990	0.9845	0.7023	0.3511	0.3735	0.2567
Exp4MF-267	MER	0.0438	0.0787	0.4822	0.4469	0.6670	0.7885	0.5563	0.1796	0.4786
Exp4MF-268	MER	0.0438	0.0640	0.7218	0.4250	0.8803	0.6473	0.3015	0.4018	0.2383
Exp4MF-269	MER	0.0438	0.0628	0.8316	0.5208	0.9521	0.4679	0.1820	0.6615	0.1546
Exp4MF-270	MER	0.0438	0.0787	0.8145	0.5531	0.9845	0.6928	0.2794	0.5184	0.1489
Exp4MF-271	MER	0.0438	0.0640	0.6747	0.5427	0.8803	0.8595	0.5301	0.2470	0.2740
Exp4MF-272	MER	0.0438	0.0628	0.7256	0.4917	0.9373	0.8509	0.4806	0.2612	0.2301
Exp4MF-273	MER	0.0438	0.0787	0.5066	0.5385	0.8803	0.7815	0.5110	0.2111	0.4078
Exp4MF-274	MER	0.0438	0.0640	0.5901	0.5344	0.7732	0.8093	0.5278	0.2160	0.3809
Exp4MF-275	MER	0.0438	0.0628	0.7320	0.4917	0.9521	0.8319	0.4418	0.2565	0.2229
Exp4MF-276	MER	0.0438	0.0787	0.7533	0.5073	0.9204	0.7375	0.3729	0.4595	0.2427
Exp4MF-277	MER	0.0438	0.0640	0.5050	0.2583	0.8314	0.4579	0.2905	0.3982	0.4123
Exp4MF-278	MER	0.0438	0.0787	0.7061	0.5469	0.9373	0.6134	0.2996	0.4596	0.2631
Exp4MF-279	MER	0.0438	0.0640	0.6826	0.6292	0.9521	0.7803	0.4054	0.3031	0.2554
Exp4MF-280	MER	0.0438	0.0628	0.5728	0.5000	0.8314	0.7687	0.4691	0.2579	0.3627
Exp4MI-281	MER	0.1502	0.0493	0.6917	0.4375	0.9521	0.6770	0.3250	0.4190	0.2442
Exp4MI-282	MER	0.1221	0.0528	0.8017	0.4833	0.9961	0.4979	0.1903	0.7229	0.1575

Exp4MI-283	MER	0.0763	0.0391	0.4583	0.3875	0.7732	0.6938	0.4386	0.2253	0.4320
Exp4MI-284	MER	0.1502	0.0493	0.8094	0.4281	0.9649	0.6330	0.2449	0.5070	0.1431
Exp4MI-285	MER	0.1221	0.0528	0.6627	0.4292	0.9913	0.8410	0.4837	0.2414	0.2516
Exp4MI-286	MER	0.0763	0.0391	0.5467	0.4260	0.8035	0.8483	0.5531	0.1686	0.3407
Exp4MI-287	MER	0.1502	0.0493	0.8036	0.4542	0.9845	0.7570	0.3271	0.4163	0.1547
Exp4MI-288	MER	0.1221	0.0528	0.8437	0.4458	0.9961	0.4269	0.1242	0.6588	0.1125
Exp4MI-289	MER	0.0763	0.0391	0.7335	0.4833	0.9521	0.6865	0.3188	0.4347	0.2190
Exp4MI-290	MER	0.1502	0.0493	0.5843	0.3833	0.7404	0.7786	0.4588	0.2343	0.3373
Exp4MI-291	MER	0.1221	0.0528	0.6561	0.4250	0.8035	0.6892	0.3516	0.4188	0.2701
Exp4MI-292	MER	0.0763	0.0391	0.7222	0.4188	0.9913	0.5045	0.2279	0.6467	0.2235
Exp4MI-293	MER	0.1502	0.0493	0.5031	0.4375	0.7404	0.8362	0.5838	0.1446	0.4166
Exp4MI-294	MER	0.1221	0.0528	0.6274	0.4625	0.9204	0.7017	0.3598	0.3182	0.2758
Exp4MI-295	MER	0.0763	0.0391	0.5426	0.3750	0.8035	0.7439	0.4464	0.2384	0.3606
Exp4MI-296	MER	0.1502	0.0493	0.6472	0.4333	0.8570	0.8098	0.4510	0.2354	0.2592
Exp4MI-297	MER	0.1221	0.0528	0.7219	0.4833	0.9015	0.7377	0.3545	0.3727	0.2254
Exp4MI-298	MER	0.1502	0.0493	0.7355	0.4375	0.9757	0.5150	0.2206	0.6060	0.2143
Exp4MI-299	MER	0.1221	0.0528	0.7684	0.4792	0.8314	0.7800	0.3564	0.3593	0.1771
Exp4MI-300	MER	0.0763	0.0391	0.6518	0.4625	0.9204	0.7466	0.3823	0.2933	0.2567
Exp5RU-301	RUL	0.1221	0.9662	0.9575	0.4802	0.6261	0.4533	0.0755	0.7708	0.0193
Exp5RU-302	RUL	0.1221	0.9513	0.9198	0.4708	0.7404	0.5569	0.1250	0.6154	0.0437
Exp5RU-303	RUL	0.1221	0.9513	0.9483	0.4750	0.7404	0.5533	0.1227	0.6612	0.0253
Exp5RU-304	RUL	0.1221	0.9689	0.8967	0.4625	0.7404	0.5747	0.1464	0.5648	0.0587
Exp5RU-305	RUL	0.1221	0.9513	0.8406	0.4875	0.7732	0.5019	0.1482	0.5713	0.0952
Exp5RU-306	RUL	0.1221	0.9662	0.9002	0.3708	0.9521	0.5860	0.1735	0.6515	0.0587
Exp5RU-307	RUL	0.1221	0.9513	0.9062	0.4792	0.7404	0.3290	0.0896	0.8467	0.0526
Exp5RU-308	RUL	0.1221	0.9513	0.7808	0.5708	0.8570	0.2331	0.0791	0.6953	0.1345
Exp5RU-309	RUL	0.1221	0.9689	0.8394	0.4833	0.7404	0.0284	0.0578	1.0000	0.0960
Exp5RU-310	RUL	0.1221	0.9513	0.8995	0.5083	0.7404	0.3160	0.0986	0.8983	0.0571
Exp5RU-311	RUL	0.1221	0.9662	0.8372	0.4917	0.6670	0.0000	0.0320	0.9655	0.0974
Exp5RU-312	RUL	0.1221	0.9513	0.8483	0.4958	0.7404	0.2625	0.0813	0.8473	0.0900
Exp5RU-313	RUL	0.1221	0.9513	0.8824	0.4958	0.7050	0.2729	0.0457	0.7975	0.0679
Exp5RU-314	RUL	0.1221	0.9689	0.9151	0.5167	0.9521	0.6209	0.1971	0.8049	0.0485
Exp5RU-315	RUL	0.1221	0.9513	0.9221	0.4667	0.5822	0.1817	0.0000	0.8364	0.0423
Exp5RU-316	RUL	0.1221	0.9662	0.7797	0.4667	0.9015	0.7996	0.3486	0.3395	0.1354
Exp5RU-317	RUL	0.1221	0.9513	0.8317	0.4500	0.7732	0.6862	0.2540	0.5225	0.1010
Exp5RU-318	RUL	0.1221	0.9513	0.8404	0.4667	0.9015	0.6856	0.2416	0.5416	0.0959
Exp5RU-319	RUL	0.1221	0.9662	0.7869	0.4708	0.9204	0.7309	0.2989	0.4667	0.1308
Exp5RU-320	RUL	0.1221	0.9513	0.7218	0.4958	0.9649	0.6890	0.3017	0.4850	0.1741
Exp6RU-321	RUL	0.2004	0.9875	0.8962	0.9250	0.8314	0.7830	0.2754	0.4095	0.0590
Exp6RU-322	RUL	0.2004	1.0000	0.8477	1.0000	0.8803	0.8080	0.3253	0.3630	0.0904
Exp6RU-323	RUL	0.2004	0.9943	0.8123	0.9292	0.9015	0.7236	0.2702	0.4158	0.1133
Exp6RU-324	RUL	0.2004	0.9875	0.8859	0.9042	0.8314	0.7611	0.2633	0.4143	0.0657
Exp6RU-325	RUL	0.2004	1.0000	0.9457	0.9583	0.7404	0.6879	0.1754	0.5076	0.0270
Exp6RU-326	RUL	0.2004	0.9943	0.9488	0.9458	0.8314	0.8051	0.2651	0.4285	0.0250
Exp6RU-327	RUL	0.2004	0.9875	0.8722	0.9750	0.8803	0.7930	0.2942	0.3796	0.0746
Exp6RU-328	RUL	0.2004	1.0000	0.9574	0.9750	0.7404	0.7303	0.2047	0.5178	0.0194
Exp6RU-329	RUL	0.2004	0.9943	0.9155	0.9583	0.9015	0.7641	0.2455	0.4349	0.0465
Exp6RU-330	RUL	0.2004	0.9875	0.8544	0.9875	0.9373	0.7608	0.2817	0.4285	0.0861
Exp6RU-331	RUL	0.2004	1.0000	0.8267	0.9292	0.9015	0.7618	0.2954	0.4069	0.1040
Exp6RU-332	RUL	0.2004	0.9943	0.9314	0.9583	0.7404	0.7230	0.2128	0.5003	0.0362
Exp6RU-333	RUL	0.2004	0.9875	0.8575	0.9125	0.9015	0.7523	0.2730	0.4112	0.0841
Exp6RU-334	RUL	0.2004	1.0000	0.8349	0.9208	0.9015	0.7655	0.2908	0.3718	0.0987
Exp6RU-335	RUL	0.2004	0.9943	0.8795	0.9292	0.9015	0.8327	0.3273	0.3534	0.0698
Exp6RU-336	RUL	0.2004	0.9875	0.8387	0.9708	0.9015	0.7561	0.2826	0.3791	0.0963
Exp6RU-337	RUL	0.2004	1.0000	0.8158	0.9125	0.9015	0.6563	0.2268	0.4534	0.1111
Exp6RU-338	RUL	0.2004	0.9943	0.8115	0.9458	0.9015	0.7338	0.2780	0.3937	0.1138
Exp6RU-339	RUL	0.2004	0.9875	0.8351	0.9250	0.9015	0.7307	0.2678	0.4360	0.0986
Exp6RU-340	RUL	0.2004	1.0000	0.8753	0.9458	0.7404	0.5622	0.1527	0.5533	0.0726

Appendix B: Program Coding

This part outlines the main codes used in MATLAB Software for the extraction of image features.

B.1 Pixel intensity values

```
dirname = 'F:\MATLAB\Th Images\Big slice 1';

fnames = dir(fullfile(dirname,'*.JPG'));


for n=1:size(fnames,1)

    fprintf('Processing %s\n',fnames(n,1).name)   % informative message to
command line


% select the image to process

    im{n} = fnames(n,1).name;


% Read image

    I = imread(im{n});

    Igray = rgb2gray(I);


% select the slice position

    rowInd = 590:1200;

    colInd = 1620:1785;

    slice = Igray(rowInd,colInd);


    sliceMatrix(n,:)=reshape(slice,1,[]);

    save('PixInt-InSlice-IgrayBS1.mat', 'sliceMatrix');

end
```

B.2 GLCM statistics

```
dirname = 'C:\Users\foibe\Documents\MATLAB\April-to final\RUL2';

fnames = dir(fullfile(dirname,'*.JPG'));


for n=1:size(fnames,1)

    fprintf('Processing %s\n',fnames(n,1).name)  % informative message to
command line


    % select the image to process

    im{n} = fnames(n,1).name;


% Read image

    I = imread(im{n});

    Igray = rgb2gray(I);


% select the slice position

    rowInd = 980:1236;

    colInd = 1760:1857;

    slice = Igray(rowInd,colInd);


    sliceMatrix(n,:)=slice(:);

    save('PixInt-SmallSlice-IgrayRUL2.mat', 'sliceMatrix');


% Create the GLCMs. Call the graycomatrix function specifying the offsets.

    glcms = graycomatrix(slice);

    glcmMatrix(n,:)=(glcms(:));


% Derive statistics from the GLCMs using the graycoprops function...
```

```
    stats = graycoprops(glcms);

    statsMatrix(n,:)=(stats(:));


% Derive Entropy from GLCMs

    E = entropy(glcms);

    EntropyMatrix(n,:)=(E(:));

    save('GLCMDefstats-Entropy-SmlInSlice-IgrayRUL2.mat',
'glcmMatrix','statsMatrix','EntropyMatrix');


% show the image with the slice position super-imposed

    imshow(Igray);

    hold on

    plot([colInd(1) colInd(end) colInd(end) colInd(1) colInd(1)],...

        [rowInd(1) rowInd(1) rowInd(end) rowInd(end) rowInd(1)],...

        '.-r','LineWidth',1);

    saveas(gcf,sprintf('%s_Igrayslice.fig',im{n}));

    saveas(gcf,sprintf('%s_rgbslice.emf',im{n}));

    close all

    end


S=statsMatrix;


cols = size(S(1).Contrast,2);

rows = length(S);


% data per feature

    contrastMat = zeros(rows, cols);

    correlMat = zeros(rows, cols);

    energyMat = zeros(rows, cols);
```

```
    homogMat = zeros(rows, cols);


for n = 1:size(S,1);

    E = S(n);

    contrastMat(n,:) = E.Contrast;

    correlMat(n,:) = E.Correlation;

    energyMat(n,:) = E.Energy;

    homogMat(n,:) = E.Homogeneity;

end


save('GLCMDef Stats-IgrayRUL2-SmallSlc.mat', 'contrastMat','correlMat',
'energyMat','homogMat');


% Calculate standard deviation for each stats measure

    Con = std(contrastMat);

    Cor = std(correlMat);

    Ene = std(energyMat);

    Hom = std(homogMat);


% Calculate standard deviation for each size entropy

    sRUL2 = std(EntropyMatrix);


save('GLCMDef Stats StdDev-IgrayRUL2-SmallSlc.mat', 'Con','Cor',
'Ene','Hom','sRUL2');
```

B.3 Neural Network function used in cross validation

```
function results = myNeuralNetfun(xtrain,ytrain,xtest,ytest)


% Solve an Input-Output Fitting problem with a Neural Network
```

```
% Script generated by NFTOOL
% Created Thu May 31 16:36:11 GMT+02:00 2012

% TRANSPOSE INPUT:
    xtrain = xtrain';
    ytrain = ytrain';
    xtest = xtest';
    ytest = ytest';

% Create a Fitting Network (TRAIN ARCHITECTURE):
    hiddenLayerSize = 10;
    net = fitnet(hiddenLayerSize);

% Choose a Performance Function
% For a list of all performance functions type: help nnperformance
    net.performFcn = 'mse';  % Mean squared error

% Choose Plot Functions
% For a list of all plot functions type: help nnplot
    net.plotFcns = {'plotperform','plottrainstate','ploterrhist', ...
  'plotregression'};

% TRAIN THE NETWORK:
    [net,tr] = train(net,xtrain,ytrain);

% TEST THE NETWORK:
    ypred = net(xtest);

% EVALUATE TEST RESULTS:
```

```
    rsq = corr2(ytest,ypred);
    error = gsubtract(ytest,ypred);
    performance = perform(net,ytest,ypred);

% Plots
% Uncomment these lines to enable various plots.
    figure, plotperform(tr)
    figure, plottrainstate(tr)
    figure, plotregression(ytest,ypred)
    figure, ploterrhist(error)

% PACKAGE RESULTS:
    results = struct('net','ypred','error','rsq','tr','performance' );
    results.net = net;
    results.ypred = ypred;
    results.error = error;
    results.rsq = rsq;
% results.r2 = r2;
    results.tr = tr;
    results.performance = performance;
end
```

B.4 Cross validation and Neural Network

```
% DIVIDE DATA into training and independent validation data
    load('LabRegressData.mat')
    numObs = length(DATA);
    rs = randperm(numObs);
    valselection = round(0.2*numObs); % 20% of data
```

```
    valindices = rs(1:valselection); % first 20%

    trainindices = rs(valselection+1:end); % last 80%

    valDATA = DATA(valindices,:);

    trainDATA = DATA(trainindices,:);


% Specify x and y training data

    xtrain = trainDATA(:,3:9);

    ytrain = trainDATA(:,2);

    xval = valDATA(:,3:9);


    yval = valDATA(:,2);

    xval = xval';

    yval = yval';


% TRAINING: Partition Data

    c = cvpartition(ytrain,'kfold',3);

    disp (c)

    cvfnc =
@(xtrain,ytrain,xtest,ytest)myNeuralNetfun2013(xtrain,ytrain,xtest,y
test);

    crossvalResults = crossval(cvfnc,xtrain,ytrain,'partition',c);


% VALIDATION

    rsq = horzcat(crossvalResults.rsq);

    [bestRsq,bestInd] = max(rsq);

    bestNet = crossvalResults(bestInd).net;

    yval_pred = bestNet(xval);

    ytrain_pred = bestNet(xtrain);
```